Understanding the Molecular Basis of Multiple Mitochondrial Dysfunctions Syndrome 1: Impact of Mutation on the Structure and Function of NFU1

Undergraduate Research Thesis

Presented in Partial Fulfillment of the Requirements for Graduation *with honors research distinction* in Biochemistry in the undergraduate colleges of The Ohio State University

By

Nathaniel Allen Wesley

The Ohio State University
May 2017

Project Advisor: Professor James A. Cowan, Department of Chemistry and Biochemistry

Abstract

Studying novel proteins and their behavior in disease states often leads to elucidation of their function *in vivo* and provides a platform to guide drug development and treatment efforts. Recent patient studies have shown that a fatal mitochondrial disease, multiple mitochondrial dysfunctions syndrome 1 (MMDS1) arises from two distinct genetic mutations near the active site of the essential iron-sulfur (Fe/S) protein NFU1. Symptoms of MMDS1 include impairment of neurological development, lactic acidosis, failure to thrive, and ultimately death in infancy – all indicative of a general failure of the metabolic system. Reduced function of target Fe/S proteins lipoic acid synthetase (LIAS) and succinate dehydrogenase (SDH) in the MMDS1 disease state suggests that multiple metabolic pathways require proper function of the native NFU1 protein through Fe/S cluster delivery and trafficking. However, the precise function of NFU1 remains unknown, and there is no treatment or cure for MMDS1. To investigate the molecular consequences of the disease-causing Gly208Cys and Gly189Arg mutations, the structure and function of the mutant human NFU1 protein forms were analyzed *in vitro* using a suite of biochemical techniques and compared to data obtained for the native construct. In the case of G208C NFU1, the mutation initiates a global structural change, which alters the monomer-dimer equilibrium such that it is unable to receive an Fe/S cluster from physiologically-relevant sources. Preliminary data suggests a similar phenomenon could be occurring in the case of G189R NFU1. In order to complement study of these mutant constructs, selective

mutations at positions 189 and 208, along with cluster-binding residues at positions 210 and 213 have provided an in-depth investigation into the effects of mutation on Fe/S cluster coordination and transfer, and corroborated conclusions drawn from study of the G208C and G189R constructs.

Acknowledgments

This work would not have been possible without the help of many dedicated colleagues and friends.

First, I would like to thank my advisor Dr. James A. Cowan, not only for his valuable guidance throughout the project development and completion, but also throughout the transition into graduate study and a research career.

I would like to thank my graduate student mentor Christine Wachnowsky for the outstanding efforts she has contributed in mentoring, collaborating with, and inspiring me throughout my time in the Cowan lab.

I would also like to thank Dr. Insiya Fidai for her friendship and encouragement to become an independent researcher, as well as her working closely alongside me and Christine at the project inception and giving feedback on our manuscripts.

I would like to thank the current and former members of the Cowan lab for creating an enjoyable work environment, and being willing to lend a hand whenever necessary.

I would like to thank Dr. Marina Bahktina for assistance with analytical ultracentrifugation experiments, and Dr. Tom Magliery, Nick Long and Sidharth Mohan for providing a thermocycler and assistance with site-directed mutagenesis.

I would like to thank my former professors at Ohio State for their support and direction in shaping my future.

And last but certainly not least, thank you to my friends and my family whose consistent love and support have made my time at Ohio State incredible and unforgettable.

Vita

May 2013 .....Cuyahoga Valley Christian Academy

May 2017 .....B.S. Biochemistry, The Ohio State University

Publications

1. Wachnowsky C.*, Wesley N.A.*, Fidai I., Cowan J.A. (2017) Understanding the Molecular Basis of Multiple Mitochondrial Dysfunctions Syndrome 1 (MMDS1)-Impact of a Disease-Causing Gly208Cys Substitution on Structure and Activity of NFU1 in the Fe/S Cluster Biosynthetic Pathway. J Mol Biol. doi: 10.1016/j.jmb.2017.01.021
2. Wesley N.A.*, Wachnowsky C.*, Fidai I., Cowan J.A. (2017) Analysis of NFU-1 Metallocofactor Binding Site Mutations: Impacts on Iron-Sulfur Cluster Coordination and Protein Structure and Function. (submitted).
3. Wesley N.A., Wachnowsky C., Fidai I., Cowan J.A. (2017) Understanding the Molecular Basis for Multiple Mitochondrial Dysfunctions Syndrome 1 (MMDS1): Impact of a Disease-Causing G189R Substitution on NFU1. (in preparation).

Fields of Study

Major Field: Biochemistry

Table of Contents

List of Tables

List of Figures

List of Equations

Chapter 1 : Introduction

Although categorized as inorganic ions, life would not be possible without the diverse range of alkali, alkaline and transition metals, along with other main group atoms that give rise to the field of bioinorganic chemistry. It is estimated that twenty-one elements, including fourteen metals, are essential for human life [1], and that forty percent of enzymes rely on a metal ion for catalysis [2] (Fig. 1.1). The alkali and alkaline ions Na^+, K^+, Mg^{2+}, and Ca^{2+} are the most abundant metal ions in biological systems, and have diverse roles in regulation of energy metabolism and cellular signaling, catalysis, structural stabilization of several classes of macromolecules, and composition of skeletal mass [3]. Transition metals (e.g. Fe^{2+}, Co^{2+}, and Ni^{2+}) possess generally less defined, yet richly diverse roles, as nature has employed these metals to perform a wide variety of redox and non-redox reactions. On account of the diverse coordination chemistry of transition metals demonstrated in their varied geometry, redox states, and kinetic and thermodynamic stabilities, metalloproteins with these cofactors are able to catalyze non-redox reactions, store and transfer cellular substrates such as oxygen, and regulate activity of other biological macromolecules [3].

Unsurprisingly, due to the complexity of the metallome and the large number of macromolecules dependent on metal ions for proper structure and function, misregulation of cellular metal ion concentrations often results in disease. Efficient metal uptake is essential, not only because the proper cellular function is strongly dependent on the

intracellular availability of metal ions, but because the extracellular availability of certain metal ions, such as iron, copper and zinc, can promote bacterial growth and virulence, and enhance microbial infection [4,5]. For example, iron availability is relevant in certain chronic disease states, such as acquired immunodeficiency disease (AIDS), in which iron is rapidly sequestered by macrophages in order to defend against infection; although the overall iron levels of the patient remain unchanged, the Fe is no longer available to tissues, causing anemia of chronic disease [5]. In addition to pathogenic disease states, accumulation of metal ions contributes to the onset and severity of various neurodegenerative disorders such as Alzheimer's and Parkinson's diseases by inducing oxidative stress and protein misfolding, disrupting mitochondrial function, and impairing the activity of metalloenzymes [6,7].

Because metal ions are necessary for life, though toxic in excess, highly-conserved and complex systems have evolved in order to acquire, transport, sequester, and incorporate these ions into cellular machinery. Of particular interest is iron (Fe), an essential nutrient utilized in a variety of biochemical and physiological processes, most notably for oxygen transport via hemoglobin, cellular respiration, and DNA synthesis [7,8]. Dietary Fe is imported from the intestines via DMT1 (divalent metal transporter 1), where it is reduced via reductase activity, exported by the basolateral iron exporter FPN, and incorporated into transferrin (Tf) for transport throughout the body [9]. Cells then obtain Fe through receptor-mediated endocytosis of Fe-bound Tf via transferrin receptors (TFR1 and TFR2) facilitating the release of the Fe, which is then incorporated into the labile Fe pool, stored in ferritin, or integrated into metalloproteins [9,10]. Regulation of intracellular Fe

concentration is achieved most importantly at the translational level via the IRE/IRP regulatory system, which is organized via the binding of multifunctional iron-regulatory proteins to regulatory mRNA motifs known as MREs [11].

Although several enzymes such as ribonucleotide reductase (RNR) utilize Fe centers to accomplish their chemistry, Fe ions are often incorporated with sulfide (S^{2-}) ions to form cofactors known as iron-sulfur (Fe-S) clusters. Fe-S clusters are highly-conserved inorganic prosthetic groups present across all kingdoms of life from bacteria to humans. Proteins that utilize an Fe-S cluster, known as Fe-S proteins, comprise the largest class of metalloproteins and are located ubiquitously throughout the mitochondria, cytosol and nucleus [12,13]. Consequently, Fe-S proteins play diverse roles in the cell. Fe-S clusters are central to the electron transfer reactions of respiratory chain complexes I-III and in photosystem I of photosynthetic organisms, while other Fe-S cluster proteins are involved in regulation of gene expression, such as aconitase or IRP1, which are activated in the absence of a [4Fe-4S] cluster cofactor [14]. Additionally, Fe-S proteins can serve as O_2 sensors, such as the bacterial FNR (fumarate and nitrate reduction) regulatory proteins, due to the sensitivity of Fe-S clusters to oxidation. Cellular roles of Fe-S clusters have expanded even further, since proteins involved in DNA replication and repair, including eukaryotic DNA polymerases and DNA helicases, have recently been shown to be Fe-S proteins [14,15]. Despite the ubiquity of Fe-S proteins, and the essential processes they catalyze, the exact function or functions of the Fe-S cluster in many of these processes, and how the Fe-S cluster is incorporated into target proteins remain unclear.

Fe-S clusters can adopt several geometries, the most abundant being the rhomboid [2Fe-2S] and the cubane [4Fe-4S] clusters (Fig. 1.2) [16], and these clusters are typically coordinated via cysteine residues [17], although non-cysteinyl ligands such as histidine [18], arginine [19], serine [20], or water [21] have been observed [14,15]. The chemical reactivity of iron and sulfur, along with the variation in geometry, oxidation state, and local protein environment enables Fe-S proteins to participate in the diverse functions described above and a wide variety of additional biological processes [22]. However, because of their oxygen sensitivity, formation and insertion of Fe-S clusters requires complex machineries, which are conserved across eukaryotic and some prokaryotic organisms, with the most common one being the ISC (iron-sulfur cluster) system (Fig 1.3), and defects in this system have been linked to a wide variety of human diseases [14,15,23].

In humans, iron-sulfur cluster biosynthesis occurs in the mitochondria via the ISC assembly pathway [24]. The first step in this pathway for reconstitution of downstream Fe-S proteins is the *de novo* formation of a transient [2Fe-2S] cluster on the scaffold protein IscU [15]. Central to this process is the cysteine desulfurase complex NFS1-ISD11, which catalyzes the conversion of cysteine to alanine for sulfur delivery to IscU, likely via a persulfide intermediate on IscU [15]. The sulfur is then reduced from elemental (S^0) to sulfide (S^{2-}) in a process involving NAD(P)H, ferredoxin reductase (FDXR), and ferredoxin 2 (Fdx2) [15]. Fe is transported into the mitochondria using the proton motive force via the mitoferrin 1/2 importers. Once imported, frataxin (FXN) or a glutaredoxin-glutathione complex are two proposed iron-donors for Fe delivery to IscU [11,14,15].

Once the [2Fe-2S] cluster is built on IscU, a chaperone system facilitates the release of the cluster from the scaffold to a cluster delivery protein glutaredoxin 5 (Glrx5) [15]. Mammals and many other eukaryotes rely on the multi-functional heat shock protein 70 (HspA9) and co-chaperone Hsc20 [14]. Glrx5 binds to this complex of the chaperone, co-chaperone, and cluster-bound IscU, so that ATP hydrolysis at HSPA9 can drive transfer of cluster from IscU to monothiol Glrx5 for downstream cluster trafficking [15,25]. Current models suggest that Glrx5 is the sole cluster transport intermediary between Fe/S scaffold machinery and downstream targets; however, a variety of other Fe/S proteins can complement this function with relatively rapid rate constants in comparison to Glrx5 [26-28].

From Glrx5, the [2Fe-2S] cluster can be incorporated into [2Fe-2S] proteins, exported into the cytosol to the cytosolic Fe-S cluster assembly (CIA) system via the ABCB7 transporter, or matured into a [4Fe-4S] cluster [15,25]. Cluster export from the mitochondria through ABCB7 is thought occur via a glutathione-coordinated [2Fe-2S] cluster complex, $[Fe_2S_2](GS)_4$, which can also function as part of the labile iron pool for Fe/S cluster delivery and trafficking [26,29-31]. The process of [4Fe-4S] cluster maturation involves proteins IscA1/2 and Iba57, which are thought to form a complex that binds free iron and a [2Fe-2S] cluster; yet it remains unknown how the IscA proteins use the iron and [2Fe-2S] cluster in the formation of the [4Fe-4S] cluster [14,15] . After the proposed formation of a [4Fe-4S] cluster on IscA1/2, a number of additional Fe-S cluster delivery proteins have been implicated in maturation of clusters at their final targets due to the connection between mutations in these assembly and export genes and human disease.

NFU1 was first thought to serve as a cluster scaffold acting in parallel to IscU, until patient studies revealed that a defect in NFU1 expression or function resulted in improper cluster assembly of certain [4Fe-4S] proteins including respiratory complexes I and II, and lipoic acid sythetase (LIAS) [15]. Likewise, BOLA3 was identified as another late-acting ISC assembly factor when it was shown that a frameshift mutation in the gene resulted in a biochemical phenotype similar to that observed in NFU1-deficient individuals, though the molecular function of BOLA3 remains unknown [15]. A third ISC targeting factor IND1, a P-loop NTPase, specifically targets only respiratory chain complex I, with other [4Fe-4S] proteins such as LIAS being unaffected [15]. However, the current model of various Fe/S biosynthesis proteins is primarily based on disease phenotypes and yeast knockouts, so further biochemical refinement is necessary for a mechanistic understanding of the molecular basis for disease.

Given the inherent structural and functional complexity of the mitochondria, combined with the necessary biosynthetic processes such as ISC assembly that occur therein, mitochondrial defects can cause a wide variety of severe and generally untreatable disorders. Figure 1.3 highlights the proteins involved in ISC assembly that have also been implicated in human diseases, such as Glrx5 and ACBC7 in sideroblastic anemia and Fxn in Friedreich's ataxia (Fig. 1.3) [15]. Multiple mitochondrial dysfunctions syndrome (MMDS) is a class of untreatable and fatal diseases that describes the severe impairment of various metabolic pathways and energy production as a consequence of single nucleotide genetic mutations in NFU1, BOLA3, IscA2, and IBA57 [15,32-38]. Further investigation into the biogenesis of essential cellular Fe-S cluster cofactors and the roles of

these late-acting ISC assembly and trafficking proteins will contribute to a better understanding of how the pathway operates, how cluster is transported *in vivo*, and why mutation causes an abrupt and severe interruption in this pathway with the potential to direct research towards finding a disease treatment. Herein, I describe investigation into two disease-causing substitutions in NFU1, as well as an examination into the effects of several Fe-S cluster binding-site mutations on Fe-S cluster coordination and NFU1 structure and function.

1.1 Figures

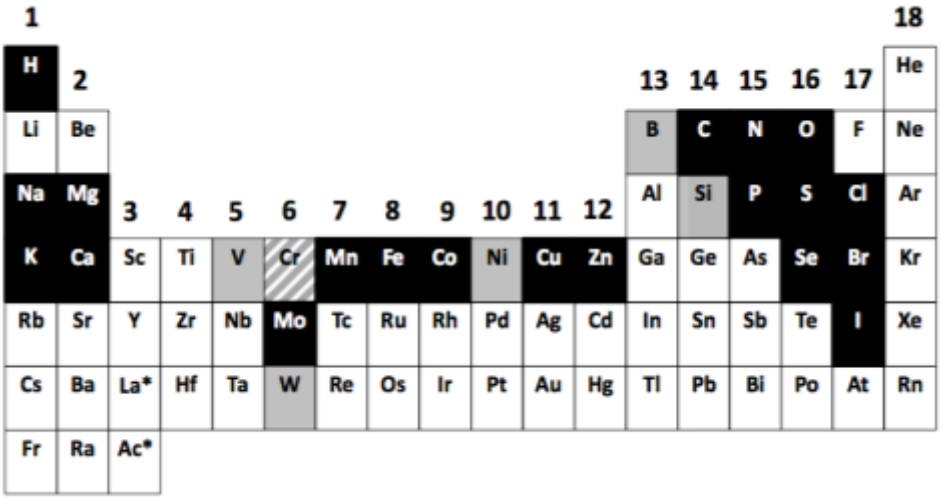

Figure 1-1 A partial representation of the periodic table of the elements indicating elements essential for life.

Elements essential for most forms of life are colored in black, with the exception of chromium (colored in a diagonal pattern) whose role in biology is still under debate. Essential elements for more restricted forms of life are shown in grey. Adapted from [1].

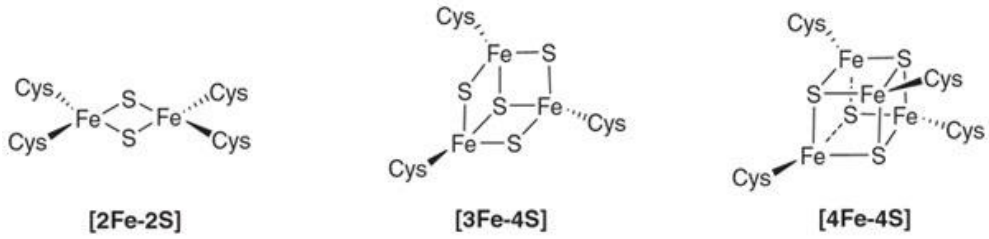

Figure 1-2 Structure of canonical [2Fe-2S], [3Fe-4S], and [4Fe-4S] clusters

shown with cysteine ligation, although alternative ligands such as serine, histidine and arginine have been observed. Adapted from [16].

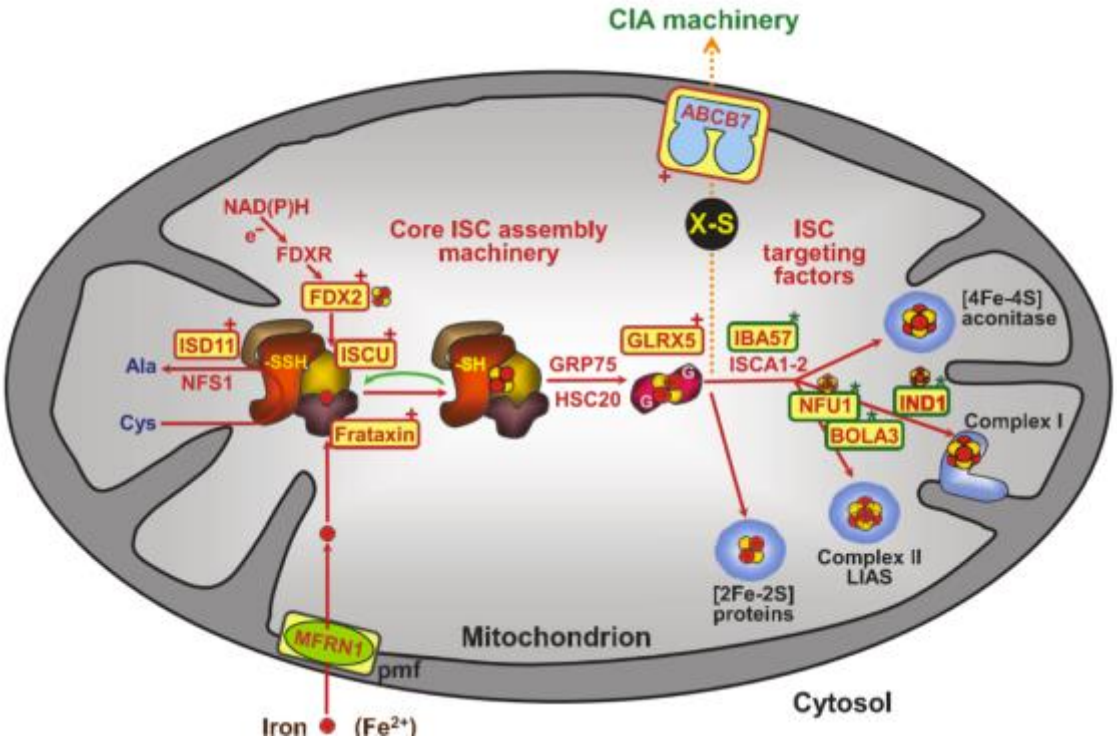

Figure 1-3 Current proposed schematic of mitochondrial ISC assembly

adapted from [15]. The various stages of cluster development are highlighted from import of ferrous ions and desulfurase activity to build a [2Fe-2S] cluster on the IscU scaffold. From IscU, the [2Fe-2S] cluster is transferred to Glrx5 via the HspA9/Hsc20 chaperone system. At this point in the ISC assembly pathway, the [2Fe-2S] cluster is exported to CIA machinery via ABCB7 as $[Fe_2S_2](GS)_4$, incorporated into various [2Fe-2S] proteins, or matured into a [4Fe-4S] cluster where it is incorporated into various [4Fe-4S] proteins by late acting ISC assembly factors. Protein names in yellow boxes highlight ISC proteins

whose genes are mutated in human Fe/S diseases. This model is primarily based on disease phenotypes and yeast knockouts, so further biochemical refinement is necessary for a mechanistic understanding of Fe/S biosynthesis. For more information see [13-15,39].

Chapter 2 : Understanding the Molecular Basis for Multiple Mitochondrial Dysfunctions Syndrome 1 (MMDS1) - Impact of a Disease-Causing Gly208Cys Substitution on Structure and Activity of NFU1 in the Fe/S Cluster Biosynthetic Pathway

2.1 Introduction

Mitochondria are complex eukaryotic organelles that serve as the site of aerobic cellular metabolism and energy production via oxidative phosphorylation. Furthermore, many important and diverse pathways for the production of essential biological cofactors are localized to the mitochondria [40-42]. Given the inherent structural and functional complexity of the mitochondria, combined with the necessary biosynthetic processes that occur there, mitochondrial defects can cause a wide variety of severe and generally untreatable disorders [40,43]. Multiple mitochondrial dysfunctions syndrome (MMDS) constitutes a class of typically fatal diseases that result from the severe impairment of various metabolic pathways and energy production as a consequence of single nucleotide genetic mutations [32,44]. Symptoms of MMDS include hypotonia, respiratory insufficiency, hyperglycinemia, encephalopathy, neurological regression, and failure to thrive, indicative of decreased functional actions of mitochondrial respiratory complexes [45-47]. Additional symptoms of MMDS are related to a deficiency of mitochondrial respiratory complexes and impaired function of lipoic acid dependent enzymes, such as pyruvate dehydrogenase (PDH) and protein H of the Glycine Cleavage System (GCS) [38,43,44]. Due to the severity and extent of symptoms described above, MMDS is typically fatal during perinatal stages [44]; however, some patients have lived until the age of two, at which point the symptoms culminated in death [32,38,45,47].

Interestingly, all four types of MMDS so far identified are associated with genes that code for metalloproteins, specifically those involved in the biosynthesis of iron-sulfur clusters: IBA57, IscA2, BOLA3, or NFU1 [32-37,44]. Further inspection of the defects caused by these iron-sulfur cluster proteins has revealed a specific impairment of downstream [4Fe-4S]-cluster-containing proteins; by contrast, [2Fe-2S]-cluster-containing proteins and cytosolic iron-sulfur cluster proteins appear unaffected [32,33,43]. All four of the identified proteins have been implicated in iron-sulfur cluster biosynthetic pathways as mediators of cluster transfer and delivery. Iron-sulfur clusters are highly conserved inorganic prosthetic groups that are present across all kingdoms of life and play diverse roles in the cell, including electron transfer, regulation of gene expression, and disulfide reduction [12,48]. Herein, we have focused on one of the aforementioned Fe/S proteins, NFU1. Human NFU1 consists of two domains, an N- and a C-terminal domain [49-52], where the latter contains a highly conserved CXXC motif [52] that identifies this domain as the Nfu domain and suggests a role in iron-sulfur cluster binding, assembly, and transport, based on comparison to homologous proteins and the high level of sequence conservation [53-57]. The thermodynamic stability of NFU1 has been studied in depth to reveal that the isolated C-terminal domain of human NFU1 exhibits characteristics of a molten globular state [49,51], while the isolated N-terminal domain demonstrates a highly ordered structure. However, when the two domains come together the overall protein maintains a relatively well-folded structure, suggesting a requirement for the unique N-terminal domain of the human protein to provide structural stabilization as well as serving a potential functional role [49,51] that may include a protein oligomerization surface or a binding site for chaperones, such as

Hsc20 [22,58]. Structure-function characteristics of human NFU1 remain unclear, because this protein has been implicated in a variety of cellular roles. NFU1 is also known as the HIRA-interacting protein, where HIRA is the histone cell cycle regulation homologue A [59]. Furthermore, it exhibits thioredoxin-like activity in the apo form [50,51], assembles and transfers a [2Fe-2S] cluster [28], assembles a [4Fe-4S] cluster [52,60], and may transfer cluster to apo aconitase [58]. Homologs of human NFU1 have been implicated in similar roles, with [2Fe-2S] [54,55,57,61] and [4Fe-4S] [53,54,56,62] cluster transfer, suggesting that both functionalities are possible and potentially physiologically relevant. Most recently, NFU1 has been implicated in the disease phenotype of MMDS1 attributed to a c.622G>T missense mutation located in the gene encoding the protein NFU1 [32,38]. This introduces a p.Gly208Cys missense mutation in the protein close to the iron-sulfur (Fe/S) cluster binding motif (Fig. 1) that alters the region around the cluster binding motif from GXCXXC to CXCXXC.

In connection with the MMDS1 disease state, human NFU1 has been proposed to be involved in the maturation of the iron-sulfur clusters on the [4Fe-4S] target proteins lipoate synthase (LIAS) and succinate dehydrogenase (SDH) [32,38,60]. In patients with MMDS1, laboratory tests have demonstrated that the level of human NFU1 protein is not diminished [32,38,63], but the activity levels of LIAS and SDH are significantly impaired, while other [4Fe-4S] targets, such as aconitase, are relatively unaffected [32,38,63]. Despite the identification of the global cellular effect of the NFU1 mutation, there remains a lack of understanding of the influence of the mutation at the molecular level. For this reason, we

have undertaken a biochemical approach to determine the impact of this mutation on the structure-function relationship of human NFU1.

2.2 Materials and Methods

2.2.1 Materials

PD10 desalting columns were purchased from GE Healthcare. Ferric chloride, sodium sulfide, DTT (Dithiothreitol), TCEP (Tris (2-carboxy-ethyl) phosphine) and L-cysteine were purchased from Fisher.

2.2.2 Mutagenesis

Stratagene QuikChange Mutagenesis was employed to introduce the p.Gly208Cys point mutation in full length human NFU1. PCR reactions contained 50 ng of native NFU1 DNA in the pET28b+plasmid, 2 units of Phusion DNA polymerase (New England Biolabs), 10x Phusion buffer (New England Biolabs), 125 ng of each primer (Integrated DNA Technologies), 0.2 mM dNTPs, and 3% DMSO. The forward primer sequence was 5'-TACAGCTGAAACTCCAG**T**GTTCTTGTACCAGCTGC-3' and the reverse primer sequence was 5'-GCAGCTGGTACAAGAA**A**CACTGGAGTTTCAGCTGTA-3' with the substituted nucleotide in bold. The thermocycle was identical to that described in the QuikChange manual: the sample was melted by heating to 95 ˚C for 1 min, followed by 16 cycles of 95 ˚C for 30 sec, 55 ˚C for 1 min and 72 ˚C for 6.5 min (Stratagene). Following amplification, samples were incubated with 7.5 units of *Dpn*I at 37 ˚C for 4 hours. Subsequently, $CaCl_2$-competent BL21 (DE3) cells were transformed via heat shock with

the mutant constructs. Mutagenesis results were confirmed by nucleotide sequencing from GENEWIZ.

2.2.3 Protein Expression and Purification

Full length human G208C NFU1 in a pET28(b+) vector in *E. coli* strain BL21(DE3) host cells was grown overnight at 37 °C in 10 mL of Luria–Bertani (LB) broth media containing kanamycin (50 μM) [50]. The overnight cultures were diluted 1:1000 in LB media containing 50 μM kanamycin until the OD_{600} reached 0.6. At this point, protein expression was induced with 0.5 mM of isopropyl β-D-1-thiogalactopyranoside (IPTG), and cultures were incubated overnight at 37 °C. Cell pellets were collected by centrifugation at 4,330*g* for 15 min at 4 °C, and resuspended in 30 mL of 50 mM HEPES, 100 mM NaCl, and pH 7.5. Resuspended pellets were incubated with 30 mg lysozyme and 0.6 mg DNase I for 30 min at 4 °C, and then lysed by use of a dismembranator. Cell lysate was centrifuged at 28,982*g* for 50 min at 4 °C, and the supernatant was applied to a TALON column. Protein was eluted with a buffer containing 50 mM HEPES, 100 mM NaCl, 150 mM imidazole, pH 7.5 and concentrated by Amicon ultrafiltration over a 10 kDa membrane.

Purification of *Hs* IscU and *Thermatoga maritima* (*Tm*) Nifs was performed as previously reported [64-66]. The expression vector for human ferredoxin-1 (*Hs* Fdx1) was kindly provided by J. Markley and protein was expressed and purified according to literature procedures [67]. Purification for human ferredoxin-2 (*Hs* Fdx2) was performed as previously reported [68]. Briefly, *Hs* Fdx1 was purified by use of DE-52 anion exchange column chromatography followed by FPLC purification with a size exclusion Superose-12

column (HR 16/50, Pharmacia) run at 0.2 mL/min with 50 mM HEPES, 100 mM NaCl, pH 7.5 at 4^0 C. All colored fractions were collected and combined. Purification for human ferredoxin-2 (*Hs* Fdx2) was performed as previously reported [68], by use of a TALON column. Protein was eluted with a buffer containing 50 mM HEPES, 100 mM NaCl, 150 mM imidazole, pH 7.5 and concentrated by amicon ultrafiltration over a 10 kDa membrane. The ferredoxins purified as holo proteins and were then subsequently converted to apo forms by treatment with 100 mM EDTA, 5mM DTT and 8M urea in a buffered solution, pH 7.5. A construct of human Grx2 (comprising residues 56-161), with a tobacco etch virus cleavable N-terminal His_6 tag in expression vector pNic-Bsa4, was kindly provided by Drs. Kavanagh, Muller-Knapp and Oppermann and protein was expressed and purified as previously reported [69]. *Schizosaccharomyces pombe* Isa1 protein was expressed and purified as previously reported [70]. Yeast Grx3 (Δ1–35) in pET28b(+) *E. coli* BL21 (DE3) was purified as noted [26]. Human HSPA9 with a N-terminal 6X-His tag was purified as previously described [71], as was human Hsc20 [72].

In all cases, protein purity was assayed by use of a 12 % SDS-PAGE gel that was visualized with Coomassie Blue staining. Imidazole was removed by dialysis at 4 °C against a buffer containing 50 mM HEPES, 100 mM NaCl, pH 7.5, and protein concentration was determined by use of the Bradford assay and confirmed by ε_{280}.

2.2.4 Differential Scanning Calorimetry (DSC)

DSC samples (0.1 mM – 0.3 mM) were dialyzed against 50 mM HEPES, 100 mM NaCl, pH 7.5 at 4 ˚C with Spectra/Por dialysis membrane (MWCO 10 000; Spectrum

Laboratories, Inc.). The resulting dialysis buffers were used as reference cell buffers for precision and repeatability. Reference buffers and protein samples were thoroughly degassed using a MicroCal Thermovac2 (Malvern Instruments, Inc.) prior to analysis on a MicroCal VP-DSC (Malvern Instruments, Inc.). The data were obtained using a differential mode at a rate of 1.0 ˚C per minute from 10 ˚C to 100 ˚C and analyzed using Origin software (Origin Labs) and fit to a non-two state model [49].

2.2.5 Variable Temperature Circular Dichroism characterization

Circular dichroism (CD) samples (10 μM) were dialyzed in phosphate buffer (40 mM phosphate, pH 7.4) with Spectra/Por dialysis membrane (MWCO 10 000; Spectrum Laboratories, Inc.). The resulting dialysis buffers were used as reference cell solvents for precision and repeatability. Prior to analyses, all sample and reference solutions were rigorously degassed with a Microcal Thermovac2 device (Malvern Instruments, Inc.). All CD data acquisitions were obtained on a JASCO J-815 CD spectrometer (JASCO) equipped with quartz cells with a 0.1 cm path length. Variable temperature studies were performed at a rate of 0.4 ° C min^{-1} from 20 to 95 °C. All data were processed with Origin 7 (Origin Laboratories). VTCD data were fit to equation 1 [49], where R is the ideal gas constant in calories per mole, T_m is the melting temperature in Kelvin, ΔH_V is the van't Hoff enthalpy, and C_p is the heat capacity. F and U represent the mean residue ellipticities (θ_{mr}) of the folded and unfolded protein, respectively.

Equation 1 One-State VTCD Unfolding Model

$$\theta =$$

$$\left\{\exp\left[\left(\frac{1}{-RT}\right)\left(\Delta H_V\left(1-\frac{T}{T_m}\right)-C_p\left((T_m-T)+T\ \ln\frac{T}{T_m}\right)\right)\right]/\left\{1+\right.\right.$$

$$\left.\left.\exp\left[\left(\frac{1}{-RT}\right)\left(\Delta H_V\left(1-\frac{T}{T_m}\right)-\ C_p\left((T_m-T)+T\ln\frac{T}{T_m}\right)\right)\right]\right\}\right\}(F-U)+U$$

2.2.6 Secondary Structure Prediction from Circular Dichroism

Protein samples at 10 μM in 40 mM phosphate, pH 7.4 were placed in a 1 mm quartz cuvette and the signal monitored from 300 – 165 nm. The buffer baseline signal was subtracted from the data sets before conversion to Δε. The resulting CD spectra were processed using the analysis program CDSSTR [73] using reference set 7 [74] found on the online server Dichroweb [75,76].

2.2.7 Reconstitution of apo proteins

NifS-mediated *in vitro* reconstitution of G208C NFU1 was completed as previously described [28,77] . Briefly, ferric chloride and L-cysteine were added to an anaerobic mixture of approximately 200 μM purified NFU1, 2 μM *T. maritima* (*Tm*) NifS, and 5 mM DTT to final concentrations of 1.6 mM $FeCl_3$ and 3.2 mM L-cysteine. Alternatively, sodium sulfide and ferric chloride were added to an anaerobic mixture of approximately 200 μM purified NFU1, 2.1 mM urea, and 5 mM DTT to final concentrations of 1 mM $FeCl_3$ and 1 mM Na_2S [26]. The final solution was incubated for 1 h with stirring at room temperature, before separation of excess iron and sulfide through a PD-10 column that was

equilibrated with an argon-purged solution of 50 mM HEPES, 100 mM NaCl, pH 7.5. Reconstituted protein was eluted with 3.5 mL of the equilibration buffer. The protein concentration was determined via the Bradford assay and the reconstitution of protein was confirmed by absorbance at 330 nm and 420 nm on a Cary WinUV spectrophotometer.

For IscU and Isa1 [78], 200 μM apo protein was incubated with 50 mM DTT, argon purged for 30 min, and then made up to 1 mM in Fe^{2+} and 1 mM in S^{2-}. After incubation for 1 h, the reaction mixture was concentrated and passed through a PD10 desalting column to remove excess of Fe^{2+} and S^{2-}, and the UV-vis spectrum was obtained for both apo and holo IscU and Isa1.

2.2.8 Reconstitution Analysis by Circular Dichroism

CD scans of apo and holo proteins were recorded on a JASCO J-815 CD spectrometer in a quartz 1 cm anaerobic cuvette. CD scans from 300 nm to 600 nm were collected to analyze signature cluster-bound protein peaks at a scan rate of 200 nm/min at 25 °C. Data were processed using JASCO Spectramanager II Analysis software and were represented in Origin 7.0.

2.2.9 Oligomerization State Determination by analytical ultracentrifugation (AUC)

Apo G208C NFU1 at 50 μM protein (OD_{280} = 1.0), in the presence or absence of 1 mM TCEP, was loaded into the ultracentrifugation chambers and sealed, using 50 mM HEPES, 100 mM NaCl, pH 7.5 as a reference, with the addition of 1 mM TCEP where needed. Reconstituted holo G208C NFU1 at 269 μM (OD_{420} = 1.5) was loaded in the same manner with the same reference buffer. Samples were centrifuged at 45,000 rpm for 6 hours to

reach complete sedimentation. The sedimentation profiles were fit using SEDFIT to the Lamm equation [79,80].

2.2.10 $[Fe_2S_2](GS)_4$ Synthesis

The cluster used was synthesized as previously reported [30]. Briefly, ferric chloride (20 mM) and sodium sulfide (20 mM) were added to 10 mL 40 mM glutathione solution, pH 8.6. A volume (40 mL) of ethanol was added to the mixture and mixed by vortexing. The precipitate was collected by centrifugation at 13,000 rpm for 10 min, washed twice with ethanol and dried under vacuum.

2.2.11 Iron Quantitation [78,81]

A solution of $[Fe_2S_2](GS)_4$ (0.05 mM, 200 µL) in H_2O or holo protein was acidified by concentrated HCl (60 µL) and heated to 100 ºC for 15 min. The resulting suspension was centrifuged at 14,000 rpm for 2 min and the supernatant (100 µL) was diluted with Tris-HCl (0.5 M, 1.3 mL, pH 8.5). Solutions of sodium ascorbate (0.1 mL, 5%) and bathophenanthroline-disulfonate (0.4 mL, 0.1%) were sequentially added to the neutralized reaction solution with mixing between each addition. The solution was incubated at 25 ºC for 1 h and iron was quantitated by measuring the absorbance at 535 nm on a UV-Vis spectrophotometer and calculated from a calibration curve made with 0.01-0.2 mM $FeCl_3$ standard solutions (Fig. S1).

2.2.12 Iron-sulfur Cluster Uptake Monitored by CD

The ability of NFU1 to take up an iron-sulfur cluster from the [2Fe-2S](GS)$_4$ complex was examined by circular dichroism (CD). CD scans were recorded on a JASCO J-815 CD spectrometer in a 1 cm anaerobic quartz cuvette from 600 – 300 nm at a scan rate of 200 nm/min at 25°C, with a 2 min interval between each accumulation. NFU1 (50 μM) in 50 mM HEPES, 100 mM NaCl pH 7.5, was thoroughly degassed in the presence of 5 mM DTT and transferred to the anaerobic cuvette. Solid [2Fe-2S](GS)$_4$ was resuspended in degassed 50 mM HEPES, 100 mM NaCl pH 7.5 and added to the argon-purged anaerobic cuvette via a gas-tight syringe to a final concentration of 400 μM to initiate the reaction. Data were processed using JASCO Spectramanager II Analysis software and analyzed in Origin 7.0. The deconvolution function from Spectramanager II analysis software was used for analysis of bands in the spectra that contained overlapping Lorentzian curves having the same full width at half maximum value that accurately distinguishes the peak positions for each band.

2.2.13 Kinetics of Fe-S cluster extraction from holo NFU1 by glutathione

Glutathione has been previously shown to extract the iron-sulfur cluster from various holo proteins to form the [2Fe-2S](GS)$_4$ complex by monitoring the change in the charge transfer bands at 330 nm and 420 nm by UV-Vis spectrophotometry [26,30] . As was done for native holo NFU1 [28], degassed, reconstituted holo G208C NFU1 in 50 mM HEPES, 100 mM NaCl, pH 7.5 was incubated with a 4- to 10-fold excess of GSH in an anaerobic cuvette and the absorbance at 420 nm on a Cary Win UV spectrophotometer was monitored every 2 min over the course of 1 h. The change in absorbance at 420 nm was plotted against

time and fit to an exponential decay to obtain the k_{obs}. A control reaction for holo G208C NFU1 in the absence of excess GSH was carried out under the same conditions to account for inherent cluster instability. Cluster extraction by GSH to form the $[2Fe\text{-}2S](GS)_4$ complex was confirmed using ESI mass spectrometry on a Bruker Micro-TOF (ESI) spectrometer and data was analyzed by use of DataAnalysis software (Bruker) [30,82].

2.2.14 Kinetic cluster transfer experiments

Kinetic cluster transfer experiments were designed based on the cluster transfer experiments by Johnson and coworkers [83,84], and refined by our own group [26,28]. Reactions were performed on a JASCO J-815 CD spectrophotometer in a 1 cm anaerobic quartz cuvette from 600 – 300 nm at a scan rate of 200 nm/min at 25°C, with a 2 min interval between each accumulation. Reactions that reached completion within the first 10 min were analyzed over a 10 nm wavelength scale based on the peak of interest with 10 second intervals between accumulations. Spectra were processed using JASCO Spectramanager II Analysis software and were represented in Origin 7.0.

Reactions in 50 mM HEPES, 100 mM NaCl, pH 7.5 were prepared by degassing a mixture of 40 μM apo protein in 5 mM DTT, and transferred to an anaerobic cuvette via a gas tight syringe. For reactions with the co-chaperone system, 22 μM HSPA9 and 22 μM Hsc20 were included. $MgCl_2$ (40 mM) and ATP (2 mM) were degassed separately and added immediately before addition of holo IscU [84-88]. Degassed holo protein at 40 μM was added to the cuvette to initiate the reaction. The concentration of [2Fe-2S] in the reaction for each holo protein was determined via standard iron quantitation methods.

Kinetics of cluster transfer was analyzed by converting the change in CD signal to the percentage of cluster transferred fit using DynaFit [89] to determine the second-order rate constants for the various reactions by best-fit simulation to second-order kinetics.

2.3 Results

Given the drastic cellular consequences of the G208C mutation on NFU1, we hypothesized that there could be two major contributors to protein impairment. Since cellular studies have shown that the protein is present at normal levels [32,38], the protein could be compromised in terms of its structural composition and recognition by partner proteins. Alternatively, it may be unable to perform functionally due to an inability to bind, receive or deliver an Fe/S cluster. By use of *in vitro* biochemical assays we set out to explore both possibilities.

2.3.1 Structural Alteration of G208C NFU1

2.3.1.1 G208C substitution does not significantly impact secondary structure

Much has been reported concerning the domain organization and protein stability of the recombinant native human NFU1 [49,51], which provided a firm benchmark for study of the effect of the G208C substitution on human NFU1 with regard to structural and stability characterization, relative to the native protein. Secondary structure and stability was examined via variable temperature circular dichroism (VTCD) and comparison of the melting profiles and thermodynamic characteristics of the native human NFU1 and the G208C mutant. Data were fit to a one-state model to reduce error in the melting event

parameters (Table 1) and yielded a satisfactory fit. Interestingly, the G208C NFU1 derivative shows a VTCD trace very similar to that of the native, with the mutant protein and the native exhibiting the same melting temperature within error, indicating that the two proteins are actually similar in their stabilities. Combining the VTCD data with an additional stability measurement, limited proteolysis (Fig. S2), we observe that the two proteins are both fairly equal in terms of stability, consistent with our other data. Both proteins exhibited reversible melting on VTCD (data not shown), indicating that the overall protein folds are relatively stable. Melting data were also fit to a two-state model (Fig. 2), due to the multidomain nature of the protein, which has been previously characterized [49]. However, the two-state model did not yield any interpretable improvements to the fit and was not considered further.

Circular dichroism was also used to examine the overall characteristics of protein secondary structure by determining the percentages of secondary structural elements: α-helix, β-sheet and random coil. The values are summarized in Table 2 and demonstrate an overall increase in random coil and loss of secondary structural elements; however, the modest change in secondary structural elements has not impacted protein stability based on the one-state VTCD results (Fig. 2; Table 1) and limited proteolysis (Fig. S2).

2.3.1.2 G208C substitution impacts tertiary structure by promoting dimerization

To clarify the results obtained via VTCD and extend the stability comparison to tertiary structural elements, Differential Scanning Calorimetry (DSC) was used to examine the thermodynamic properties of the NFU1 G208C mutant by determining the heat capacity

of the protein in comparison to the native. The DSC profile of native human NFU1 (Fig. 3A) matches the parameters determined in prior literature [49] in that the protein follows a two-state melting process with T_{m1} of 59.4 ± 0.20 °C and a second melting event at 72.6 ± 0.04 °C (Table 3). The lowest T_m value for native protein corresponds to the melting of the C-terminal domain and the higher melting temperature represents the melting of the well-folded N-terminal domain [49]. The DSC profile for the G208C derivative interestingly exhibited a three phase melting process (Fig. 3B): the first broad melting peak is indicative of the molten globular C-terminal domain with T_{m1} of 49 ± 6 ˚C, a second sharp peak not seen in the native melting profile with T_{m2} of 64 ± 2 ˚C and an additional shoulder from the structured N-terminal domain with T_{m3} of 74 ± 4 ˚C (Table 3). The similarity of melting temperatures and van't Hoff enthalpies (within error) for the transitions in the substituted protein, relative to the native NFU1 (Table 4), confirm the comparable stabilities of each.

Previous DSC analysis of human NFU1 ascribed the two peaks in the melting trace as arising from C-terminal domain unfolding at low temperature, due to its molten globular nature, and N-terminal domain unfolding at higher temperature [49,51]. For this reason, the presence of a third peak in the DSC trace for G208C NFU1 was quite surprising. An additional protein domain could not have been introduced by the point mutation, so we sought to understand the origin of the new peak by application of analytical ultracentrifugation (AUC) to examine oligomerization effects. AUC was completed for apo G208C NFU1 in the presence and absence of 1 mM TCEP to eliminate the potential for oligomerization due to disulfide bonds. In the absence of TCEP, a G208C NFU1

monomer was observed at 22.6 kDa (expected MW: 23.9 kDa) as 29% of the total observed species (Fig. 4, black). Dimer at 41.6 kDa accounted for 58%, and some higher order oligomer at 74.0 kDa, potentially corresponding to a tetrameric form, constituted 6% of the sample. However, in the presence of 1 mM TCEP (Fig. 4, red), monomer was still observed at 22.9 kDa, accounting for 30%. The percent of dimer at 41.9 kDa, was also practically unchanged at 60%. The largest change observed was for the higher order oligomeric species. A species at 83.5 kDa was observed as ~ 1.5% of the total species. The apo protein percentages contrast sharply with the AUC data collected for the native protein, which showed the monomer and dimer in approximately equal percentages [28], suggesting that the point mutation propagates the protein's tendency to oligomerize, but not via disulfide bonding and could explain the additional melting peak present in the DSC trace. However, the apparent modest decrease in thermodynamic stability and increased propensity towards dimer formation does not alter the protein's susceptibility to degradation in limited proteolysis (Fig. S2), reducing the likelihood that the point mutation initiates a major structural change of the protein. The mutant protein is not significantly less stable than the native form; however, the minor structural changes from secondary structure composition seem to promote a greater tendency to dimerize, and these perturbations may have large impacts on function and partner recognition.

2.3.2 Functional Impairment of G208C NFU1

2.3.2.1 G208C NFU1 can be reconstituted, but is primarily dimeric

Following the thermodynamic and structural comparisons of G208C NFU1 with the native protein, we next examined the functional changes resulting from the mutation in order to link the oligomeric changes to the downstream effects. Similar to the native protein, G208C NFU1 could be reconstituted *in vitro* by use of *Tm* NifS and L-cysteine, and yielded a UV spectrum with typical iron-sulfur cluster charge-transfer bands at 330 and 420 nm (Fig. 5A, blue trace). However, in contrast to the native protein, which cannot be reconstituted with inorganic sulfide, G208C NFU1 was found to be readily reconstituted with ferric chloride and sodium sulfide to yield a native-like UV spectrum and a slightly more prominent 420 nm signature (Fig. 5A, green trace). Additionally, both reconstitution methods resulted in similar UV and CD spectra relative to native NFU1, although with a slight increase in intensity at certain wavelengths (Fig. 5). Inasmuch as native human NFU1 has been shown to bind a [2Fe-2S] cluster under enzymatic reconstitution conditions [28], the similarity in UV and CD spectra suggests that the G208C mutant is capable of binding the same type of cluster. Based on iron quantitation, reconstitution via sodium sulfide resulted in the highest maximum yield, with 0.86 [2Fe-2S] cluster/dimer, while reconstitution with L-cysteine gave 0.76 [2Fe-2S] cluster/dimer. However, both of these yields are in line with what has been typically achieved for the native protein, which yielded 0.75 [2Fe-2S] cluster/dimer [28]. Therefore, the G208C mutant is capable of binding an iron-sulfur cluster and in a similar environment to the native form. Protein oligomerization around the cluster was confirmed via AUC. Holo G208C was monitored at 420 nm to measure the cluster-bound form of the protein. The majority (65.6%) of the holo protein exists as a dimer with a minor tetrameric species (Fig. S3B), in contrast to the native protein, which demonstrated slightly

more tetramer than dimer. For both the native and the mutant, no clear additional peaks were observed in the AUC trace [28,58]. The remaining percentages correspond to protein aggregation and crashing out. The G208C mutation alters the ability of NFU1 to oligomerize in both the apo and holo forms relative to native protein. These data are confirmed by the AUC of the holo protein at 280 nm (Fig. S3A).

2.3.2.2 G208C NFU1 cannot take up Fe/S clusters from relevant donor sources

Our previous analysis of native human NFU1 [28] has shown that the human protein was capable of receiving and transferring cluster from other Fe/S proteins, as well as from a physiologically relevant glutathione-bound iron-sulfur cluster complex [2Fe-2S](GS)$_4$. This complex can be delivered to a number of iron-sulfur cluster proteins [26,30] and is a viable substrate for the mitochondrial ABCB7 transporter [29,82], suggesting a possible role for the [2Fe-2S](GS)$_4$ complex as a component of the labile iron pool. Native human NFU1 can take up a [2Fe-2S] cluster from the complex with a second-order rate constant of 1930 $M^{-1}min^{-1}$ [28], as observed by circular dichroism (CD). However, G208C NFU1 is unable to take up a cluster from this complex, even with an 8-fold excess of the complex (data not shown).

Likewise, G208C NFU1 was unable to receive a Fe/S cluster from donor proteins. We have previously demonstrated that [2Fe-2S] cluster proteins are able to transfer an iron-sulfur cluster to native human NFU1 [27,90]. Therefore, we have examined the ability of the G208C mutant protein to be reconstituted in the same way using CD spectroscopy. Holo reconstituted human IscU was added to apo G208C; however, no change in CD signal was

observed that would represent the unique spectrum of holo G208C NFU1 (Fig. 5B), indicating that human IscU is incapable of transferring cluster into G208C NFU1 (data not shown). Because involvement by Hsc co-chaperones has been implicated in IscU-promoted cluster delivery to target proteins [22,25,44], we also examined the kinetics of transfer from holo human IscU to apo human NFU1 and G208C NFU1 in the presence of HSPA9, Hsc20, $MgCl_2$ and ATP. With the chaperones, IscU was unable to transfer cluster in to either the native or the mutant (Fig. S4), even though transfer from IscU to the native protein can proceed without the chaperone system [90]. Similarly, we monitored the ability of *S. pombe* Isa1 to transfer a cluster into G208C NFU1, since that transfer was also observed for native NFU1 [27]; however, the appearance of the G208C NFU1 signature peaks was not observed, even over the course of 3 h (data not shown). Minor peak shifts were seen, but the overall signal mainly resembled Isa1, indicating possible formation of a heterodimeric complex. Nevertheless, no clear transfer was demonstrated from Isa1 to G208C NFU1. All of the donor sources for cluster that we examined were unable to reconstitute G208C NFU1 with an Fe/S cluster.

2.3.2.3 Chemically Reconstituted G208C NFU1 can still transfer Fe/S clusters to target proteins, albeit with perturbed second-order rate constants

Our previous work with the native form of NFU1 has characterized aspects of NFU1 in Fe/S cluster delivery and trafficking. As such, the $[2Fe\text{-}2S](GS)_4$ complex could be formed by cluster extraction from the [2Fe-2S] cluster-bound native NFU1 under conditions of excess glutathione (GSH), with a second-order rate constant of 130 ± 22 $M^{-1}min^{-1}$ [28].

Excess GSH is also able to extract the [2Fe-2S] cluster from holo G208C NFU1, and the decrease in absorbance at 420 nm was monitored over the course of an hour (Fig. 6A, red trace). The decrease in absorbance was not due to cluster breakdown on G208C NFU1, since a control in the absence of excess GSH (Fig. 6A, black trace) demonstrated very little change in absorbance. The change in absorbance data was determined at four different GSH concentrations and k_{obs} was calculated from each concentration. The data were fit to a linear equation to determine the overall second-order rate constant for GSH extraction of $140 \pm 20\ M^{-1}min^{-1}$ (Fig. 6B), which is in the same range as the second-rate constant found for the native protein, indicating that dimerization has not influenced the ability to transfer a cluster out of G208C NFU1 to this target. Extraction of the cluster by GSH to form the $[2Fe\text{-}2S](GS)_4$ complex was confirmed by appearance of the cluster m/z peak of 1427.3 in ESI-MS, which corresponds to an adduct of the complex with one sodium [30,82] (Fig. S5).

G208C NFU1 is also capable of transferring the [2Fe-2S] cluster to other apo protein targets. As found for native human NFU1, cluster transfer to ferredoxins 1 and 2 (Fdx1 and Fdx2) [28] and glutaredoxins 2 and 3 (Grx2 and Grx3) was observed [27]. Cluster transfer was monitored by use of CD spectroscopy because unique spectra are generated for each iron-sulfur cluster bound protein [91]. Although some these previous transfer reactions were not carried out in the preferred pseudo first-order kinetics range, as a result of limitations from detection sensitivity and protein solubility, we have developed a method to provide estimates for second-order rate constants in cluster transfer reactions using DynaFit software [89], similar to previously published literature [54,83,88]. We

have shown in test cases that the apparent second-order rate constant obtained in this manner shows close agreement with the rate constant determined from more traditional concentration dependence measurements [26,28]. Herein, we have used those same methods to determine apparent second-order rate constants for mutant NFU1 for comparison with the native transfer rates. Reconstituted holo G208C NFU1 was added to apo human Fdx1 and the increase in CD signal at 445 nm was monitored (Fig. 7A and 7B) and used to yield a second-order rate constant for the transfer of [2Fe-2S] cluster of $2600 \pm 300\ M^{-1}min^{-1}$. Similarly, cluster transfer from G208C NFU1 to human Fdx2 yielded an overall second-order rate constant of $1200 \pm 200\ M^{-1}min^{-1}$ (Fig. 7C and 7D). Cluster transfer kinetics for transfer to glutaredoxins was executed in the same manner as for the ferredoxins. Following addition of holo reconstituted G208C NFU1 to either apo Grx3 or apo Grx2, the change in CD signal was monitored. Since the glutaredoxins utilize glutathione as endogenous ligands, an excess of GSH was included in the reactions to be able to reconstitute a functional glutaredoxin protein. The $[2Fe\text{-}2S](GS)_4$ complex is CD silent [30]. Given that no intermediate spectra were observed during the transfer from either native NFU1 or G208C NFU1 to glutaredoxins, the data is consistent with direct cluster transfer to the putative partner protein with no intermediate species formed by extraction of the cluster to form a transitory complex. In both cases, rapid transfer was observed such that by the end of 2 min the spectra already resembled those of the target holo proteins. For that reason, cluster transfer kinetics were monitored over 10 sec intervals, instead of 2 min intervals. Transfer to apo human Grx2 was also complete within the first 15 min (Fig. 8A and 8B), and based on the initial [2Fe-2S] cluster concentration of holo G208C NFU1,

resulted in a large second-order rate constant of 22400 ± 5000 $M^{-1}min^{-1}$. Cluster transfer from holo G208C NFU1 to apo *S. cerevisiae* Grx3 (Fig. 8C and 8D) was complete within the first 15 min and yielded a second-order rate constant of 14500 ± 3500 $M^{-1}min^{-1}$.

G208C NFU1 was capable of delivering a [2Fe-2S] cluster to the same target proteins that have been examined for kinetic transfer from the native form. However, the rates of these transfer reactions are significantly different, especially when examining interactions with the glutaredoxin proteins.

2.4 Discussion

Previously we have examined and characterized the iron-sulfur cluster protein NFU1 in terms of its stability and iron-sulfur cluster binding and transfer capabilities [28,50,51] . Based on our findings from studies of the native human protein, we decided to investigate an important disease-causing mutation of NFU1. A genetic point mutation converts a glycine at position 208 of the amino acid sequence to a cysteine (G208C), resulting in the disease condition known as Multiple Mitochondrial Dysfunctional Syndrome 1 (MMDS1), where symptoms primarily result in death during the infant stage of life [32,38]. Accordingly, to better determine the cause of the human disease phenotype and understand its molecular basis, we have characterized the stability and iron-sulfur cluster binding and transfer capabilities of the substituted G208C NFU1 protein. Given our two potential hypotheses for the disease phenotype (altered protein structure and recognition, or perturbation to Fe/S cluster uptake or transfer), we began with an examination of protein structure and stability, specifically in terms of secondary and tertiary structure

characteristics. Initial analysis via VTCD demonstrated no significant change in secondary structure thermodynamics, suggesting that the native and mutant forms of NFU1 are relatively similar. However, modest changes were observed in secondary structure composition and DSC traces. G208C NFU1 exhibited an overall increase in random coil (Table 2), which does not demonstrate significant effects on stability. The major structural or stability impacts are reflected in the DSC trace, in conjunction with AUC, to show an increased tendency of the protein to oligomerize, specifically to the dimeric form.

The DSC trace of the mutant protein showed a new melting peak (Fig. 3A and 3B), relative to the recombinant native protein, which is consistent with a modest change in secondary structure that could perturb the dimerization interface. Examination by AUC showed that the dimer was present in the majority (Fig. 4), which contrasts with the more equal distribution of monomer and dimer for the native protein [28], suggesting the monomer-dimer equilibrium for apo to be skewed in the direction of dimer. The increased concentration of dimer could affect the DSC trace by altering the melting process. For the native protein, the unfolding of the dimer is concurrent with the melting of the molten globular C-terminal domain to yield a partially unfolded monomer [92,93], as observed by the first transition in Figure 3A. Following this concerted melting process, the remainder of the protein melts to yield completely unfolded monomers, represented by the three-state mechanism shown in equation 2. However, G208C NFU1 exists primarily as a dimer, which shifts the unfolding process to exhibit a new and distinct melting peak in the DSC trace. The mechanism (equation 3) would now be reflective of a four-state melting process, in which the destabilized, molten globular C-terminal domain of the mutant protein begins

to melt (the first transition of three), reducing dimer stability and causing the dimer to unfold in the second melting event (Fig. 2B) [92,93]. Lastly, the N-terminal domain melts to complete the unfolding process, just as it had for the native.

Equation 2 Two-Phase Unfolding Process

$$(NC)_2 \overset{T_{m1}}{\longleftrightarrow} 2(NC_U) \overset{T_{m3}}{\longleftrightarrow} 2(N_U C_U)$$

Equation 3 Three-Phase Unfolding Process

$$(NC)_2 \overset{T_{m1}}{\longleftrightarrow} (NC_U)_2 \overset{T_{m2}}{\longleftrightarrow} 2(NC_U) \overset{T_{m3}}{\longleftrightarrow} 2(N_U C_U)$$

(U – represents unfolded protein)

Since the DSC and secondary structure data suggested a change in structure for the mutant protein, we submitted the protein sequence to Phyre2 [94] for structure prediction by homology modeling, which utilized the NMR structure of the C-terminal domain of mouse NFU1 (PDB ID: 1VEH) and the NMR structure of the C-terminal domain of human NFU1 (PDB ID: 2M5O) to generate a model for G208C NFU1. The resulting model predicts that the placement of the cysteines will change with the mutation (Fig. 9). The CXXC domain exists as a flexible loop, while the G208C NFU1 protein has an altered loop, which appears to lock the position of the C at residue 213 as the beginning of an α-helix (Fig. 9). The replacement of the flexible glycine [95], with a more rigid cysteine has altered the cluster binding loop such that the overall structure of the protein has changed, and could promote an interaction interface to support an increase in the presence of dimers, although how this change at the C-terminal domain might impact the overall protein is currently unknown.

Inasmuch as the investigation of the biochemical consequences of the G208C substitution demonstrate a structural change that promotes dimerization, but no major change in protein stability, we next examined how this mutation and its structural perturbations would impact function. Our studies of native NFU1 demonstrated a bound [2Fe-2S] cluster that can be transferred in and out of the protein by interactions with either other iron-sulfur cluster proteins or a physiologically relevant [2Fe-2S](GS)$_4$ complex [28]. Similarly, the G208C NFU1 derivative was capable of undergoing reconstitution *in vitro* through the use of either sodium sulfide, or L-cysteine with *Tm* NifS as a sulfide source (Fig. 4), while native NFU1 can only be reconstituted using L-cysteine with *Tm* NifS; however, reconstitution yields in all cases were similar. Following reconstitution, both UV and CD spectra look analogous, indicating the presence of a similarly bound [2Fe-2S] cluster. The cluster on holo G208C NFU1 was stable over the course of an hour and remained bound to the protein even in the presence of 5 mM DTT (Fig. S6).

Although G208C NFU1 was capable of being reconstituted using *in vitro* methods, the protein was unable to accept cluster from other physiologically relevant sources, and most likely reflects deficiencies in reconstitution expected inside the cell. Also, in contrast to native protein, the G208C variant is unable to take up the [2Fe-2S](GS)$_4$ complex [28]. Likewise, the mutant protein is unable to receive a [2Fe-2S] cluster from typical iron-sulfur scaffold proteins such as Isa1 and IscU (Table 5), which have been shown to deliver a cluster into native NFU1 [27,90]. Current models for Fe/S cluster biogenesis indicate that transfer from IscU is promoted with assistance from heat shock chaperone proteins [22,25,44,96]. We have found that transfer from holo IscU to apo native NFU1 or G208C

NFU1 does not occur in the presence of the chaperones (Fig. S4), which is similar to transfer from holo human IscU to apo ferredoxin 2 (Fig. S7) or ferredoxin 1 [87], where transfer is unaffected in the case of the former, and inhibited for the latter, in the presence of chaperones. Inhibition most likely arises from stabilization of the cluster on holo IscU [87] that slows its ability to transfer the cluster. In the case of transfer to human NFU1 in the presence of chaperones, we postulate that no transfer is observed, at least on the time scale considered, due to possible steric interaction of NFU1 with the chaperone proteins [58,97] in conjunction with the stabilization of cluster on IscU.

Heat shock chaperones are highly conserved across bacteria, yeast and humans, and serve crucial roles in Fe-S cluster biogenesis, mediating cluster delivery to key targets such as glutaredoxins and succinate dehydrogenase [22,98]. As such, they have been studied in all of those organisms. Moreover, because the process of Fe-S cluster biosynthesis is highly conserved, the co-chaperone system is believed to play similar roles across various organisms, however, minor kinetic differences have been observed when making comparisons between organisms. For example, heat shock chaperones are observed to greatly increase the rate of transfer from IscU in *Azotobacter vinelandii* (22-fold to Fdx and 670-fold to Grx5) [84,88] and on a more minor scale (5-10 fold) in *E. coli* [85,86], but have actually been shown to slow a transfer reaction in humans [87]. The observed differences in rate enhancement across these organisms suggest that the chaperone systems could participate in distinct roles in support of Fe/S cluster biogenesis and/or trafficking, depending on the particular organism. In this case the human chaperone system appears to

block IscU-mediated cluster delivery to NFU1 (Table 5), but serves no clear role in rate enhancement in subsequent delivery to Fdx's (Table S1).

Since the mutant form of NFU1 cannot receive cluster from traditional sources, in contrast to the native protein (Table 5), this readily explains the detrimental phenotype and symptoms observed for those with the point mutation. Derivative G208C NFU1 not receive a cluster *in vivo* and would therefore be unable to transfer a cluster to downstream partners. The predicted change in structure (Fig. 9), suggesting that the CXXC loop in G208C NFU1 has been locked into a specific orientation, may align the cysteines in such a way that they no longer exhibit the conformational flexibility required for cluster uptake and reconstitution in the cell. Alternatively, the increased proportion of dimeric protein could sterically block the CXXC motif from cluster uptake. In either case, the protein cannot accept a pre-formed [2Fe-2S] cluster, since cluster assembly on G208C NFU1 is observed only under *in vitro* reconstitution conditions employing inorganic iron and sulfide. In addition to the possibility of impaired accessibility of the CXXC cluster binding motif, the replacement of a glycine with a cysteine near the cluster binding site could perturb cluster coordination, where the new cysteine now functions as a cluster ligand. This alternative is currently under investigation to determine if the CXXC motif is solely responsible for cluster coordination even with the added cysteine in the new CXCXXC sequence.

The inability of the mutant protein to receive cluster from relevant sources shows good correlation with the increased presence of dimer. In our examination of the native NFU1, cluster uptake from the [2Fe-2S](GS)$_4$ complex was only possible when the protein was

monomeric [28]. Kinetic assays for cluster uptake have revealed a model consistent with experimental data, where the cluster is taken up first by a monomer of NFU1, followed by formation of complete holo NFU1 when a second monomer is added to form the [2Fe-2S] cluster-bound dimer (Fig. 10). Cluster uptake into a preformed dimer did not occur and was not supported experimentally [28]. Since the mutant is primarily in the dimer form, the oligomeric state would prevent cluster uptake into G208C NFU1. A similar mechanism for cluster transfer from other holo proteins is most likely in place, where dimer formation is preventing G208C NFU1 from efficiently receiving cluster (Figure 10). A model, in which the monomeric form of NFU1 is the active species, is consistent with the emerging evidence for a functional NFU1-BolA complex involved in Fe/S cluster biogenesis [60,99], due to the fact that NFU1 would need to be capable of forming cluster-bridged homo- and heterodimeric species.

The structural change promoting dimer formation and the downstream consequences of this oligomerization could explain the dominant negative phenotype recently observed by introducing the MMDS1 mutation in yeast [60]. In utilizing yeast as a model system, Melber and colleagues introduced the MMDS1 mutation and found that co-expression of wild-type yeast Nfu1 could not rescue the effects [60]. Having a mutation that promotes protein oligomerization, thereby preventing cluster uptake and downstream transfer, readily explains this phenotype. Native human NFU1 has a natural tendency to dimerize [28] and the G208C mutation amplifies this characteristic. Therefore, it is plausible that a mixture of native and mutant Nfu1, such as in the co-expression system mentioned above, would also show high levels of dimer, in which the native protein could exist as both

monomeric and dimeric states, the mutant would be primarily dimeric, and heterodimers could be formed between the native and the mutant monomeric proteins. With all of the dimers present, cluster uptake would be impaired and downstream cluster transfer perturbed, as we have shown here.

These kinetic limitations and alterations to the Fe/S biosynthesis pathway could generate the drastic consequences and the dominant negative phenotype. However, yeast is not the best model for human NFU1 concerning the MMDS1 condition. Yeast Nfu1 has been observed to behave differently from human NFU1 inasmuch as deletion of Nfu1 is not lethal [100], and negative effects are only exhibited when grown on specific media, which may be reflective of a conditional need for Nfu1 in yeast with a bypass mechanism in place to allow for survival [60]. Furthermore, introduction of the G208C equivalent mutation in yeast results in functional consequences that are not observed in patients, such as aconitase depletion [60]. Together, these differences may speak to potentially dissimilar functions across yeast and human Nfu-type proteins [60], indicating that these types of studies need to be addressed in an *in vivo* system that better replicates the MMDS1 disease condition in conjunction with *in vitro* studies, which are unique in being able to address issues at the molecular level, such as the dimerization effect.

While G208C NFU1 does not appear to have a mechanism of efficient *in vivo* reconstitution, the derivative did retain cluster transfer activity and was able to deliver clusters to both human ferredoxin 1 and 2 (Fig. 7), at a modest rate of approximately half of the second-order rate constant observed for the native protein (Table 5) [28]. A greater change in the transfer abilities of G208C NFU1 was noted for transfer of cluster to

glutaredoxins (Fig. 8). The point mutation results in a changed preference for the glutaredoxins. Our previous work has indicated that [2Fe-2S] cluster from native NFU1 to apo Grx3 was a kinetic sink at 36000 $M^{-1}min^{-1}$, while transfer to Grx2 occurred, but at around the same level as other transfers from NFU1 (Table 5) [27,90]. However, the mutant form of the protein now kinetically prefers cluster transfer to Grx2 by increasing the second-order rate constant seven-fold over transfer to Grx3, which decreased by three-fold. Although Grx2 is primarily present in the mitochondria [101], where Grx3 is cytosolic [102], the large change in second-order rate constants reflects a kinetically altered iron-sulfur cluster transfer pathway due to a single point mutation, which, again, could suggest why such severe phenotypes are observed, as there could be drastic downstream consequences for minor perturbations to the transfer pathway.

MMDS1 was only recently identified as a disease condition, with the first case studies emerging in 2011 [32,38]; however, the number of patients diagnosed with MMDS1 due to the G208C NFU1 mutation has been growing since its initial disease classification. At least 22 patients have been diagnosed since 2011 [32,38,45,46], but it is speculated that this is a highly underdiagnosed condition [46]. Patient case studies describing the same symptoms and disease characteristics, which were attributed to defects in the iron-sulfur cluster biosynthetic pathway, were first published in 2001; [103] but, in the absence of information provided by the human genome project, the exact cause of the disease remained unclear, suggesting the first subset of under-diagnosis. Furthermore, the disease symptoms resemble the majority of mitochondrial or energetic disorders and the patients often died of respiratory or mitochondrial failure, and so the exact cause of death had not

been investigated in depth and the number of cases of MMDS1 is likely to be much higher [46]. Since the disease has only been examined recently, it is also possible that the majority of downstream target proteins for NFU1 that result in the severity of the disease condition are unknown.

Our investigation into the G208C NFU1 mutation has elucidated key facts regarding the actual structural and functional impairments caused by the mutant NFU1 in MMDS1. While several questions remain to be answered, such as the exact link between NFU1 and lipoic acid synthase or succinate dehydrogenase [38,63], we postulate that the mutation alters the structure of the NFU1 protein such that the protein exists in a primarily dimeric state, which prevents it from being able to be reconstituted effectively with an iron-sulfur cluster *in vivo*. The kinetics of [2Fe-2S] cluster transfer have been perturbed due to the mutation, but the connection between the mutant NFU1 and how it interacts with other potential target proteins remains under investigation.

2.5 Figures and Tables

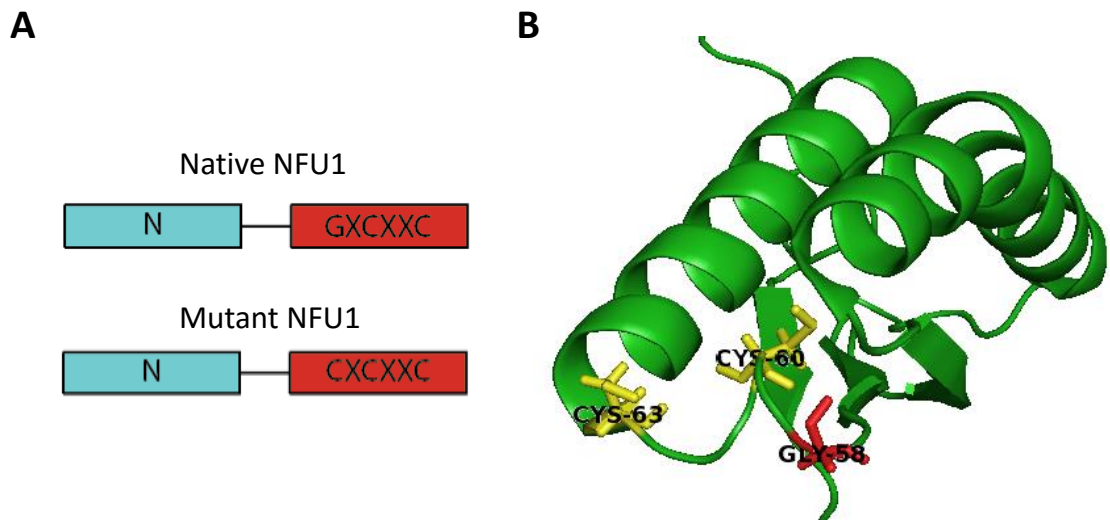

Figure 2-1. (**A**) A representation of the two-domain composition of the native and G208C mutant NFU1 proteins

with the N-terminal domain in blue and the C-terminal domain in red. NFU1 features the functional CXXC Fe/S cluster binding motif in its C-terminal domain. This pattern is altered in the mutant protein with the mutation of a nearby glycine residue at position 208 to cysteine, which gives a CXCXXC motif. (**B**) Solution NMR structure of human C-terminal domain of the NFU1 protein (PDB ID: 2M5O) with the cluster binding cysteines shown in yellow [58]. The glycine at position 208 in the full-length protein (58 above), which is mutated to a cysteine in MMDS1, is colored red. Numbering is consistent with the C-terminal construct used in the structure determination.

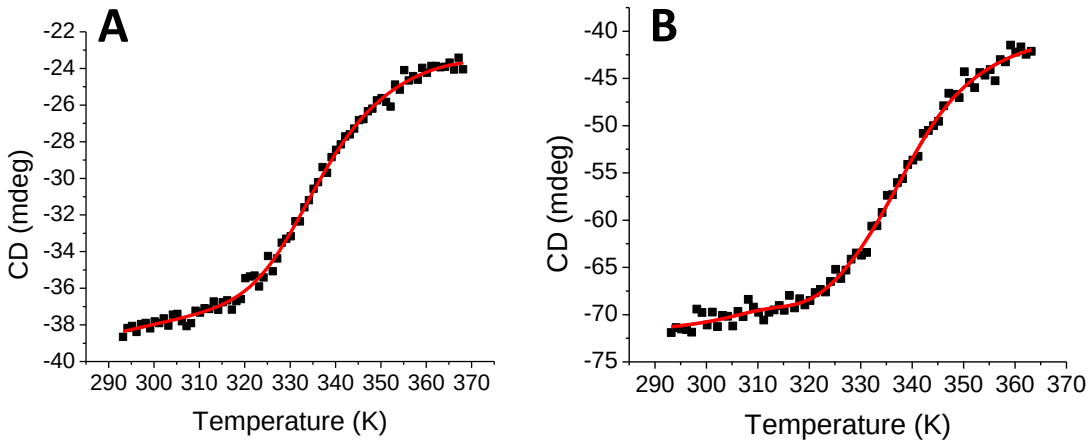

Figure 2-2 VTCD traces

for the melting of 10 μM native human NFU1 (**A**) and G208C NFU1 (**B**) in 40 mM phosphate, pH 7.4. Data were fit to equation 1 to obtain T_m and ΔH_V, which are shown in Table 1. CD units of ellipticity (mdeg) were used directly without conversion to molar ellipticity because the van't Hoff enthalpies are independent of such a factor [49].

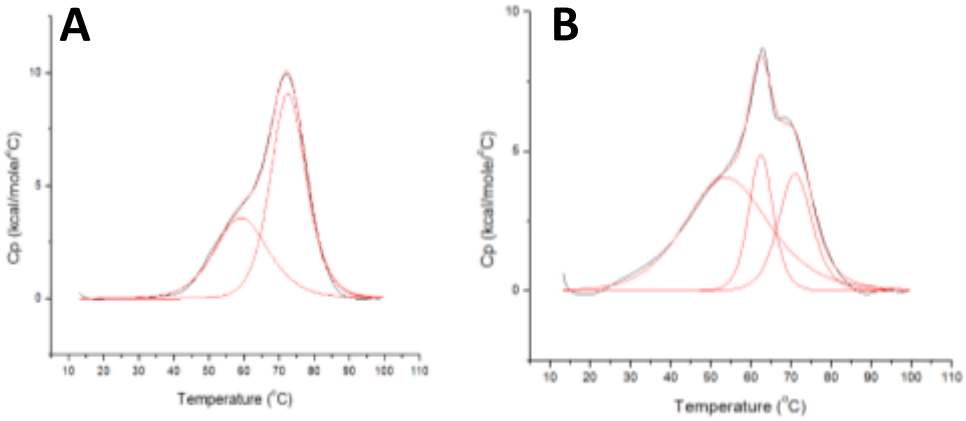

Figure 2-3 Differential scanning calorimetry profiles

for (**A**) 0.2 mM native human NFU1, (**B**) 0.3 mM G208C human NFU1. Both of the proteins were in 50 mM HEPES, 100 mM NaCl, and pH 7.4. The data were fit using Origin 7.0 to obtain T_m, ΔH_{cal}, and ΔH_V, all of which are listed in Tables 3 and 4.

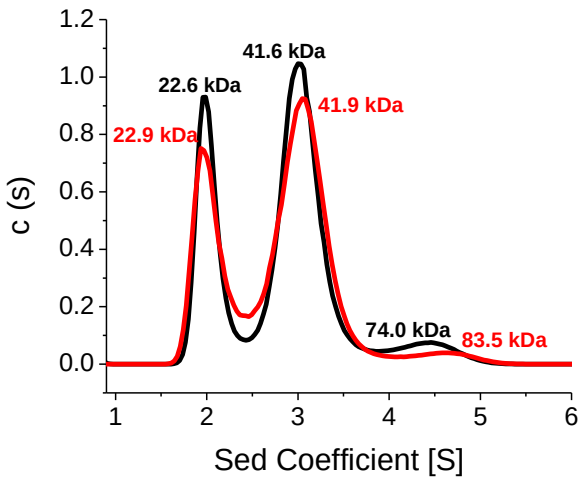

Figure 2-4 Analytical ultracentrifugation profiles for G208C NFU1.

(**A**) Apo G208C was sedimented in the absence of TCEP (black) and in the presence of 1 mM TCEP (red). Sedimentation was monitored at 280 nm. The first peak of the black trace at 22.6 kDa accounts for 29% of the sample, the second peak at 41.6 kDa accounts for 58%, and the third peak at 74.0 kDa accounts for 6%. The first peak of the red trace at 22.9 kDa accounts for 30% of the sample, the second peak at 41.9 kDa accounts for 60%, and the third peak at 83.5 kDa accounts for 1.5%. The AUC results were fit to the Lamm equation [79,80] using a continuous distribution model to obtain the peaks and molecular weights shown above.

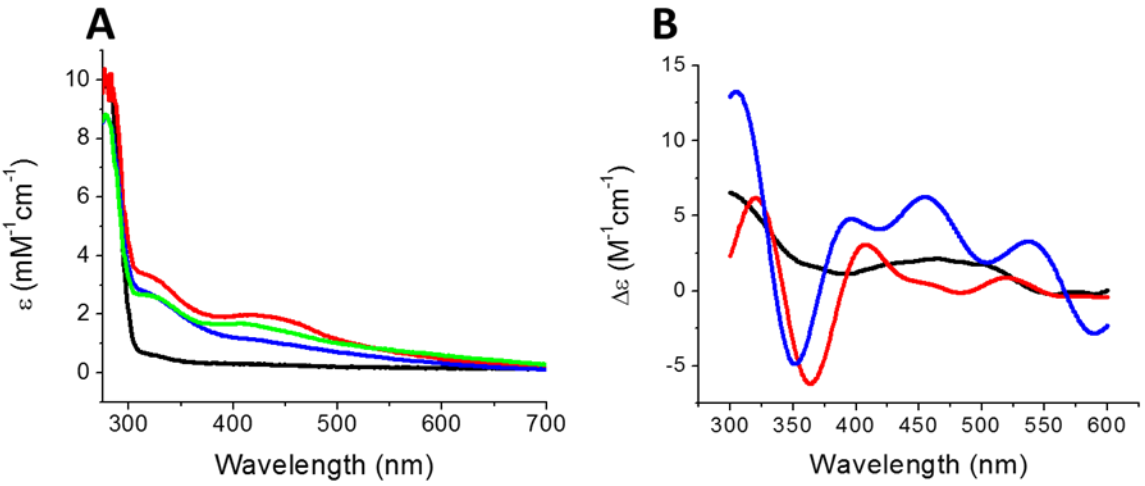

Figure 2-5 UV (**A**) and CD (**B**) spectra following reconstitution

of native and G208C NFU1. In both spectra, the black trace corresponds to apo G208C NFU1, and the red trace to native reconstituted holo NFU1. In (**A**), the blue trace is holo G208C NFU1 reconstituted with *Tm* NifS and L-cysteine, while the green trace is holo G208C NFU1 reconstituted with ferric chloride and sodium sulfide. In (**B**), the blue trace is holo reconstituted NFU1, since both reconstitution methods resulted in the same spectra.

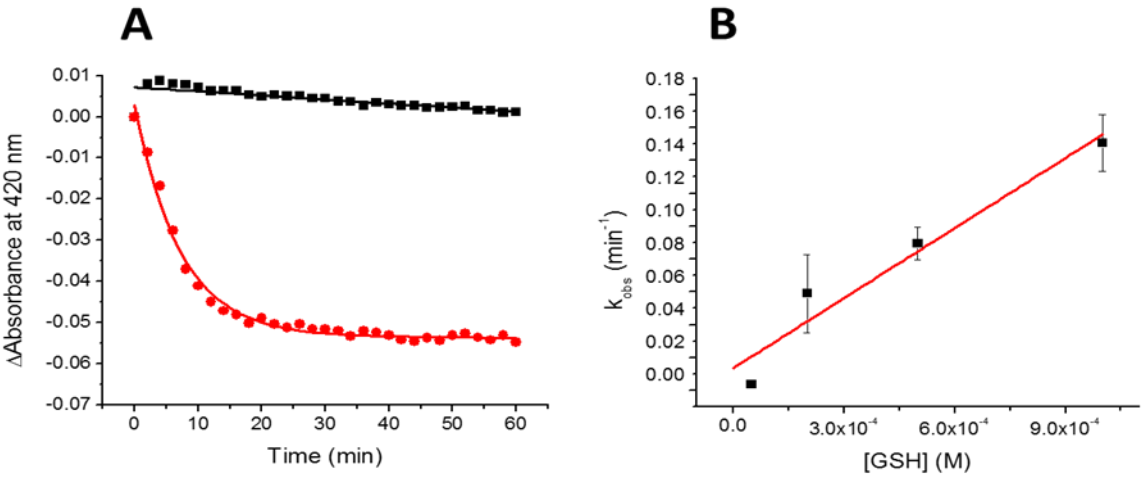

Figure 2-6 GSH extraction

of the [2Fe-2S] cluster from 10 µM reconstituted holo G208C human NFU1 to form the $[2Fe\text{-}2S](GS)_4$ complex. The change in absorbance at 420 nm was monitored over the

course of an hour and data were fit to an exponential to obtain the k_{obs}. (**A**) Shows a representative trace of extraction by 1 mM GSH (red trace). The black trace shows a control of reconstituted holo G208C human NFU1 in the absence of GSH to demonstrate the rate of general cluster instability or breakdown. The concentration of GSH was varied, while keeping the concentration of G208C NFU1 constant to obtain a second-order rate constant. (**B**) The k_{obs} data were plotted against the concentration of GSH and fit to a linear equation to determine an overall second-order rate constant of 140 ± 20 $M^{-1}min^{-1}$.

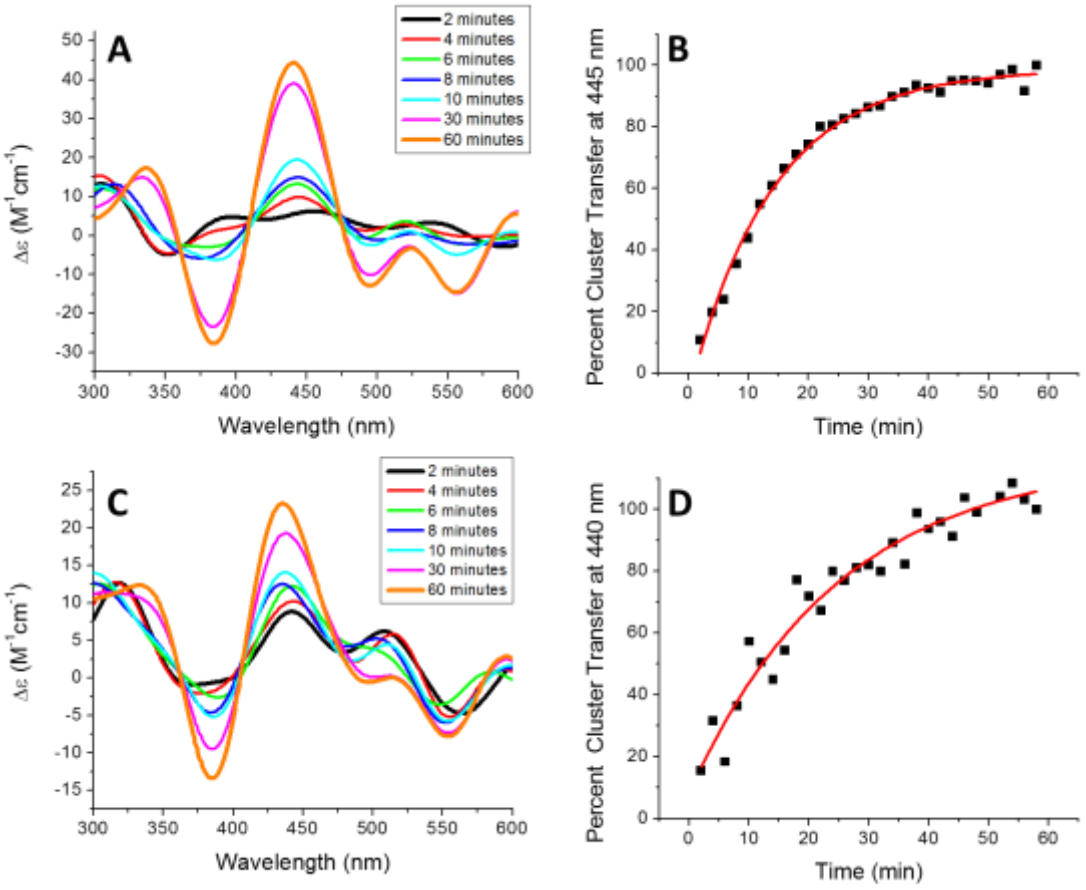

Figure 2-7 Kinetics of [2Fe-2S] cluster transfer

from holo reconstituted human G208C NFU1 to apo human ferredoxins. (**A**) Time course for cluster transfer to ferredoxin 1(Fdx1) monitored by CD in 50 mM HEPES, 100 mM NaCl, pH 7.5. Spectra were recorded every 2 min after the addition of holo NFU1, and converted to percent cluster transfer (**B**) to yield an apparent second-order rate constant from DynaFit of 2600 ± 300 $M^{-1}min^{-1}$ based on the concentration of the [2Fe-2S] cluster [89]. (**C**) Time course for cluster transfer from holo human NFU1 to apo human ferredoxin

2 (Fdx2) recorded by CD under the same conditions as for Fdx1. (**D**) The CD signal was again converted to the percentage of cluster transferred with time to yield an apparent second-order rate constant of 1200 ± 200 $M^{-1}min^{-1}$.

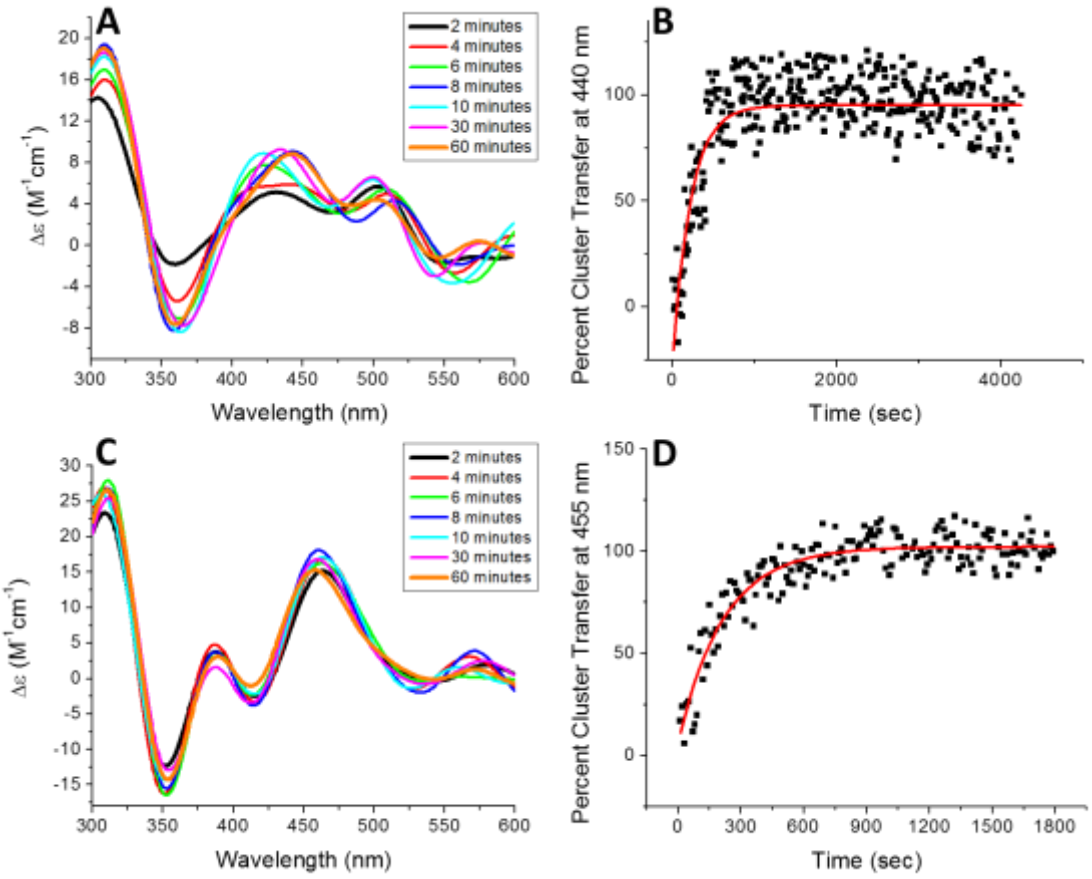

Figure 2-8. Kinetics of [2Fe-2S] cluster transfer

from holo reconstituted human G208C NFU1 to apo glutaredoxins. (**A**) Time course for cluster transfer to apo human Grx2 monitored by CD in 50 mM HEPES, 100 mM NaCl, and pH 7.5 with 3 mM GSH. Spectra were recorded every 2 min after the addition of holo NFU1. However transfer was too rapid to monitor, so cluster transfer was monitored from 435-445 nm every 10 sec and converted to percent cluster transfer (**B**) to determine an apparent second-order rate constant using DynaFit of 22400 ± 5000 $M^{-1}min^{-1}$ based on the concentration of the [2Fe-2S] cluster [89]. (**C**) Time course for cluster transfer to apo *S. cerevisiae* Grx3 monitored by CD under identical conditions. Again, cluster transfer was too rapid to monitor, and so transfer was monitored from 450-460 nm every 10 sec and

converted to percent cluster transfer (**D**) to determine an apparent second-order rate constant of 14500 ± 3500 $M^{-1}min^{-1}$.

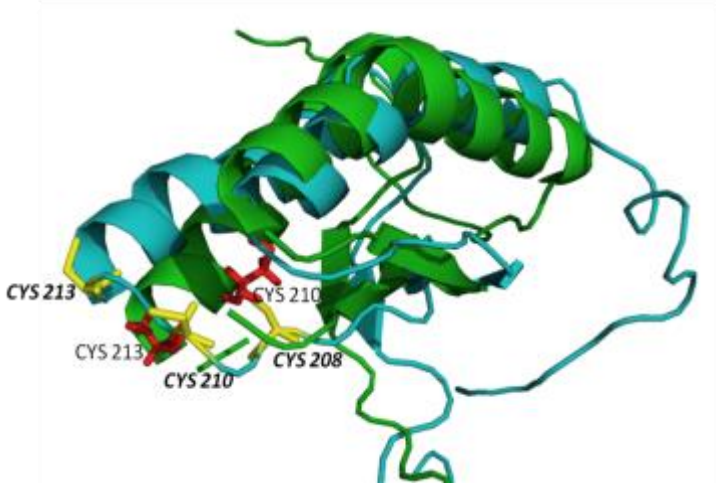

Figure 2-9 Alignment of the human C-terminal domain of the NFU1 protein

(PDB ID: 2M5O) (green trace) and corresponding cysteines in red. The Phyre2 homology modeled structure generated for G208C NFU1 is shown in blue with the cysteines colored yellow.

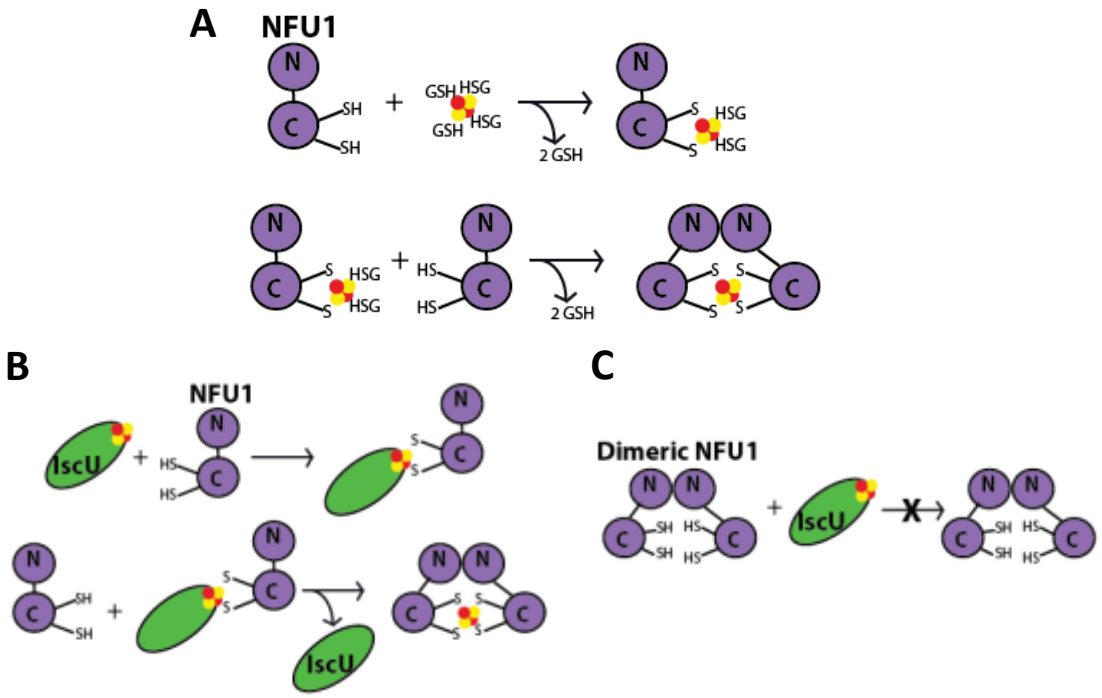

Figure 2-10 (**A**) A model for [2Fe-2S] cluster uptake by monomeric NFU1

represented by the N- and C-terminal domains, from the [2Fe-2S](GS)$_4$ cluster complex to form an intermediate [2Fe-2S] species with two exogenous GSH ligands. A second monomeric NFU1 displaces the GSH molecules to form [2Fe-2S] dimeric NFU1. Adapted from [1]. (**B**) A model for [2Fe-2S] cluster uptake by monomeric NFU1, from a [2Fe-2S] cluster scaffold, such as IscU. Holo IscU interacts with monomeric NFU1 to form a transient heterodimeric complex. A second NFU1 monomeric displaces the now apo IscU to form the holo NFU1 dimer. In a case where NFU1 is a pre-formed dimer (**C**)**,** such as in the G208C mutant, the dimeric NFU1 is unable to form the transient complex with holo IscU and therefore unable to receive the [2Fe-2S] cluster.

	T_m (°C)	ΔH_V (kcal/mol)
Native NFU1	65 ± 1	26 ± 2
G208C NFU1	65 ± 2	31 ± 2

Table 2-1 Variable temperature circular dichroism results.

Native NFU1 and G208C NFU1 at 10 µM were subjected to melting from 20 to 95 °C at 0.4 °C per min. Table 1 shows the data fit to a one-state melting process using equation 1.

	α-helix	β-sheet	Random Coil
Native NFU1	47 %	21 %	33 %
G208C NFU1	37 %	17 %	46 %

Table 2-2. Percentages of secondary structural elements

measured by circular dichroism and analyzed using the analysis program CDSSTR [73] on the online Dichroweb server [75,76].

	T_{m1} (°C)	T_{m2} (°C)	T_{m3} (°C)
Native NFU1	59.3 ± 0.2	--	73 ± 3
G208C NFU1	49 ± 6	64 ± 2	74 ± 4

Table 2-3. Melting temperatures as determined from DSC.

The DSC profiles used for fitting are shown in Figure 2.

	ΔH_{cal1} (kcal/mol)	ΔH_{V1} (kcal/mol)	ΔH_{cal2} (kcal/mol)	ΔH_{V2} (kcal/mol)	ΔH_{cal3} (kcal/mol)	ΔH_{V3} (kcal/mol)
Native NFU1	73 ± 2	41 ± 2	--	--	122 ± 1	74 ± 5
G208C NFU1	5.2 ± 0.4	33 ± 4	39 ± 2	50 ± 2	24 ± 4	74 ± 4

Table 2-4. Enthalpies of melting determined by DSC.

The DSC profiles used for data fitting are shown in Figure 2.

	Rate Constant for Native NFU1 ($M^{-1}min^{-1}$)	Rate Constant for G208C NFU1 ($M^{-1}min^{-1}$)
Human NFU1 to human Fdx1	4700 ± 800 [28]	2600 ± 300
Human NFU1 to human Fdx2	3900 ± 1200 [28]	1200 ± 200
Human NFU1 to human Grx2	3740 ± 77 [27]	22400 ± 5000
Human NFU1 to *S. cerevisiae* Grx3	36200 ± 7700 [90]	14500 ± 3500
S. pombe Isa1 to human NFU1	6700 ± 1560 [27]	No transfer
$[2Fe\text{-}2S](GS)_4$ to human NFU1	1930 ± 210 [28]	No transfer
Human IscU to human NFU1	4750 ± 8 [90]	No transfer

Human IscU to human NFU1 with HSPA9/Hsc20 and MgATP	No transfer	No transfer
Human NFU1 to GSH to form [2Fe-2S](GS)$_4$ complex	130 ± 22 [28]	140 ± 20

Table 2-5. Apparent second-order rate constants determined using CD for [2Fe-2S] cluster transfer to and from G208C NFU1.

Native transfer rates were previously determined using the same CD method [27,28,90].

Chapter 3 : Understanding the Molecular Basis for Multiple Mitochondrial Dysfunctions Syndrome 1 (MMDS1): Impact of a Disease-Causing Gly189Arg Substitution on Structure and Activity of NFU1 in the Fe/S Cluster Biosynthetic Pathway

3.1 Introduction

Study of novel proteins and their behavior in disease states has often led to elucidation of their function *in vivo*. For example, although a clinical description of cystic fibrosis was outlined in the 1930s, it was not until the 1980s that genetic analysis implicated mutation on chromosome 7, now known as the cystic fibrosis transmembrane conductance regulator (CFTR) gene, as the etiological factor of cystic fibrosis. The discovery then led to an in-depth analysis of the protein and its polymorphisms to understand its function and role in disease [104]. Similarly, an investigation of thiazolidinedione binding, a class of drugs used to treat type 2 diabetes, led to discovery of a novel integral mitochondrial protein mitoNEET, which is now thought to have a key role in regulation of electron transfer and oxidative phosphorylation and potentially contribute to the etiology of type 2 diabetes [105,106]. Discovery of these proteins and examination of their function has guided ongoing efforts for drug development and disease cure.

Likewise, a fatal mitochondrial disease, multiple mitochondrial dysfunctions syndrome 1 (MMDS1) has been shown to arise from point mutations in NFU1, an essential iron-sulfur (Fe/S) protein implicated in multiple metabolic pathways and in energy production through Fe/S cluster delivery and trafficking [15,32,38,46,63,103,107]. A number of recent studies have offered insight into the natural cellular roles of this protein by investigating the downstream Fe/S proteins affected by substitution of one disease-causing residue in close proximity to the cluster binding site (Gly208Cys) [32,38,103]. The

reduced function of target Fe/S proteins lipoic acid synthetase (LIAS) and succinate dehydrogenase (SDH) in the MMDS1 disease state suggests pathways that require proper function of the native NFU1 protein for cluster delivery [15,96]. However, the precise function of NFU1 in humans remains unknown.

Analysis of the G208C NFU1 construct by our laboratory revealed an altered monomer-dimer equilibrium *in vitro,* which prevented reconstitution from physiologically-relevant sources, suggesting the molecular basis for MMDS1 is the inability of NFU1 to accept cluster *in vivo* [108]. Recently, a heterozygous Gly189Arg substitution also on NFU1 has been shown to impact metabolic pathways related to the G208C substitution, despite lying farther from the cluster binding site (Fig. 1) [47,109]. In previously documented MMDS1 patient cases, the G208C mutation was either homozygous or heterozygous in conjunction with a deleterious frame-shift mutation, but heterozygous mutation alone was insufficient to display the disease phenotype, as the parents and siblings of the patients showed no symptoms [32,38]. However, in contrast to the G208C mutation, the G189R mutation has been reported as heterozygous, though present with either a G208C or frame-shift mutation [47,109]. Interestingly, patients with this mutation experience milder symptoms and a later age of onset when compared with those with the G208C mutation, suggesting a similar yet less severe impairment of function. In order to understand the molecular basis for the milder MMDS1 phenotype of the G189R derivative, we have undertaken a close examination of the effects of amino acid substitution at position 189 on the structure and function of NFU1 in comparison to the previously documented native and G208C constructs to aid in our understanding of its cellular role.

3.2 Materials and Methods

3.2.1 Protein preparation protocols

Stratagene QuikChange Mutagenesis was employed to introduce the p.Gly189Arg, p.Gly189Ala, and p.Gly189Lys point mutations in to the full length human NFU1 gene in the pET28b(+) plasmid [Primers in SI] [108]. Mutant and wild-type constructs in BL21 DE3 cells were over-expressed in *E. coli*, and the proteins were purified using a TALON column as previously described [28]. A construct of human Grx2 (comprising residues 56-161), with a tobacco etch virus cleavable N-terminal His_6 tag in expression vector pNic-Bsa4, was kindly provided by Drs. Kavanagh, Muller-Knapp and Oppermann and protein was expressed and purified as previously reported [69]. *Schizosaccharomyces pombe* Isa1 protein was expressed and purified as previously reported [70]. Yeast Grx3 (Δ1–35) in pET28b(+) *E. coli* BL21 (DE3) was purified as noted [26].Purification of *Hs* IscU and *Thermatoga maritima* (*Tm*) Nifs was performed as previously reported [64-66]. Purified NFU1 constructs were reconstituted anaerobically with $FeCl_3$ and L-cys as previously described, as were reconstitutions for Isa1 and ISU with FeCl3 and Na_2S [28,108]. Successful reconstitutions were confirmed by UV, CD and iron quantitation [81,110].

The expression vector for human ferredoxin-1 (*Hs* Fdx1) was kindly provided by J. Markley and protein was expressed and purified according to literature procedures [67]. Purification for human ferredoxin-2 (*Hs* Fdx2) was performed as previously reported [68]. The ferredoxins purified as holo proteins and were subsequently converted to apo forms [27,28].

3.2.2 Thermodynamic analyses and oligomeric state determination

Differential scanning calorimetry (DSC) was performed using a MicroCal VP-DSC (Malvern Instruments, Inc.) on 200 μM samples using a differential mode of 0.1 ˚C per minute from 10 ˚C to 100 ˚C, and analyzed using Origin software (Origin Labs) [49,108]. For variable temperature circular dichroism (VTCD), 10 μM protein samples were dialyzed into 40 mM phosphate buffer, pH 7.4 for acquisition via a JASCO J-815 CD spectrometer with 0.1 cm quartz cells. Variable temperature studies were performed at a rate of 0.4 ° C min^{-1} from 20 to 95 °C monitoring signal at 222 nm, and data processed with Origin 7 (Origin Laboratories) [49,108]. Secondary structure prediction of 10 μM samples in phosphate buffer (40 mM, pH 7.4) were obtained using CD by scanning from 300 – 165 nm. The resulting CD spectra were processed using the analysis program CDSSTR [73] using reference set 7 [74] found on the online server Dichroweb [75,76]. Analytical ultracentrifugation (AUC) was employed to determine the oligomeric state of the NFU1 constructs. Apo proteins at 50 μM were monitored at 280 nm in the presence and absence of 1 mM TCEP, and the sedimentation profiles were fit to the Lamm equation using SEDFIT [79,111].

3.2.3 Kinetic analysis for second-order rate constant determination

Kinetic cluster transfer experiments using CD were based on the cluster transfer experiments by Johnson and coworkers [83,84], and refined by our own group [26,28]. All cluster transfer experiments were carried out on a JASCO J-815 CD spectrometer with

a 1 cm anaerobic quartz cuvette by scanning from 600 – 300 nm at 200 nm/min at 25 °C after of the degassed holo protein or degassed glutathione-complexed [2Fe-2S] cluster ([2Fe-2S](GS)$_4$) complex. CD data were converted to the percentage of cluster transferred based on the concentration of [2Fe-2S] cluster and fit using DynaFit [89] to determine the second-order rate constants by best-fit simulation to second-order kinetics [27,90].

Cluster extraction from holo NFU1 constructs was conduction on UV-Visible spectrophotometry by scanning from 800 - 200 nm at 600 nm/min at 25°C after the addition of holo protein. Glutathione concentrations were varied from 0.2 – 2 mM, and the reaction course monitored via the change in absorbance at 420 nm. The k_{obs} was plotted against GSH concentration and fit linearly to obtain the second-order rate constant [26,28].

3.3 Results and Discussion

In this work, we have extended our analysis to a second disease causing mutation of NFU1. Patients have been found with a genetic point mutation that converts a glycine at position 189 of the amino acid sequence to an arginine (G189R), and when heterozygous with the previously discussed p.G208C substitution mutation or a c.146delC null mutation, also results in the disease condition known as MMDS1, although generally with milder symptoms in comparison to the homozygous G208C [46,109]. Although the 189 position is farther in sequence from the cluster-binding CXXC motif, the solution NMR of the C-terminal domain (PDB ID: 2M5O) overlay with the Swiss Model homology model of the G189R mutant shows that Gly189 lies close in space to the binding pocket (Figure 1).

Furthermore, the G189R mutation introduces a significantly larger and positively charged side chain in the place of a flexible, small aliphatic one that could potentially affect the secondary Fe/S coordination sphere and thus Fe/S cluster transfer behavior, in addition to a disruption of global protein structure. Given that the heterozygous G189R/G208C disease phenotype is less severe than the homozygous G208C, yet still disease causing, whereas G208C and null mutation carriers remain unaffected, we sought to understand the molecular basis of disease of the G189R NFU1 mutation, particularly how this construct can disrupt protein structure or function by introducing 3 different amino acid substitutions at this position: G189R, G189K, and G189A.

Initially, secondary structure and stability were examined via variable temperature CD (VTCD) by comparison of the melting profiles and thermodynamic characteristics with the native human NFU1 and the G208C mutant. All of the 189 constructs were fit to a two-state model (equation 4), clearly reflecting the multi-domain nature of the protein (Fig. 2, Table 1) [49]. Interestingly, T_m1 and ΔH_1 values, corresponding to the unfolding of the C-terminal domain, are significantly lower in the 189 constructs than the native construct, whereas T_m2, corresponding to the unfolding of the N-terminal domain, is elevated in the 189 constructs relative to the native, potentially pointing to a destabilizing effect of the 189 mutation in the C-terminal domain that is compensated by increased ordering in the N-terminal domain. Both proteins exhibited reversible melting on VTCD (data not shown), indicating that the overall protein folds are relatively stable.

CD was also used to examine the overall characteristics of protein secondary structure by determining the percentages of secondary structural elements: α-helix, β-sheet,

and random coil. The values are summarized in Table 2 and demonstrate an overall increase in random coil with a corresponding loss of secondary structural elements, most noticeably in the G189A construct. However, the modest change in secondary structural elements likely does not explain the changes in protein stability seen in the VTCD results, as the changes in either T_m or ΔH values do not correlate to changes in the relative abundance of random coil.

Additional thermodynamic and structural characterization of G189X NFU1 using differential scanning calorimetry (DSC) reveals significant destabilization of the C-terminal domain as reflected in T_m1 and ΔH_{v1} values and broadening of the peak corresponding to the C-terminal domain unfolding (Figs. 3, S2; Tables 3, 4). N-terminal domain melting temperatures (T_m3) are comparable to the native, although enthalpies of unfolding (ΔH_{v3}) are lower for the G189X derivatives, indicating the substitution mutations have a global destabilizing effect.

As previously documented for the case of the G208C substitution, mutation at position 189 also strongly influences monomer-dimer equilibrium. Examination by analytical ultracentrifugation revealed that the 189 constructs strongly prefer monomer, as opposed to the relatively equal monomer to dimer ratio observed in the native, and the substantially increased the amount of dimer relative to the native in the G208C mutant (Figs. 4, S3). In addition to the destabilizing effect of mutation, the dramatic decrease in the relative abundance of dimer also likely contributes to the decreased melting temperature and lower enthalpies of unfolding of the C-terminal domain (T_m1), as it has

been proposed that a dimer unfolding event occurs alongside the unfolding of the C-terminal domain [108].

Although mutation introduces small changes in thermodynamic parameters relative to the native and causes a primarily monomeric apo state, no significant changes in global stability were observed, so we sought to evaluate any differences in function relative to the native construct. Like the native and G208C constructs, the G189 derivatives were capable of undergoing reconstitution *in vitro* through the use of $FeCl_3$ and L-cysteine with *Tm* NifS as a sulfide source. Following reconstitution, both UV and CD spectra look analogous to those reported for the native and G208C form, indicating the presence of a similarly bound [2Fe-2S] cluster. The cluster-bound 189 constructs also form as a dimer around the Fe-S cluster, as confirmed by AUC with monitoring at 420 nm (data not shown), with similar reconstitution yields to those observed for the native and G208C forms.

The 189 constructs are also capable of conducting cluster uptake and transfer. Similar to the G208C construct, yet despite being largely monomeric, none of the 189 derivatives were able to accept cluster from the [2Fe-2S](GS)$_4$ complex, though this has been shown to be a viable substrate for reconstitution for proteins like NFU1 and export by the ABCB7 transporter [26,28,31,108,112]. Likewise, the 189 derivatives were unable to receive a Fe/S cluster from the donor protein Isa1, a proposed Fe/S cluster scaffold protein, indicating that one putative *in vivo* reconstitution pathway could be interrupted in the G189R NFU1 MMDS1 disease state. However, in contrast to the G208C derivative, all 189 derivatives were able to accept cluster from human IscU, with transfer to G189R yielding a similar second-order rate constant to that of transfer to the native protein of 5700

± 1400 M^{-1} min^{-1}, though the G189A and G189K constructs demonstrated slightly slower uptake (Figure 5, Table 4). In the heterozygous G189R/G208C MMDS1 disease state, reconstitution of NFU1 *in vivo* is likely being impaired due to the inability of both NFU1 mutants to receive an Fe-S cluster from the IscA1/2 assembly complex, yet not completely halted due to the apparently functioning IscU pathway for the G189R protein. The partially-functioning Fe/S trafficking pathway could explain the milder phenotype experienced by patients with the G189R mutation.

Our previous work with the native and G208C forms of NFU1 has shown that a [2Fe-2S](GS)$_4$ complex could be formed by Fe-S cluster extraction from the [2Fe-2S] cluster-bound native NFU1 under conditions of excess GSH, with a second-order rate constant of 130 ± 22 M^{-1} min^{-1} for the native and 140 ± 20 M^{-1} min^{-1} for the G208C mutant [28,108]. Excess GSH is also able to extract the [2Fe-2S] cluster from the 189 NFU1 derivatives, and the decrease in absorbance was not due to cluster breakdown on the NFU1 constructs, since a control in the absence of excess GSH demonstrated very little change in absorbance. Second-order rate constants for GSH extraction were determined as 1850 ± 30 M^{-1} min^{-1} for the G189R derivative and 1200 ± 70 M^{-1} min^{-1} for the G189K derivative, which corresponds to a tenfold increase over that for the native and G208C constructs (Table 4). The extraction rate constant for G189A though elevated, was still on the same order of magnitude of the native construct. The dramatic increase observed for the G189R and G189K mutants suggests that the structural change and subsequent charge or steric effects which impact the monomer-dimer equilibrium and prevent efficient Fe/S cluster uptake from sources aside from IscU could simultaneously be promoting Fe/S cluster

lability and impairing its ability to effectively transfer cluster for *in vivo* reconstitution of downstream target proteins for final delivery to proteins like LIAS and SDH.

Once reconstituted, the G189X NFU1 derivatives are also capable of transferring the [2Fe-2S] cluster to apo protein targets. As found for native and G208C human NFU1, cluster transfer to ferredoxins (Fdx) 1 and 2 (Fdx1 and Fdx2) [28] and glutaredoxins (Grx) 2 and 3 (Grx2 and Grx3) was observed [27], as monitored by the use of CD spectroscopy as previously reported [26,28,54,89,91,113]. Reconstituted holo G189X NFU was added to apo human Fdx1, and the increase in CD signal at 445 nm was monitored (Fig. 6 A and B) and used to yield a second-order rate constant for the transfer of [2Fe-2S] cluster of 12,500 ± 1000 M^{-1} min^{-1} for G189R, about three-fold increase from the native, whereas the other two mutants demonstrated transfer rates similar to the native (Table 4). Cluster transfer from holo G189X NFU1 to human Fdx2 was monitored in a similar fashion and yielded an overall second-order rate constant in the range of that observed for the native. Cluster transfer kinetics for transfer to Grx was executed in the same manner, though since the Grxs utilize GSH as endogenous ligands, an excess of GSH was included in the reactions. Rapid transfer to the Grxs was observed for both Grx2 and Grx3 such that by the end of 2 min, the spectra already resembled those of the target holo proteins. For that reason, cluster transfer kinetics were monitored over 10-s intervals, instead of 2-min intervals. Transfer to apo human Grx2 resulted in a second-order rate constant of 2700 ± 770 M^{-1} min^{-1} for G189R, and similarly lower values observed for the other constructs (Table 4). Cluster transfer from holo G208C NFU1 to apo *Saccharomyces cerevisiae* Grx3 was complete within the first 2 min and yielded a second-order rate constant of 39,500 ±

8000 M^{-1} min^{-1} for G189R, essentially unchanged from the native (Table 4). Because the G189R NFU1 and the other mutant derivatives were capable of delivering a [2Fe-2S] cluster to the same target proteins that have been examined for kinetic transfer from the native form with second-order rate constants in close agreement with those observed for the wild-type, the disease phenotype is likely arises from an inability to effectively receive, hold on to a cluster under physiological GSH levels, and traffic an Fe/S cluster to downstream targets, rather than a disruption in the downstream transfer kinetic pathway.

Our investigation into the G189R NFU1 mutation, as well as two other substitutions at position 189 has elucidated key facts regarding the structural and functional changes of NFU1 in the presence of the G189R substitution, and the how these alterations could contribute to the MMDS1 phenotype. Although mutation does not greatly affect thermodynamic parameters like ΔH and Tm, there is a small structural change which significantly impacts the monomer-dimer equilibrium. As a result, mutant NFU1 has an impaired although not eliminated ability to receive cluster from physiologically-relevant sources and increased Fe/S cluster lability when present in near cellular concentrations of GSH. The relatively unaffected cluster transfer kinetics from NFU1 also suggest a problem with Fe/S cluster reconstitution or stability *in vivo* as opposed to an inability to transfer the cluster to downstream targets once bound, since transfer rates were similar to the native protein. Nevertheless, it remains unclear how NFU1 interacts with other potential target proteins in the MMDS1 disease state, such as LIAS and SDH, and the connection between NFU1 mutation and impaired interaction with these targets remains under investigation.

3.4 Figures and Tables

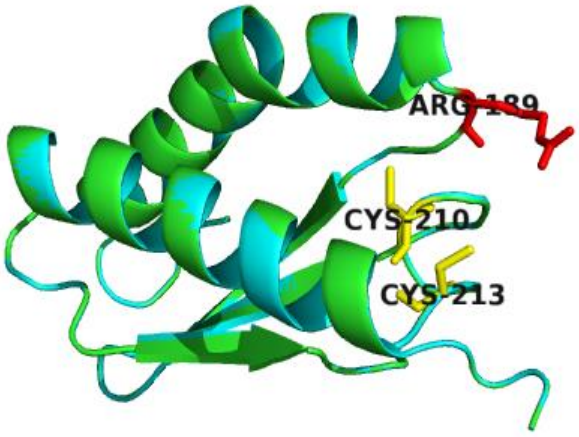

Figure 3-1 Alignment of the human C-terminal domain of the NFU1 protein

(PDB ID: 2M5O; green trace), with corresponding cysteines in yellow. The Swiss-Model homology modeled structure generated for G189R NFU1 is shown in cyan with the arginine colored red. Numbering correlates with the full-length protein sequence.

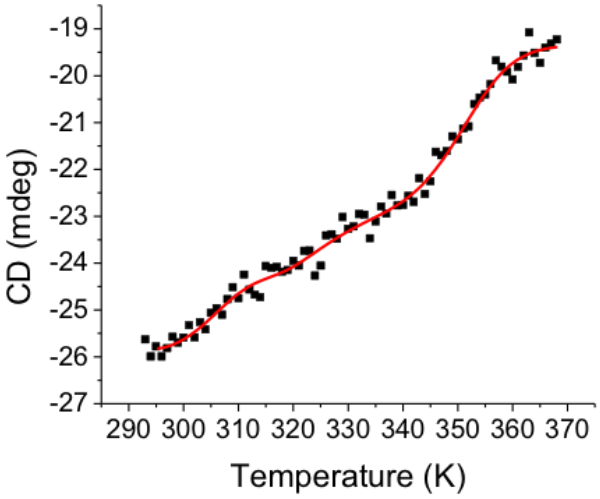

Figure 3-2 VTCD trace for the melting of 10 μM G189R human NFU1

in 40 mM phosphate, pH 7.4. Data were fit to a two-state model (equation 4) to obtain T_m and ΔH_V, which are shown in Table 1. CD units of ellipticity (mdeg) were used directly without conversion to molar ellipticity because the van't Hoff enthalpies are independent of such a factor [49]. Equation in SI.

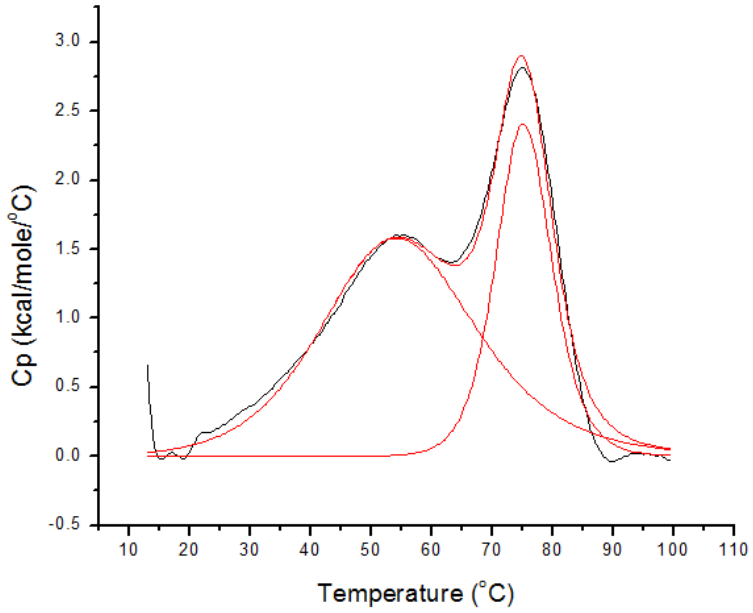

Figure 3-3 Differential scanning calorimetry profiles for 0.2 mM G189R human NFU1

The protein was in 50 mM HEPES, 100 mM NaCl, and pH 7.4. The data were fit using Origin 7.0 to obtain T_m and ΔH_V values, all of which are listed in Tables 3 and 4.

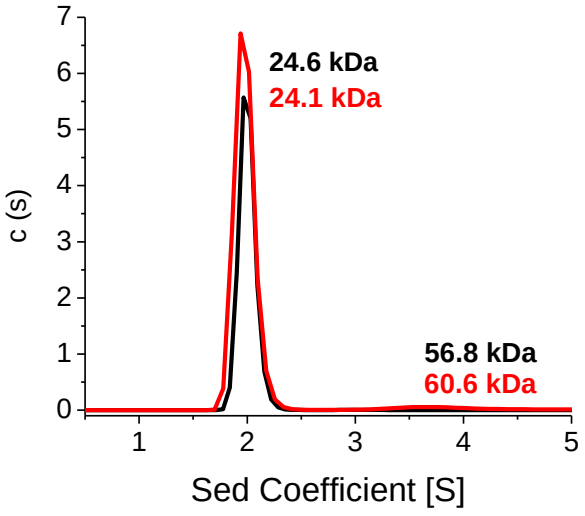

Figure 3-4 AUC profile for apo G189R NFU1

Apo protein was sedimented in the absence of TCEP (black) and in the presence of 1 mM TCEP (red). Sedimentation was monitored at 280 nm. The first peak of the black trace at 24.6 kDa accounts for 95% of the sample, the second peak at 56.8 kDa accounts for 4%. The first peak of the red trace at 24.1 kDa accounts for 94% of the sample, the second peak at 60.6 kDa accounts for 4%. The AUC results were fit to the Lamm equation [79,111] using a continuous distribution model to obtain the peaks and molecular weights shown above.

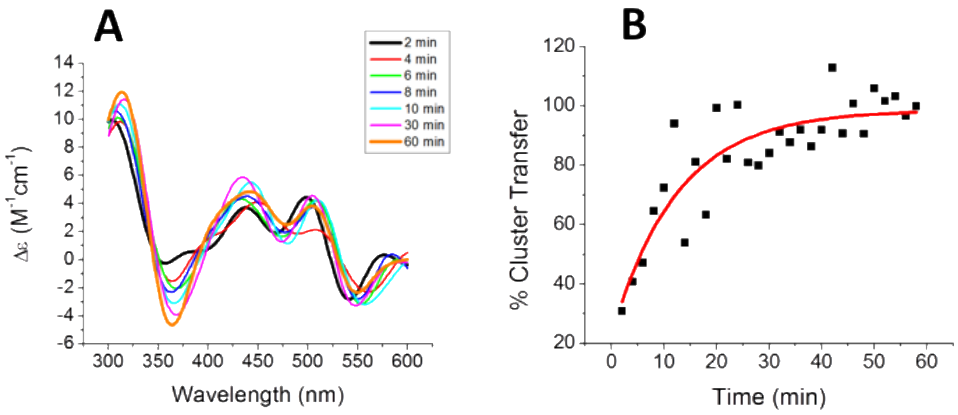

Figure 3-5 Kinetics of [2Fe-2S] cluster transfer from holo reconstituted human IscU to human G189R NFU1.

(**A**) Time course for cluster transfer to human G189R NFU1 monitored by CD in 50 mM Hepes and 100 mM NaCl (pH 7.5). Spectra were recorded every 2 min after the addition of holo IscU and were converted to (**B**) percent cluster transfer to yield an apparent second-order rate constant from DynaFit of 5700 ± 1400 M^{-1} min^{-1} based on the concentration of the [2Fe-2S] cluster [89].

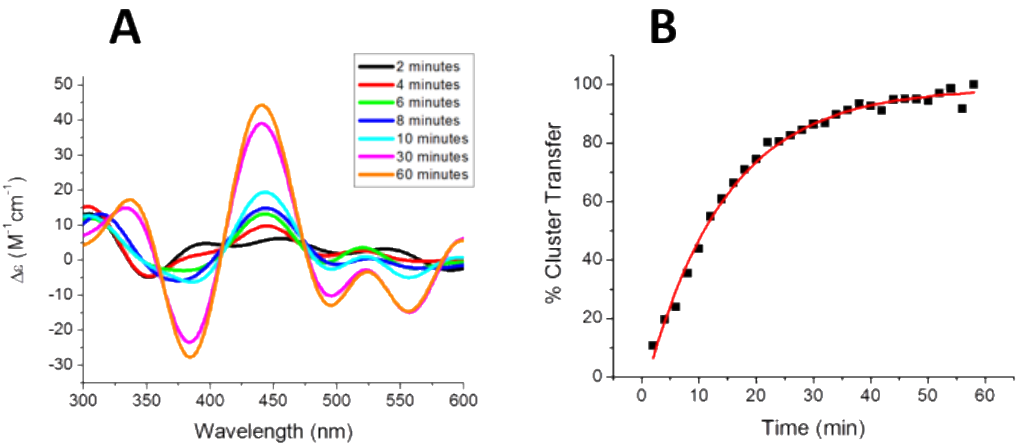

Figure 3-6 A representative [2Fe-2S] cluster transfer from holo reconstituted human G189R NFU1 to apo human ferredoxin 1 (Fdx1).

(**A**) Time course for cluster transfer to Fdx1 monitored by CD in 50 mM Hepes and 100 mM NaCl (pH 7.5). Spectra were recorded every 2 min after the addition of holo G189R NFU1 and were converted to (**B**) percent cluster transfer to yield an apparent second-order rate constant from DynaFit of 12,500 ± 1000 M^{-1} min^{-1} based on the concentration of the [2Fe-2S] cluster [89].

	T_m1 (˚C)	ΔH_v1 (kcal/mol)	T_m2 (˚C)	ΔH_v2 (kcal/mol)
Native NFU1	55 ± 3	33 ± 2	74 ± 2	36 ± 3
189R NFU1	38 ± 1	16 ± 1	79 ± 2	34 ± 4
189A NFU1	40 ± 3	21 ± 1	80 ± 3	32 ± 1
189K NFU1	42 ± 4	24 ± 4	77 ± 2	40 ± 1

Table 3-1 VTCD data

Native NFU1 and G189X NFU1 at 10 µM were subjected to melting from 20 to 95 °C at 0.4 °C per min. Table 1 shows the data fit to a two-state melting process.

	α-helix	β-sheet	Random Coil
Native NFU1	47 %	21 %	33 %
189R NFU1	37 %	19 %	44 %
189A NFU1	23 %	20 %	57 %
189K NFU1	40 %	17 %	44 %

Table 3-2 Percentages of secondary structural elements

measured by CD and analyzed using the analysis program CDSSTR [73] on the online Dichroweb server [75,76].

	Tm1 (°C)	Tm2 (°C)	Tm3 (°C)
Native NFU1	60 ± 1	--	73 ± 1
G208C NFU1	49 ± 6	64 ± 2	74 ± 4
G189R NFU1	52 ± 5	--	75 ± 1
G189A NFU1	53 ± 3	--	77 ± 1
G189K NFU1	49 ± 2	--	80 ± 4

Table 3-3 Melting temperatures as determined from fits to the DSC data

The DSC profiles used for fitting are shown in Figure 3 and Figure S2. Native and G208C data were previously reported [108].

	ΔH_{v1} (kcal/mol)	ΔH_{v2} (kcal/mol)	ΔH_{v3} (kcal/mol)
Native NFU1	41 ± 2	--	74 ± 5
G208C NFU1	33 ± 4	50 ± 2	74 ± 4
G189R NFU1	24 ± 1	--	65 ± 20
G189A NFU1	29 ± 2	--	55 ± 3
G189K NFU1	28 ± 6	--	44 ± 6

Table 3-4 Enthalpies of melting determined by DSC.

The DSC profiles used for data fitting are shown in Figure 3 and Figure S2. Native and G208C data were previously reported [108].

	Native	G208C	G189R	G189A	G189K
Human NFU1 to human Fdx1	4700 ± 800	2600 ± 300	12500 ± 1000	3300 ± 750	2500 ± 930
Human NFU1 to human Fdx2	3900 ± 1200	1200 ± 200	3100 ± 250	3400 ± 200	21000 ± 2900
Human NFU1 to human Grx2	3740 ± 77	22400 ± 5000	2700 ± 770	1500 ± 500	2100 ± 300
Human NFU1 to *S. cerevisiae* Grx3	36200 ± 7700	14500 ± 3500	39500 ± 8000	29000 ± 3700	6700 ± 1900
Human IscU to Human NFU1	4750 ± 8	No transfer	5000 ± 1200	3200 ± 30	3000 ± 110
S. pombe Isa to human NFU1	6700 ± 1560	No transfer	No transfer	1750 ± 110	No transfer
$[2Fe\text{-}2S](GS)_4$ to human NFU1	1930 ± 210	No transfer	No transfer	No transfer	No transfer
Human NFU1 to $[2Fe\text{-}2S](GS)_4$	130 ± 22	140 ± 20	1800 ± 30	360 ± 70	1200 ± 70

Table 3-5 Second-order rate constants for [2Fe-2S] cluster transfer to and from NFU1.

Native transfer rates were previously determined using the same CD method [27,28,90,108]. All values have units of M^{-1} min^{-1}.

Chapter 4 : Analysis of NFU-1 Metallocofactor Binding Site Mutations: Impacts on Iron-Sulfur Cluster Coordination and Protein Structure and Function

4.1 Introduction

Iron-sulfur (Fe/S) cluster assembly *in vivo* occurs via three organized Fe/S cluster biosynthetic pathways. The Isc (iron-sulfur cluster) system is the predominant pathway for cluster assembly in humans, with *de novo* [2Fe-2S] cluster biosynthesis on the scaffold protein IscU [96], which are then transferred to target proteins via a series of chaperones and delivery proteins. One such delivery protein, NFU1 can bind a [2Fe-2S] cluster [28] that is then transferred to other partner proteins. NFU1 is comprised of two domains; a structure-defining N-terminal domain, and a functional molten globular C-terminal domain that holds the cluster binding site at a highly-conserved CXXC motif [49,51,114]. The molten globular nature of the cluster binding domain is believed to provide the structural flexibility required for function in iron-sulfur cluster uptake and delivery [49,108].

Recently, a point mutation in NFU1 (p.Gly208Cys) that lies in close proximity to the Fe/S cluster binding site has been implicated as the cause of the Multiple Mitochondrial Dysfunction Syndrome 1 (MMDS1) disease state [38]. This substitution alters the protein sequence surrounding the cluster binding motif, changing the native sequence from GXCXXC to CXCXXC [38], with a subsequent structural change that is intimately tied to its function [108]. Other consequences of this point mutation may arise because a potential third ligand for cluster coordination has been introduced and Fe/S cluster function is

inextricably linked to cluster geometry and coordination. Fe/S centers are generally ligated via cysteine residues in highly-conserved motifs [17], such as the CXXC sequence of native NFU1; however, non-cysteinal ligands such as histidine [18], serine [20], and a variety of other amino acids [19] have been observed. Furthermore, non-protein derived ligands have been shown to function as cluster ligands, such as a water molecule in the iron-sulfur cluster scaffold IscU [21] and S-Adenosylmethionine (SAM) in lipoic acid synthase [20]. The impact of cluster coordination extends beyond the primary coordination sphere by controlling protein structure around the cluster-binding site [12], which can effect changes in both overall protein structure and function. Properties such as reduction potential, can be specifically tuned based on the amino acids in the inner and outer cluster coordination sphere [12,115].

For NFU1, the altered (CXCXXC) motif in the mutant protein resembles other cluster-binding sequences that have been previously identified. The same sequence occurs twice in a small T antigen from Merkel cell polyomavirus that is capable of binding a [2Fe-2S] cluster at one site, and a [4Fe-4S] cluster with a fourth ligand of uncertain identity at another [116]. Similarly, a cytosolic Fe/S cluster assembly protein, anamorsin (Dre2 in yeast) utilizes a CXXCXC sequence to bind a [2Fe-2S] cluster that resembles the motif found in the NFU1 disease state [117]. These two proteins exhibit very different cellular roles, demonstrating the importance of the Fe/S cluster coordination state on overall protein structure and function, and the role of perturbations to the cluster binding motif to alter functional characteristics. Therefore, the question remains as to what impact the change in

cluster-binding motif has on NFU1 structure-function characteristics, and how this change contributes to the MMDS1 disease state.

In this paper, we have selectively mutated the glycine at position 208 and the cysteine residues at positions 210 and 213 to alter the cluster binding motif. By analysis of these complementary mutations we conclude that the introduction of a third cysteine does not increase the number of cysteine ligands to the iron-sulfur cluster, and that modulation of ligating residues does not cause a significant change in structure. Rather, mutation at position 208 dominates subsequent coordination to the cluster, forcing a change in cysteine ligation that results in the structural and functional effects observed *in vitro*. These results clarify how the G208C mutation inhibits cluster uptake by NFU1, most likely giving rise to the MMDS1 disease state.

4.2 Materials and Methods

4.2.1 Mutagenesis

Strategene QuikChange Mutagenesis was employed to introduce a series of point mutations in full length human NFU1. The PCR reaction contained 50 ng of native NFU1 DNA in pET28b(+) plasmid, 2 units of Phusion DNA polymerase (New England Biolabs), 10x Phusion buffer (New England Biolabs), 125 ng of each primer (Integrated DNA Technologies), 0.2 mM dNTPs, and 3% DMSO. The native plasmid was utilized to generate two single mutant variants: p.Gly208Ala and p.Gly208Ser (primers in Table S1). The p.Gly208Cys mutant plasmid was generated as previously described [108]. In all cases, the thermocycle was identical to that described in the QuikChange manual: the sample was

melted by heating to 95 ˚C for 1 min, followed by 16 cycles of 95 ˚C for 30 sec, 55 ˚C for 1 min and 72 ˚C for 6.5 min (Stratagene). Following amplification, samples were incubated with 7.5 units of *Dpn*I at 37 ˚C for 4 h, and $CaCl_2$-competent BL21 (DE3) cells subsequently transformed via heat shock with the mutant constructs. Mutagenesis results were confirmed by nucleotide sequencing from GENEWIZ. The p.Gly208Cys DNA was then used to introduce the second point mutation at either the 210 or 213 positions following the protocol outlined above (primers in Table S1).

4.2.2 Protein expression and purification

All of the NFU1 constructs in a pET28(b+) vector in *E. coli* strain BL21(DE3) host cells were grown overnight at 37 °C in 10 mL of Luria–Bertani (LB) broth media containing kanamycin (50 μM) [50]. The overnight cultures were diluted 1:1000 in LB media containing 50 μM kanamycin until the OD_{600} reached 0.6. At this point, protein expression was induced with 0.5 mM of isopropyl β-D-1-thiogalactopyranoside (IPTG), and cultures were incubated overnight at 37 °C. Cell pellets were collected by centrifugation at 4,330*g* for 15 min at 4 °C, and resuspended in 30 mL of 50 mM HEPES, 100 mM NaCl, pH 7.5. Resuspended pellets were incubated with 30 mg lysozyme and 0.6 mg DNase I for 30 min at 4 °C, and then lysed by use of a dismembranator. Cell lysate was centrifuged at 28,982*g* for 50 min at 4 °C, and the supernatant applied to a TALON column. Protein was eluted with a buffer containing 50 mM HEPES, 100 mM NaCl, 150 mM imidazole, pH 7.5 and concentrated by Amicon ultrafiltration over a 10 kDa membrane.

Purification of *Hs* ISU and *Thermatoga maritima* (*Tm*) Nifs was performed as previously reported [64-66]. The expression vector for human ferredoxin-1 (*Hs* Fdx1) was kindly provided by J. Markley and protein was expressed and purified according to literature procedures [67]. Purification of human ferredoxin-2 (*Hs* Fdx2) was performed as previously reported [68]. Briefly, *Hs* Fdx1 was purified by use of DE-52 anion exchange column chromatography followed by FPLC purification with a size exclusion Superose-12 column (HR 16/50, Pharmacia) run at 0.2 mL/min with 50 mM HEPES, 100 mM NaCl, pH 7.5 at 4^0 C. All of the colored fractions were collected and combined. Purification for human ferredoxin-2 (*Hs* Fdx2) was performed by use of a TALON column as previously reported [68]. Protein was eluted with a buffer containing 50 mM HEPES, 100 mM NaCl, 150 mM imidazole, pH 7.5 and concentrated by amicon ultrafiltration over a 10 kDa membrane. The ferredoxins purified as holo proteins and were subsequently converted to the apo form by treatment with 100 mM EDTA, 5mM DTT and 8M urea in a solution of 50 mM HEPES, 100 mM NaCl, pH 7.5. A construct of human Grx2 (comprising residues 56-161), with a tobacco etch virus cleavable N-terminal His_6 tag in expression vector pNic-Bsa4, was kindly provided by Drs. Kavanagh, Muller-Knapp and Oppermann and protein was expressed and purified as previously reported [69]. *Schizosaccharomyces pombe* Isa1 protein was expressed and purified as previously reported [70]. Yeast Grx3 (Δ1–35) in pET28b(+) *E. coli* BL21 (DE3) was purified as described [26].

In all cases, protein purity was assayed by use of 12 % SDS-PAGE that was visualized with Coomassie Blue staining. Imidazole was removed by dialysis at 4 °C against a buffer containing 50 mM HEPES, 100 mM NaCl, pH 7.5, and protein

concentration was determined by the Bradford assay and confirmed by absorbance measurements by use of the protein's extinction coefficient at 280 nm.

4.2.3 Differential scanning calorimetry

DSC samples (0.15 mM – 0.2 mM) were dialyzed against 50 mM HEPES, 100 mM NaCl, pH 7.5 at 4 ˚C with Spectra/Por dialysis membrane (MWCO 10 000; Spectrum Laboratories, Inc.). The resulting dialysis buffers were used as reference cell buffers for precision and repeatability. Reference buffers and protein samples were thoroughly degassed using a MicroCal Thermovac2 (Malvern Instruments, Inc.) prior to analysis on a MicroCal VP-DSC (Malvern Instruments, Inc.). The data were obtained using a differential mode at a rate of 1.0 ˚C per minute from 10 ˚C to 100 ˚C, analyzed using Origin software (Origin Labs), and fit to a non-two state DSC curve fitting model to account for the multiple protein domains [49].

4.2.4 Variable temperature circular dichroism characterization

Circular dichroism (CD) samples (10 μM) were dialyzed in phosphate buffer (40 mM phosphate, pH 7.4) with Spectra/Por dialysis membrane (MWCO 10,000; Spectrum Laboratories, Inc.). The resulting dialysis buffers were used as reference cell solvents for precision and reproducibility. Prior to analyses, all sample and reference solutions were rigorously degassed with a Microcal Thermovac2 device (Malvern Instruments, Inc.). All CD data acquisitions were obtained on a JASCO J-815 CD spectrometer (JASCO) equipped with quartz cells with a 0.1 cm path length. Variable temperature studies were

performed at a rate of 0.4 ° C min^{-1} from 20 to 95 °C, and all data were processed with Origin 7 (Origin Laboratories). VTCD data were fit to equation (1) for T_m and ΔH_V determination for a one-state melting model indicative of a one-phase transition [49], where R is the ideal gas constant in calories per mole, T_m is the melting temperature in Kelvin, ΔH_V is the van't Hoff enthalpy, and C_p is the heat capacity. F and U represent the mean residue ellipticities (θ_{mr}) of the folded and unfolded protein, respectively. Data were fit to a one-state model to examine the possibility of a concerted secondary structure melting process of both the N- and C-terminal domains (equation 1).

$$\theta = \left\{\exp\left[\left(\frac{1}{-RT}\right)\left(\Delta H_V\left(1-\frac{T}{T_m}\right)-C_p\left((T_m-T)+T\ \ln\frac{T}{T_m}\right)\right)\right]/\left\{1+\exp\left[\left(\frac{1}{-RT}\right)\left(\Delta H_V\left(1-\frac{T}{T_m}\right)-\ C_p\left((T_m-T)+T\ln\frac{T}{T_m}\right)\right)\right]\right\}\right\}(F-U)+U$$

4.2.5 Secondary structure prediction from circular dichroism

Protein samples at 10 µM in 40 mM phosphate, pH 7.4 were placed in a 1 mm quartz cuvette and the signal monitored from 300 – 165 nm. The baseline signal from the buffer was subtracted before converting the data to Δε. The resulting CD spectra were processed using the analysis program CDSSTR [73] using reference set 7 [74] found on the online server Dichroweb [75,76].

4.2.6 Reconstitution of apo proteins

NifS-mediated *in vitro* reconstitution of G208C NFU1 was completed as previously described [28,77]. Briefly, ferric chloride and L-cysteine were added to an anaerobic mixture of approximately 200 μM purified NFU1, 2 μM *T. maritima* (*Tm*) NifS, and 5 mM DTT to final concentrations of 1.6 mM $FeCl_3$ and 3.2 mM L-cysteine. Alternatively, sodium sulfide and ferric chloride were added to an anaerobic mixture of approximately 200 μM purified NFU1, 2.1 mM urea, and 5 mM DTT to final concentrations of 1 mM $FeCl_3$ and 1 mM Na_2S [26]. The final solution was incubated for 1 h with stirring at room temperature, before separation of excess urea, iron and sulfide through a PD-10 column that was equilibrated with an argon-purged solution of 50 mM HEPES, 100 mM NaCl, pH 7.5. Reconstituted protein was eluted with 3.5 mL of the equilibration buffer and concentration determined by both the Bradford assay and by absorbance at 330 nm and 420 nm on a Cary WinUV spectrophotometer.

For ISU and Isa1 [78], 200 μM apo protein was incubated with 50 mM DTT, argon-purged for 30 min, and then made up to 1 mM in Fe^{2+} and 1 mM in S^{2-}. After incubation for 1 h, the reaction mixture was concentrated and passed through a PD10 desalting column to remove excess DTT, Fe^{2+} and S^{2-}, and the UV-vis spectrum was obtained for each of apo and holo ISU and Isa1.

4.2.7 Reconstitution analysis by circular dichroism

CD scans of apo and holo proteins were recorded on a JASCO J-815 CD spectrometer in a quartz 1 cm anaerobic cuvette. CD scans from 300 nm to 600 nm were collected to analyze signature cluster-bound protein peaks at a scan rate of 200 nm/min at

25 °C. Data were processed using JASCO Spectramanager II Analysis software and were represented in Origin 7.0.

4.2.8 Oligomerization state determination by analytical ultracentrifugation

The four NFU1 double mutant variants at 50 μM protein concentration (OD_{280} = 1.0), in the presence or absence of 1 mM TCEP, were loaded into the ultracentrifugation chambers and sealed. Buffer samples containing 50 mM HEPES, 100 mM NaCl, pH 7.5 were used as a reference, with the addition of 1 mM TCEP where needed. Reconstituted holo NFU1 mutant variants at an OD_{420} = 1.5 were loaded in the same manner with the same reference buffer. Samples were centrifuged at 45,000 rpm for 6 h to reach complete sedimentation, and the sedimentation profiles were fit using SEDFIT to the Lamm equation [79,80].

4.2.9 $[Fe_2S_2](GS)_4$ Synthesis

The cluster used was synthesized as previously reported [30]. Briefly, ferric chloride (20 mM) and sodium sulfide (20 mM) were added to 10 mL 40 mM glutathione solution, pH 8.6. A volume (40 mL) of ethanol was added to the mixture and mixed by vortexing. The precipitate was collected by centrifugation at 13,000 rpm for 10 min, washed twice with ethanol and dried under vacuum.

4.2.10 Iron quantitation

A solution of $[Fe_2S_2](GS)_4$ (0.05 mM, 200 µL) in H_2O or holo protein was acidified by concentrated HCl (60 µL) and heated to 100 ºC for 15 min. The resulting suspension was centrifuged at 14,000 rpm for 2 min and the supernatant (100 µL) was diluted with Tris-HCl (0.5 M, 1.3 mL, pH 8.5). Solutions of sodium ascorbate (0.1 mL, 5%) and bathophenanthroline-disulfonate (0.4 mL, 0.1%) were sequentially added to the neutralized reaction solution with mixing between each addition. The solution was incubated at 25 ºC for 1 h and iron was quantitated by measuring the absorbance at 535 nm on a UV-vis spectrophotometer and calculated from a calibration curve made with 0.01-0.2 mM $FeCl_3$ standard solutions (Fig. S1) *[78,81]*.

4.2.11 Iron-sulfur cluster uptake monitored by CD

The ability of the NFU1 double mutants to take up an iron-sulfur cluster from the $[2Fe\text{-}2S](GS)_4$ complex was examined by circular dichroism (CD). CD scans were recorded on a JASCO J-815 CD spectrometer in a 1 cm anaerobic quartz cuvette from 600 – 300 nm at a scan rate of 200 nm/min at 25°C, with a 2 min interval between each accumulation. The protein (50 µM) in 50 mM HEPES, 100 mM NaCl pH 7.5, was thoroughly degassed in the presence of 5 mM DTT and transferred to the anaerobic cuvette. Solid $[2Fe\text{-}2S](GS)_4$ was resuspended in degassed 50 mM HEPES, 100 mM NaCl pH 7.5 and added to the argon-purged anaerobic cuvette via a gas-tight syringe to a final concentration of 400 µM to initiate the reaction. Data were processed using JASCO Spectramanager II Analysis software and analyzed in Origin 7.0. The deconvolution function from Spectramanager II analysis software was used for analysis of bands in the

spectra that contained overlapping Lorentzian curves having the same full width at half maximum value that accurately distinguishes the peak positions for each band.

4.2.12 Kinetics of [2Fe-2S] cluster extraction by glutathione from holo NFU1

Glutathione has been previously shown to extract the iron-sulfur cluster from various holo proteins to form the $[2Fe\text{-}2S](GS)_4$ complex by monitoring the change in the charge-transfer bands at 330 nm and 420 nm by UV-Vis spectrophotometry [26,30]. As was done for native holo NFU1 [28], degassed, reconstituted holo double mutant NFU1 in 50 mM HEPES, 100 mM NaCl, pH 7.5 was incubated with a 4- to 10-fold excess of GSH in an anaerobic cuvette and the absorbance at 420 nm on a Cary Win UV spectrophotometer was monitored every 2 min over the course of 1 h. The change in absorbance at 420 nm was plotted against time and fit to an exponential decay to obtain k_{obs}. A control reaction for holo double mutants in the absence of excess GSH was carried out under the same conditions to account for inherent cluster instability. Cluster extraction by GSH to form the $[2Fe\text{-}2S](GS)_4$ complex was confirmed using ESI mass spectrometry on a Bruker Micro-TOF (ESI) spectrometer and data was analyzed by use of Bruker DataAnalysis software [30,82].

4.2.13 Kinetic cluster transfer experiments

Kinetic cluster transfer experiments were designed based on the cluster transfer experiments by Johnson and coworkers [83,84], and refined by our own group [26,28]. Reactions were performed on a JASCO J-815 CD spectrophotometer in a 1 cm anaerobic

quartz cuvette from 600 – 300 nm at a scan rate of 200 nm/min at 25°C, with a 2 min interval between each acquisition. Reactions that reached completion within the first 10 min were analyzed over a 10 nm wavelength scale, based on the peak of interest, with 10 second intervals between acquisitions. Spectra were processed using JASCO Spectramanager II Analysis software and were represented in Origin 7.0.

Reactions in 50 mM HEPES, 100 mM NaCl, pH 7.5 were prepared by degassing a mixture of 40 μM apo protein in 5 mM DTT, and transferred to an anaerobic cuvette via a gas tight syringe. Degassed holo protein at 40 μM was added to the cuvette to initiate the reaction. The concentration of [2Fe-2S] in the reaction for each holo protein was determined via standard iron quantitation methods.

Kinetics of cluster transfer was analyzed by converting the change in CD signal to the percentage of cluster transferred. The plot of time versus percent cluster transfer was fit using DynaFit [89] to obtain the second-order rate constant by a best fit simulation to second-order kinetics.

4.3 Results

To more thoroughly understand the impact of the altered Fe/S cluster binding motif in the MMDS1 disease state, we have generated a series of point substitutions of NFU1 to investigate the occurrence of Cys ligation to the bound cluster (Table 1). Single mutant constructs were created where the glycine residue at position 208 was mutated either to alanine, a more rigid and slightly bulkier residue that is sterically similar to cysteine, or to serine, a ligand that is capable of binding a Fe/S cluster, though less favorably than cysteine [65,118]. These selections allow for the separation of effects on cluster binding that are observed in the G208C construct as a result of changes in size or ligation behavior relative to the identity of the residue at this position. Additionally, double mutant constructs were created where the 208 cysteine mutation was retained, while the cysteine residues at positions 210 and 213 were substituted with either alanine or serine in order to investigate differences in cluster-binding and transfer behavior as the typical CXXC motif was interrupted. Each of these six protein constructs was then purified and characterized with regard to structural and functional properties of their apo and holo protein states.

4.3.1 Apo protein stability characterization of single mutant constructs

Detailed secondary and tertiary protein characterization has already been reported for native human NFU1 [49] and the G208C mutant variant [108]. These results demonstrated that the mutant protein maintains less overall secondary structure in the monomeric form, which alters the monomer-dimer equilibrium to favor the dimer species. The increased presence of dimer has been shown to prevent cluster uptake from

physiologically-relevant sources *in vivo*, likely giving rise to the MMDS1 phenotype [108]. To examine additional single mutations at the 208 position, secondary structure and stability were likewise examined via variable temperature circular dichroism (VTCD), and the melting profiles and thermodynamic characteristics contrasted to those obtained from the native human NFU1 and the G208C mutant (Figure 1; Figure S1). Data were fit to a one-state model (Table 2), indicative of a concerted unfolding mechanism of both the N- and C-terminal domains [119]. The native NFU1 and mutant constructs all show similar melting traces, with no significant deviations in the melting temperature and enthalpy of unfolding, within error, indicating relatively comparable secondary structural stability.

Circular dichroism was also utilized to examine the overall characteristics of protein secondary structure by determining the percentages of secondary structural elements: α-helix, β-sheet and random coil. The values are summarized in Table 3. Substitutions at residue 208 were observed to increase the relative amount of random coil while decreasing α-helical content, but did not perturb overall secondary structure stability, based on the VTCD results (Figure 1; Table 2). The G208C construct maintains the closest semblance to the native, followed by G208S then G208A.

Differential scanning calorimetry (DSC), was also utilized to determine the thermodynamics and heat capacity of unfolding for all of the mutant variants, relative to the native protein (Tables 4 and 5). The DSC profile for the G208A and G208S variants did not show the additional third peak observed for G208C that was ascribed to dimer unfolding [108], but rather they resembled the two-state melting process of the native protein with the first event at T_m1 = 48 ± 8 °C and the second at T_m2 = 74 ± 6 °C for the

G208A construct, and T_m1 = 61 ± 3 °C and T_m2 = 75 ± 1 °C for the G208S construct. The lower T_m values correspond to the melting of the C-terminal domain and the higher melting temperatures represent melting of the well-folded N-terminal domain [49]. Although the mutant melting temperatures are similar to the native state, the mutant constructs show lower van't Hoff enthalpies than the native, reflecting the higher percentage of random coil from secondary structure contributions.

Because the prominent third DSC peak observed in the G208C derivative was not observed for the G208A and G208S mutant variants, analytical ultracentrifugation (AUC) experiments were then performed to investigate whether the mutations had any effect on oligomerization trends as previously noted for the G208C construct. AUC was completed for both apo G208A and G208S NFU1 in the presence and absence of 1 mM TCEP to eliminate the potential for oligomerization due to disulfide bond formation. Both mutant constructs showed a strong preference for the monomer form (expected: 23.9 kDa) which contributed 70% of the species for G208A and 90% of the species for G208S (Figure 3; Table 6). Dimer for G208A and G208S accounted for 22% and 8% of the species, respectively. No higher order species were observed for G208S, although a peak at 102 kDa as 2% of the species could reflect a small tendency of G208A towards tetramer formation, similar to prior observations for G208C [108]. Even in the presence of TCEP, these values remain essentially unchanged. This supports a crucial role for residue 208 in determining oligomerization trends independent of disulfide bonding or cofactor binding. The increased presence of dimer exhibited by the G208C mutation is thought to be the underlying cause for the observed functional impairment of Fe/S cluster binding [108], a

conclusion that is supported by the drastic changes in oligomeric ratios as the residue at position 208 is altered.

4.3.2 Apo protein stability characterization of double mutant constructs

Stability characterization was conducted on the G208C/C210X (where X=S/A) and G208C/C213X (X=S/A) double mutant constructs in addition to the single mutant constructs. Data were again fit to a one-state model (Table 7), indicative of a concerted unfolding mechanism of both the N- and C-terminal domains. The native NFU1 and mutant constructs all show similar melting traces (Figure 4; Figure S2), though the double mutants generally have slightly higher melting temperatures and enthalpies of unfolding indicative of an energetically favorable change in secondary structure. Similar results were observed independent of the replacement residue or residue position.

However, analysis of protein secondary structures using circular dichroism shows a dramatic dependence on the position of the mutation, with the 210 double mutants showing a substantial decrease in the amount of α-helix, complemented by an equal increase in the amount of random coil. The values are summarized in Table 8. It is interesting to note that this increase in random coil does not correlate with a decrease in stability as evidenced by the thermodynamic parameters obtained from VTCD, suggesting that the protein is adopting an equally stable conformer despite the lack of canonical ordered secondary structure.

Differential scanning calorimetry was again performed to investigate any tertiary structure perturbations that may have appeared in conjunction with the previously

identified alterations in secondary structure. Interestingly, although the G208C mutation was incorporated, none of the double mutant constructs displayed the three-phase melting trace observed for the G208C single mutant (Figure 5); rather, all four double mutant DSC traces resembled the native curve with a two-phase melting event indicative of the separate N- and C-terminal melting events already discussed, with dimer dissociation inseparable from those events [49]. The respective first melting events show little deviation from that of the native, with the notable exception of G208C/C213S, which occurs about 4 ˚C higher at $T_m1 = 63 \pm 1$ ˚C (Table 9). The second melting event has slightly more variance, with a noticeable increase for G208C/C210A which occurs at $T_m2 = 79 \pm 1$ ˚C and a noticeable decrease for G208C/C213A which occurs at $T_m2 = 66 \pm 2$ ˚C. Alternatively, the serine double mutants maintain their similarity with the native construct, with their second melting events occurring at $T_m2 = 74 \pm 2$ ˚C for the G208C/C210S construct and $T_m2 = 72 \pm 2$ ˚C for the G208C/C213S construct (Table 9). Conversely, all double mutants display a noticeable decrease in their enthalpies of melting, indicating an overall destabilizing effect initiated by the mutations, which is not present at the secondary structure level (Table 10).

Although minor changes to melting temperature and thermodynamic stability are present as a result of the point substitutions, the most dramatic effects were observed in AUC experiments to examine oligomerization behavior. As discussed previously, all samples were run in the presence and absence of 1 mM TCEP in order to separate oligomerization effects due to disulfide bonding from those due to electrostatic interaction. All double mutants displayed a substantially decreased preference for the monomer state (expected: 23.9 kDa) with oligomeric effects again dependent on the position, as the C213

constructs displayed an increased preference for higher-order oligomers with trimer species for C213A at 15.2 % and C213S forming a tetramer comprising 47% of the species (Figure 6; Table 11); whereas no higher-order oligomers are observed for the native construct [108]. Higher-order oligomerization effects are less pronounced for the G208C/C210 constructs, although there is still a decreased preference for monomer (Figure 6; Table 11). Due to the consistent increased preference of the double mutant constructs for higher-order oligomeric species, and the large variance observed for the G208 single mutant constructs, it is likely that the G208C mutation dominates this effect.

4.3.3 Holo protein functional characterization of single mutant constructs

Following a thermodynamic and structural analysis of the two single mutants, in comparison to the native construct and the disease-causing G208C construct, the functional changes resulting from the mutation were next examined to understand how the differences in oligomeric state impacted Fe/S cluster binding and transfer behavior. Similar to the native and G208C constructs, the single mutants were readily reconstituted *in vitro* by use of $FeCl_3$, L-cysteine and *Tm* NifS, and yielded UV spectra displaying typical iron-sulfur cluster charge-transfer bands at 330 and 420 nm (Fig. 9). Native NFU1 and the G208C construct have been shown to bind a [2Fe-2S] cluster under similar reconstitution conditions [28,108], while UV and CD spectra reveal no significant differences between samples, consistent with the G208A and G208S constructs also binding a [2Fe-2S] cluster in a similar environment and further evidenced by the quantitative transfer to [2Fe-2S]

ferredoxins. Based on iron quantitation, reconstitution yields of 0.84 [2Fe-2S]/dimer for G208A and 0.86 [2Fe-2S]/dimer for G208S were obtained, both similar to the yield achieved for previous NFU1 reconstitutions [28,108]. Protein oligomerization around the cluster was confirmed by use of AUC, with monitoring at 420 nm to follow the cluster-bound form of the protein. Oligomeric species were the major constituents of G208A and G208S holo samples, with a preference for tetramer formation in the G208A sample and dimer formation in the G208S sample (data not shown).

Our previous analysis of both the native human NFU1 and the G208C constructs showed that the native human protein was capable of receiving and transferring cluster from other Fe/S proteins [27,28,90]; whereas the G208C construct was incapable of receiving an Fe/S cluster from any physiologically-relevant source, but could transfer a cluster once reconstituted, though with perturbed kinetic preferences [108]. Native NFU1 was also able to receive cluster from a physiologically-relevant glutathione-bound iron-sulfur cluster complex $[2Fe\text{-}2S](GS)_4$, but not the G208C construct [28,108]. This glutathione complex has been shown to be taken up by a number of apo iron-sulfur cluster proteins [26,30] and is a viable substrate for the mitochondrial ABCB7 transporter [29,82], suggesting a possible role for the $[2Fe\text{-}2S](GS)_4$ complex as a component of the labile iron pool. Native human NFU1 can take up a [2Fe-2S] cluster from the complex with a second-order rate constant of 1930 $M^{-1}min^{-1}$ [28], as observed by circular dichroism (CD) [28]. The G208A construct was also able to take up a [2Fe-2S] cluster moderately faster with a larger second-order rate constant of 3500 $M^{-1}min^{-1}$ (Figure 7). However, the G208S construct was unable to receive cluster from the complex (data not shown).

Conversely, only the G208S construct was able to receive cluster from two donor proteins *S. pombe* Isa1 and human IscU, in contrast to both the G208C and the G208A constructs. We have previously demonstrated that these [2Fe-2S] cluster scaffold proteins are able to transfer an iron-sulfur cluster to native human NFU1 [27,90]. Therefore, we have examined the ability of the single mutant proteins to be reconstituted in the same way by use of CD spectroscopy. Holo reconstituted human IscU was added to apo G208S (Fig. 8C) and the resulting spectral change was used to extract a second-order rate constant of 2300 ± 90 M^{-1} min^{-1}, slightly smaller than the value of 4750 ± 8 M^{-1} min^{-1} observed with the native protein. Likewise, *S. pombe* Isa1 was added to the apo single mutant targets and reacted for 1 h (Fig. 8A). The G208S construct could again receive cluster with a smaller second-order rate constant of 3200 ± 850 $M^{-1}min^{-1}$ compared to 6700 $M^{-1}min^{-1}$ for native NFU1 (Table 12). Because the transfer was rapid, it was also monitored at 360 nm at 10 sec intervals to confirm the second-order rate constant (Fig. 8D).

Our previous work with native and G208C forms of NFU1 has quantitatively addressed a role for NFU1 in Fe/S cluster delivery and trafficking. As such, the [2Fe-2S](GS)$_4$ complex could be formed by cluster extraction from both the [2Fe-2S] cluster-bound native protein and G208C NFU1 under conditions of excess glutathione (GSH), with similar second-order rate constants of 130 ± 22 $M^{-1}min^{-1}$ and 142 ± 24 $M^{-1}min^{-1}$, respectively [28]. Excess GSH is also able to extract the [2Fe-2S] cluster from holo G208A and G208S NFU1, and the decrease in absorbance at 420 nm was monitored over the course of an hour (Fig. 9A). The decrease in absorbance was not due to cluster breakdown on the NFU1 constructs, since a control in the absence of excess GSH

demonstrated very little change in absorbance (Fig 9B). The change in absorbance data was determined at six different concentrations of excess GSH and k_{obs} plotted against GSH concentration (Fig. 9C), and the initial slope fit to a linear equation to determine the second-order rate constant for GSH extraction of the [2Fe-2S] cluster from G208A of 520 ± 80 $M^{-1}min^{-1}$ (Table 12). The plot was also fit to a saturation kinetics model to determine the K and k_1 values (12); however, this was the only mutant construct to demonstrate this behavior. By contrast, the G208S construct displayed no dependence on the concentration of glutathione, and a rate constant of 205 ± 71 $M^{-1}min^{-1}$ was determined.

Both single mutants were also capable of transferring the [2Fe-2S] cluster to other apo protein targets. As found for the native and G208C human NFU1, cluster transfer to ferredoxins 1 and 2 (Fdx1 and Fdx2) and glutaredoxins 2 and 3 (Grx2 and Grx3) was observed [27,28,90,108]. Cluster transfer was monitored by use of CD spectroscopy, because unique spectra are generated for each iron-sulfur cluster bound protein, converted to percent cluster transfer and fit using DynaFit [89] to determine the second-order rate constants [91], which are summarized in Table 12. Reconstituted holo G208A or G208S were added to apo human Fdx1 and the increase in CD signal at 445 nm was monitored (Fig. 10) and used to yield second-order rate constants for transfer of [2Fe-2S] cluster of 12000 ± 2800 $M^{-1}min^{-1}$ for G208A and 19000 ± 1700 $M^{-1}min^{-1}$ for G208S, both of which are significantly larger than the observed 4700 $M^{-1}min^{-1}$ for native NFU1. Similarly, cluster transfer from the single mutants to Fdx2 yielded an overall second-order rate constant of 13000 ± 1500 $M^{-1}min^{-1}$ for G208A and 20000 ± 510 $M^{-1}min^{-1}$ for G208S, again larger than

the observed 3800 $M^{-1}min^{-1}$ for the native protein. Transfer was monitored at 10 s intervals at 440 nm for both Fdx1 and Fdx2 to capture the rapid transfer reaction that was too fast to be observed with 2 min intervals.

Cluster transfer kinetics for transfer to glutaredoxins was conducted in the same manner as for the ferredoxins. The change in CD signal was monitored following addition of holo reconstituted single mutant NFU1 to either apo Grx2 or apo Grx3. Since the glutaredoxins utilize glutathione as endogenous ligands, an excess of GSH was included in these reactions to be able to reconstitute a functional glutaredoxin protein. Although excess GSH has been shown to extract the cluster from Fe-S proteins [26,28,30], transfer from NFU1 to the glutaredoxins was direct as no intermediate spectra were observed during the transfer which would represent formation of a transitory complex. Consistent with no intermediates of a [2Fe-2S](GS)$_4$ complex [30], the observed rates were faster than those obtained for direct reconstitution using the [2Fe-2S](GS)$_4$ complex. Transfer to Grx2 yielded a slightly higher second-order rate constant of 6300 ± 380 $M^{-1}min^{-1}$ for G208A, while G208S was found to transfer with a slower rate constant of 1500 ± 97 $M^{-1}min^{-1}$, in comparison to the 3700 $M^{-1}min^{-1}$ observed for native. However, cluster transfer to Grx3 occurred at much slower rates for both single mutant constructs in comparison to the native protein. Specifically, single mutant transfers to Grx3 yielded second-order rate constants of 5600 ± 170 $M^{-1}min^{-1}$ and 2900 ± 420 $M^{-1}min^{-1}$ for G208A and G208S, respectively, in comparison to the 36,000 $M^{-1}min^{-1}$ observed for native NFU1.

4.3.4 Functional characterization of double mutant holo protein constructs

Similar to the native and single mutant constructs, all of the double mutant constructs were readily chemically reconstituted using ferric chloride, L-cysteine and *Tm* NifS, and yielded the expected charge transfer bands at 420 nm and 330 nm indicative of [2Fe-2S] cluster binding (Fig. 11A). Based on iron quantitation, reconstitution yields varied from 0.62 cluster/dimer for C210A, 0.86 for C213A, 0.65 for C210S, and 0.57 for C213S, which are slightly lower than those typically achieved for the native construct [28,108]. Protein oligomerization around the cluster was confirmed by use of AUC, while monitoring at 420 nm to assess the cluster-bound form of the protein. Dimeric and tetrameric species accounted for the majority of holo samples, with a preference for dimer formation for C210A and C210S, and tetramer formation in the C213A and C213S samples (data not shown).

Analysis of the native protein has demonstrated its ability to receive a [2Fe-2S] cluster from holo donor proteins IscU and Isa1, as well as the [2Fe-2S](GS)$_4$ complex [27,28,90]; however, similar to the G208C mutant, none of the double mutants were able to receive cluster from any physiologically-relevant source (data not shown).

Chemically reconstituted NFU1 double mutants were able to transfer the [2Fe-2S] cluster to various targets. As such, the cluster on the mutants constructs could be extracted in the presence of excess glutathione, as observed for the native protein and G208 single mutants [28,108]. Cluster transfer was monitored at 420 nm using UV-vis over the course of 1 h, and the corresponding decrease in absorbance was used to calculate k_{obs}. The extraction reaction was run at five different concentrations of glutathione, which were fit

using linear regression to obtain a second-order rate constant (Figure 11, Table 13; Figure S3). Both C210 double mutants yielded smaller rate constants, relative to the native NFU1, with transfer occurring at 60 ± 3 $M^{-1}min^{-1}$ for C210A and 81 ± 8 $M^{-1}min^{-1}$ for C210S.The rate constant for the C213A construct is comparable to that of native protein, at 133 ± 5 $M^{-1}min^{-1}$. Only C213S showed a significantly larger rate constant than native, at 250 ± 10 $M^{-1}min^{-1}$.

Similar to the native and single mutant constructs, the holo double mutant constructs were each capable of delivering an iron-sulfur cluster to apo protein targets, although with perturbed rate constants. Cluster transfer reactions were monitored over the course of 1 h by CD, as outlined earlier. Most holo double mutants transferred cluster to Fdx1 and Fdx2 targets more rapidly than the native protein, with a dramatic increase in rate observed for the C210A and C213A constructs (Table 13). All transfers to Grx3 were demonstrably slower than observed for native, with the smallest second-order rate constant observed for the C210S construct. The most varied response among the double mutants was observed in transfer to Grx2. None of the C210 double mutants were able to transfer cluster to Grx2, whereas the C213A transfer yielded a higher second-order rate constant, and the C213S transfer yielded a slightly lower rate constant (Table 13). Representative transfers are shown in Fig 12.

4.4 Discussion

Mutations of the human Fe/S protein NFU1 have been implicated in Multiple Mitochondrial Dysfunctions Syndrome 1 (MMDS1), with the majority of patients showing a glycine to cysteine mutation at residue 208 [32,38,43,47]. Previous *in vitro* studies

reported from our laboratory have examined the G208C mutation and suggest the disease condition to be a result of increased dimer formation in the apo state, which impairs cluster delivery to NFU1 from physiologically relevant sources and prevents downstream cluster transfer to key apo targets [108]. However, an additional disruptive possibility exists with the G208C mutation, in that the presence of an additional cysteine near the Fe/S cluster binding motif of CXXC may interfere or perturb the cluster coordination sphere due to the presence of a third potential cluster binding ligand. For this reason, we have sought to examine the influence of this extra cysteine on protein structure-function relationship and cluster stability via a series of residue substitutions in the cluster binding pocket (Table 1). Derivatives were made that 1) examined the role of position 208 (G208A and G208S), and 2) analyzed the possibility of altered cluster coordination motifs on NFU1 through a series of double mutant constructs that created either CXCXXA/S or CXA/SXXC motifs by substituting residues at positions 210 or 213 (Table 1). Alanine and serine are sterically similar to cysteine, but differ in polarity and ability to bind a Fe/S cluster. Replacement of a cysteine residue at position 210 or 213, by either an alanine or serine to create double mutants, has allowed us to delineate structural and functional effects based on position and residue.

To begin to examine the cluster binding motif and any alterations introduced by substitutions, we began with an analysis of apo protein stability characteristics. Purified protein constructs were first examined thermodynamically in terms of secondary and tertiary structure in the apo state using VTCD and DSC. No significant differences were observed in terms of melting temperature or enthalpy of melting when evaluating

secondary structure via VTCD for both the single and double mutant constructs (Tables 2 and 7), despite different contributions to secondary structural elements (Tables 3 and 8). Therefore, increasing the amount of random coil has not perturbed the overall level of protein stability for these NFU1 constructs such that there is no observable difference in melting temperature. Similar patterns were observed with DSC analysis, since there were no major differences in melting temperature or van't Hoff enthalpy relative to the native construct (Tables 4, 5, 9, and 10). Although no thermodynamic differences were observed, significant changes were observed in the shape of the DSC traces.

Our previous characterization of the native human NFU1 demonstrated two peaks in the melting trace, which were attributed to the molten globular C-terminal domain melting at the lower temperature and the structured N-terminal domain melting at the higher temperature [49]. However, characterization of the G208C apo state showed three melting peaks, which we attributed to the C-terminal domain unfolding followed by dimer dissociation and finally the N-terminal domain unfolding, based on the high percentage of dimer observed in AUC [92,93,108]. Surprisingly, none of the other 208 single mutants or the double mutant constructs demonstrated a third peak in the melting trace, which caused them to more resemble the native form (Figures 2 and 5). For the 208 single mutants, this likely correlates with the significantly lower percentages of dimer observed in AUC (Table 6, Figure 3). However for the double mutants, because the dimer form is still present, dimer unfolding most likely occurs in a concerted manner with the C-terminal domain, which has been observed for the native form of the protein [92,93,108]. The minor differences observed with the C-terminal melting temperature most likely reflect the percentage of

oligomer, which could shift the T_m either slightly higher or lower depending on the inherent stability of the complex.

Differences observed in the oligomeric states of the apo protein highlight the importance of the residue at position 208. Replacement of glycine with either alanine or serine, both with increased α-helical propensity [95], severely shifted the oligomeric state towards monomer (Table 6, Figure 3); whereas the native glycine and mutant cysteine, both with a decreased α-helical propensity [95], promoted dimer formation [108]. This trend extends to the double mutant variants, and provides a ready explanation for the observed changes in global structure. Having both the G208C mutation and the mutation at position 210 maintained the oligomeric trends of the single mutant form (Table 11, Figure 6), confirming the importance of the amino acid at position in 208 in dictating oligomerization trends. Furthermore, in addition to maintaining the dimer state, protein derivatives of G208C, with substitutions at 213, promote tetramer formation to almost a quarter or a half of the overall composition (Table 11), again highlighting the importance of residue 208 and showcases the functional role of the cluster binding motif in regulating structure-function relationships of human NFU1. Minor mutations to this motif promote global change in protein structure that both alter protein oligomerization, and influence downstream cluster binding and transfer capabilities.

The crucial nature of this structure-function relationship is observed in the ability of these NFU1 mutant variants to receive a Fe/S cluster from physiologically relevant sources. In the case of the G208C single mutant, the high prevalence of dimer prevented cluster uptake from either the $[2Fe\text{-}2S](GS)_4$ complex or scaffold donor proteins, such as

IscU, even in the presence of chaperones [108]. In accordance with this observation for G208C NFU1, the primarily monomeric G208A and G208S derivatives (Table 6) were both able to receive cluster from donor proteins (Table 12), and G208A was even able to take up cluster from the [2Fe-2S](GS)$_4$ complex (Fig 13). Similarly, all of the double mutants were unable to receive cluster from the same sources (Table 13), due to their high percentages of dimer and other higher-order oligomeric states (Fig 13). The inability of the double mutants to receive cluster was not due to dysfunctional Fe/S cluster binding motifs, as those same motifs have already been observed in nature [120-123] and the mutants were all able to undergo chemical reconstitution and cluster transfer to [2Fe-2S] cluster proteins (Table 13).

All of the mutant constructs made and tested herein were able to undergo reconstitution and transfer their Fe/S cluster to downstream targets. AUC of the holo proteins confirmed that the cluster-bound forms maintain oligomeric states similar to those observed in the native form, indicating a binding scenario similar to the native. However, just as the mutations altered the oligomeric states of the apo form, the cluster transfer activities of the holo form were also perturbed. In terms of the single mutant constructs, the second-order rate constants for transfer to either the ferredoxins or free GSH were drastically increased, while the rate constants for Grx3 were found to decrease (Table 12). This contrasts with the transfer reactions observed for G208C, which showed decreased rate constants for transfer to the ferredoxins, and unaffected transfer to free GSH [108]. Since the rates were so drastically different with the single mutants, which were designed to maintain the CXXC cluster binding motif on human NFU1, it is likely that the structural

change that perturbs the oligomeric state simultaneously dictates the effects observed on transfer reactivity; inasmuch as the mutation at position 208 alters the structural characteristics that in turn promotes transfer to ferredoxins with increased cluster reactivity. However, in the case of Grx3, the transfer reaction is slowed, most likely reflecting a structural change that either blocks a protein-protein interaction or perturbs the recognition surface in a unique way given the dimeric nature of Grx3, in contrast to monomeric ferredoxins.

Likewise, double mutant derivatives demonstrated the same overall trends with faster transfer to the ferredoxins and slower transfer to Grx3 (Table 13). Even with their altered cluster coordination spheres, a similar phenomena may be occurring in terms of the oligomeric states. The new coordination scheme could make the holo form of human NFU1 less stable and make cluster transfer to ferredoxin easier. Similarly, the new ligation sphere may alter protein structure and interfere with cluster transfer to Grx3 in the same manner as for the single mutants. Interestingly, the S variants of the double mutants, either at position 210 or 213, demonstrated transfer rates to the ferredoxins most like the native human NFU1 (Table 13). In these constructs, one possible explanation is that the serine can function as a cluster ligand to maintain the original spacing of the archetypical CXXC motif, as the supported by the native-like kinetic transfer rates [65,118]; however, UV and CD of the holo double mutant constructs yield similar spectra, which contrasts with prior optical characterization of cysteine to serine rubredoxin and ferredoxin mutants that demonstrate similar, yet less intense UV spectra and shifted peaks in CD spectra [118,124]. Alternatively, the serine substitution may perturb the structure of the reconstituted form

less than the equivalent alanine substitution promoting similar cluster transfer properties to the native protein.

For all of the mutant variants examined, the second-order rate constants for transfer to Grx2 did not seem to follow a clear trend. For the single mutants, the rate constant increased for G208A and decreased for G208S (Table 12). In terms of the double mutants, the rate constant for G208C C213A increased, but was observed to decrease for G208C C213S, while the 210 variants showed no transfer reaction at all (Table 13). These results reflect a very nuanced view of protein-protein interaction that is sensitive to minor perturbations in protein structure or oligomeric state, which is unique for each of the different constructs.

Together the rate data, in combination with the apo protein stability data and information on oligomeric states, provide insight into structure-function relationships for human NFU1. Our mutational analysis suggests that the G208C mutation does not contribute to cluster binding, but instead alters the overall structure-function relationships of the protein through changes in oligomerization state, and it is these more global structural changes, rather than any direct change in cluster coordination, that result in downstream effects that are manifest as MMDS1.

4.5 Figures and Tables

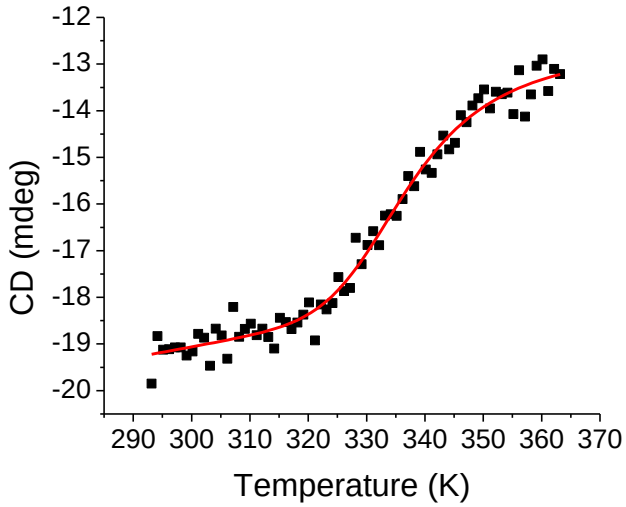

Figure 4-1 A representative VTCD trace for the melting of 10 μM G208A

in 40 mM phosphate, pH 7.4. Data were fit to equation 1 to obtain T_m and ΔH_V, which are shown in Table 2. CD units of ellipticity (mdeg) were used directly without conversion to molar ellipticity because the van't Hoff enthalpies are independent of such a factor [49].

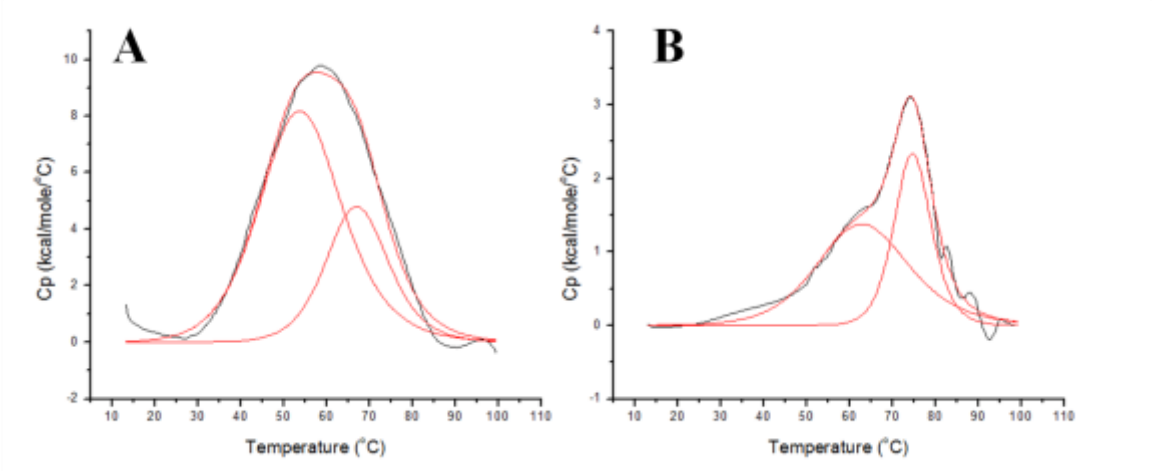

Figure 4-2 Differential scanning calorimetry profiles

for (**A**) G208A NFU1 and (**B**) G208S human NFU1.Both of the proteins were in 0.2 mM solutions in 50 mM HEPES, 100 mM NaCl, and pH 7.4. The data were fit using Origin 7.0 to obtain T_m, ΔH_{cal}, and ΔH_V values, all of which are listed in Tables 4 and 5.

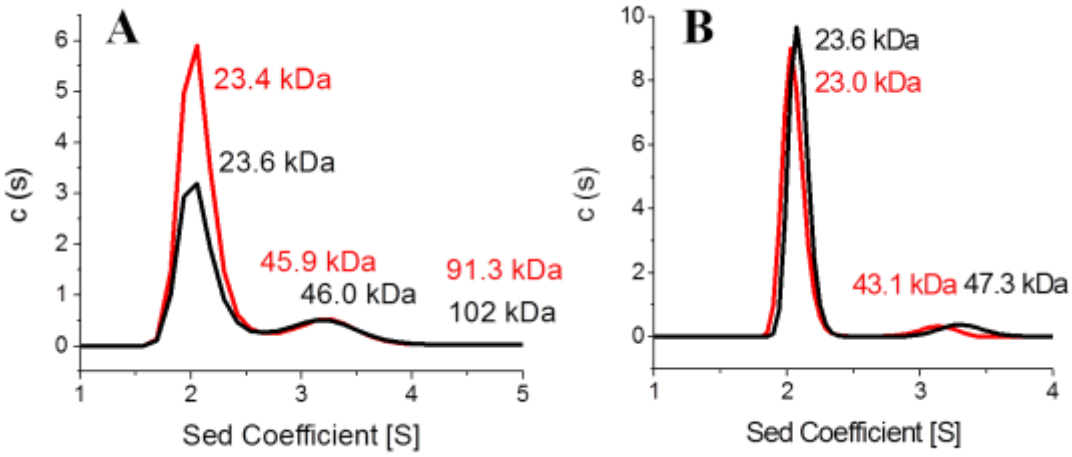

Figure 4-3 Analytical ultracentrifugation profiles for G208A and G208S NFU1.

(**A**) Apo G208A was sedimented in the absence of TCEP (black) and in the presence of 1 mM TCEP (red). Sedimentation was monitored at 280 nm. (B) Apo G208S was also sedimented in the absence of TCEP (black) and in the presence of 1 mM TCEP (red) and monitored at 280 nm. The AUC results were fit to the Lamm equation [79] using a continuous distribution model to obtain the peaks and molecular weights shown above. The AUC results are summarized in Table 6.

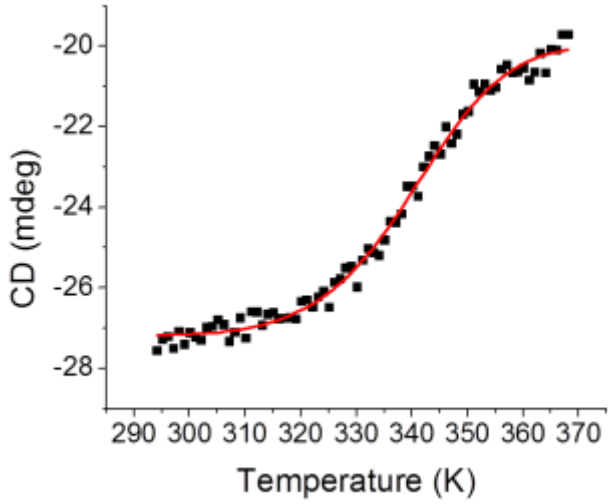

Figure 4-4 A representative VTCD trace

for the melting of 10 μM G208C C213A NFU1 in 40 mM phosphate, pH 7.4. Data were fit to equation 1 to obtain T_m and ΔH_V, which are shown in Table 2. CD units of ellipticity (mdeg) were used directly without conversion to molar ellipticity because the van't Hoff enthalpies are independent of such a factor [49].

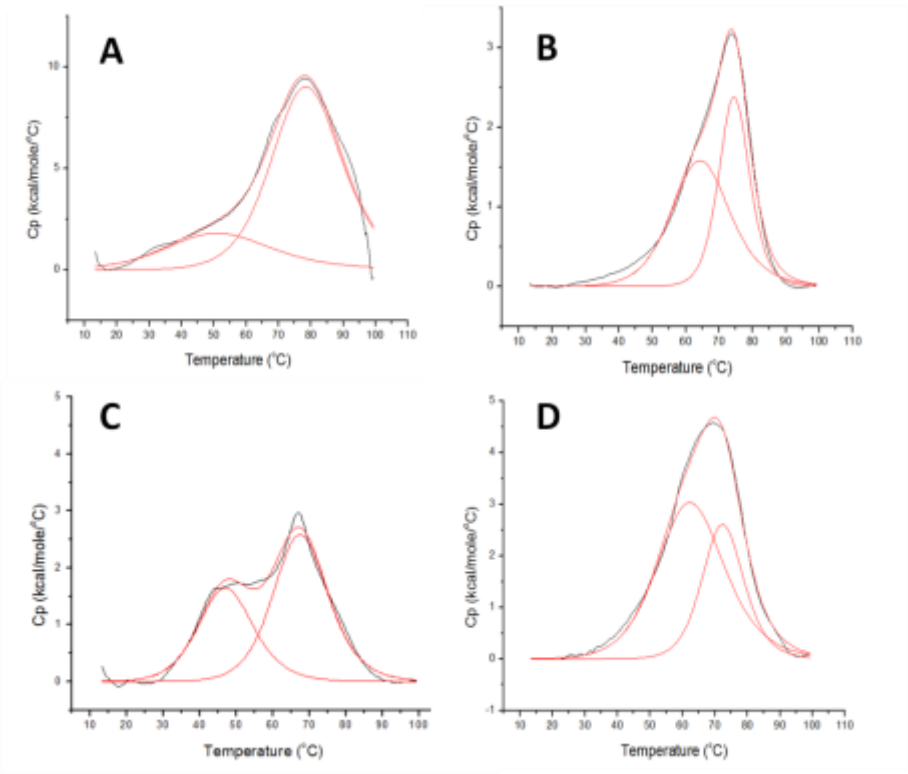

Figure 4-5 Differential scanning calorimetry profiles for the NFU1 double mutants.

(**A**) G208C C210A NFU1, (**B**) G208C C210S NFU1, (**C**) G208C C213A NFU1, and (**D**) G208C C213S NFU1. All of the proteins were 0.2 mM and in 50 mM HEPES, 100 mM NaCl, and pH 7.4. The data were fit using Origin 7.0 to obtain T_m, ΔH_{cal}, and ΔH_V values, all of which are listed in Tables 9 and 10.

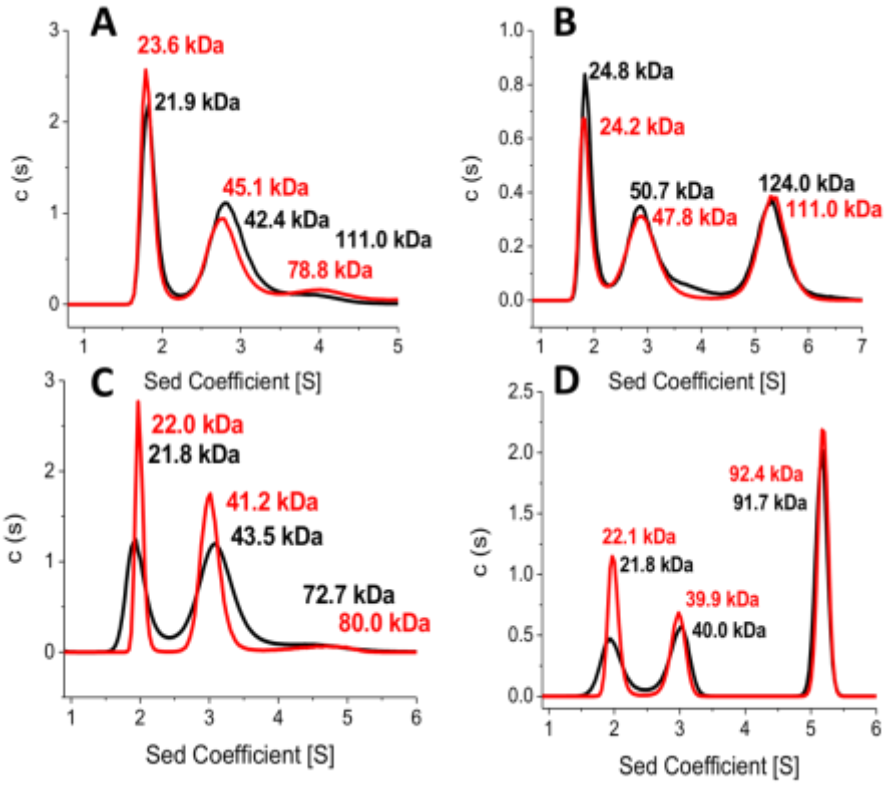

Figure 4-6 Analytical ultracentrifugation profiles for the NFU1 double mutants.

(**A**) Apo G208C C210A was sedimented in the absence of TCEP (black) and in the presence of 1 mM TCEP (red). Sedimentation was monitored at 280 nm. (**B**) Apo G208C and C213A, (**C**) Apo G208C and C210S, and (**D**) Apo G208C and C213S were also sedimented in the absence of TCEP (black) and in the presence of 1 mM TCEP (red) and monitored at 280 nm. The AUC results were fit to the Lamm equation [79,111] using a continuous distribution model to obtain the peaks and molecular weights shown above. The AUC results are summarized in Table 11.

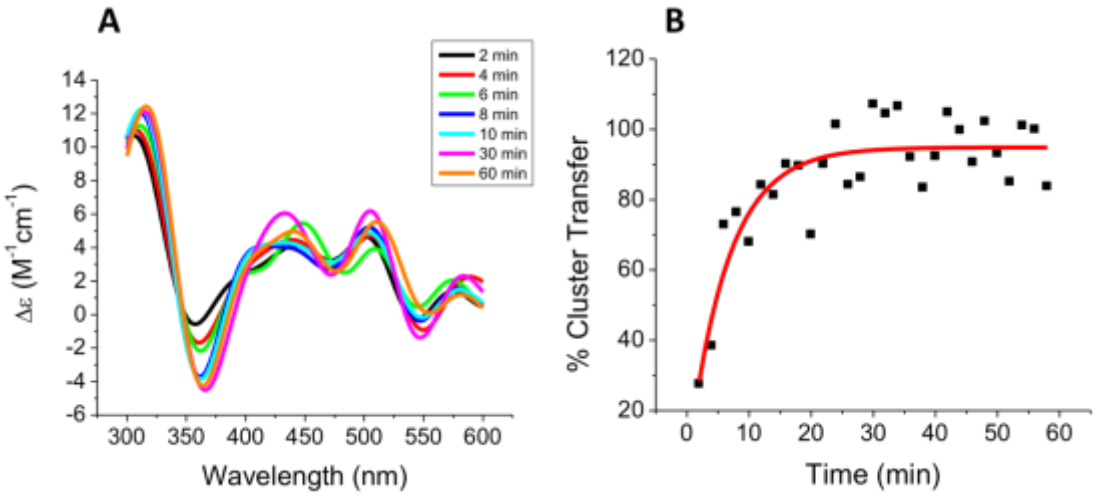

Figure 4-7 Kinetics of [2Fe-2S] cluster transfer from the [2Fe-2S](GS)$_4$ complex to apo G208A NFU1.

(**A**) Time course for cluster transfer monitored by CD in 50 mM HEPES, 100 mM NaCl, pH 7.5. Spectra were recorded every 2 min after the addition of the [2Fe-2S](GS)$_4$ complex and converted to percent cluster transfer (**B**) and fit using DynaFit [89] to yield the apparent second-order rate constant of 3500 ± 480 $M^{-1}min^{-1}$.

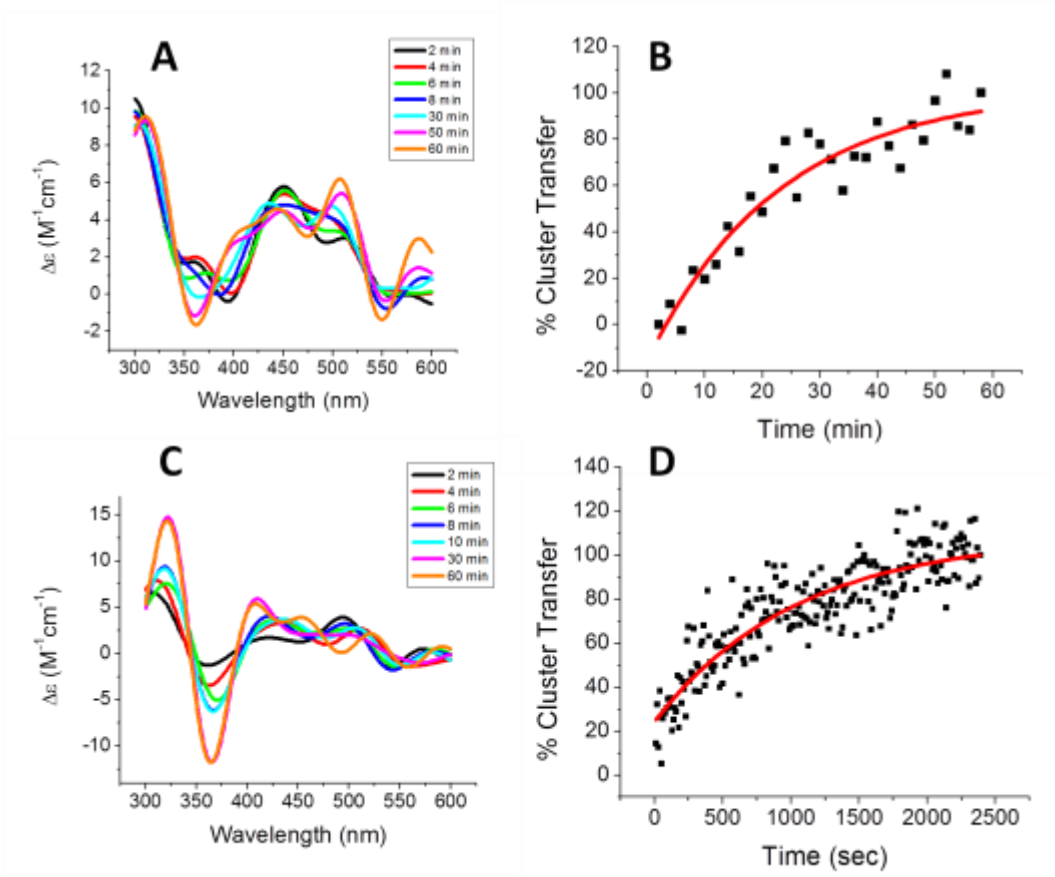

Figure 4-8 Kinetics of [2Fe-2S] cluster transfer from holo reconstituted Fe/S cluster donors IscU and Isa1 to apo G208S NFU1.

(**A**) Time course for cluster transfer from Isa1 to G208S NFU1 monitored by CD in 50 mM HEPES, 100 mM NaCl, pH 7.5. Spectra were recorded every 2 min following the addition of holo Isa1, and converted to percent cluster transfer (**B**) and fit using DynaFit [89] to yield an apparent second-order rate constant 3200 ± 850 M^{-1} min^{-1} based on the concentration of the [2Fe-2S] cluster. (**C**) Time course for cluster transfer from holo IscU to apo G208A NFU1 recorded by CD under the same conditions as for Isa1. (**D**) Due to the rapid cluster transfer, the reaction was run again at intervals of 10 sec, and the CD signal was converted to the percentage of cluster transferred with time to yield an apparent second-order rate constant of 2300 ± 90 M^{-1} min^{-1}.

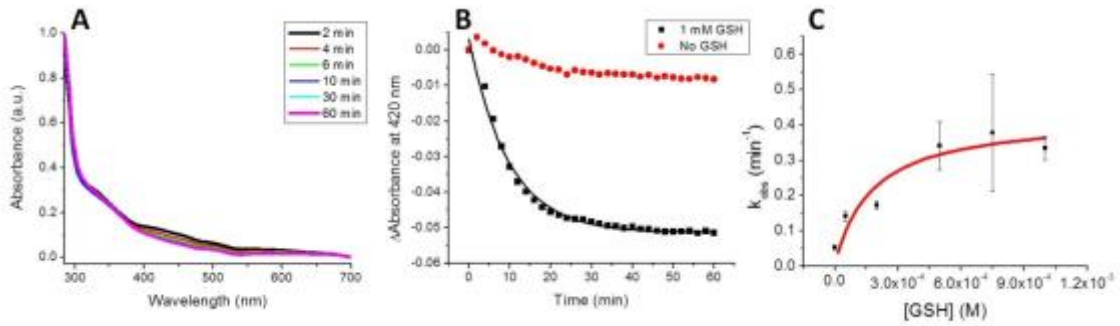

Figure 4-9 GSH extraction of the [2Fe-2S] cluster

from 10 μM reconstituted holo G208A human NFU1 to form the $[2Fe\text{-}2S](GS)_4$ complex. The change in absorbance at 420 nm was monitored over the course of one hour and data were fit to an exponential to obtain the k_{obs}. (**A**) Shows a representative UV trace of the reconstituted G208A in the presence of 200 μM GSH and the corresponding decrease in absorbance at 420 nm over the course of 1 h. (**B**) The change in absorbance at 420 nm was plotted against time for each of the different concentrations of GSH and fit to an exponential to obtain the k_{obs} for each concentration. Sample traces are shown for 1 mM GSH (black) and no GSH (red). (**C**) k_{obs} data was plotted against GSH concentration to determine an overall second-order rate constant of 520 ± 80 $M^{-1}min^{-1}$, an apparent dissociation constant K_D of 0.426 M and a first order rate constant k_1 for formation of the $[2Fe\text{-}2S](GS)_4$ complex of 1.7 x 10^{-4} min^{-1}, similar to values obtained with other glutathione extraction reactions [26].

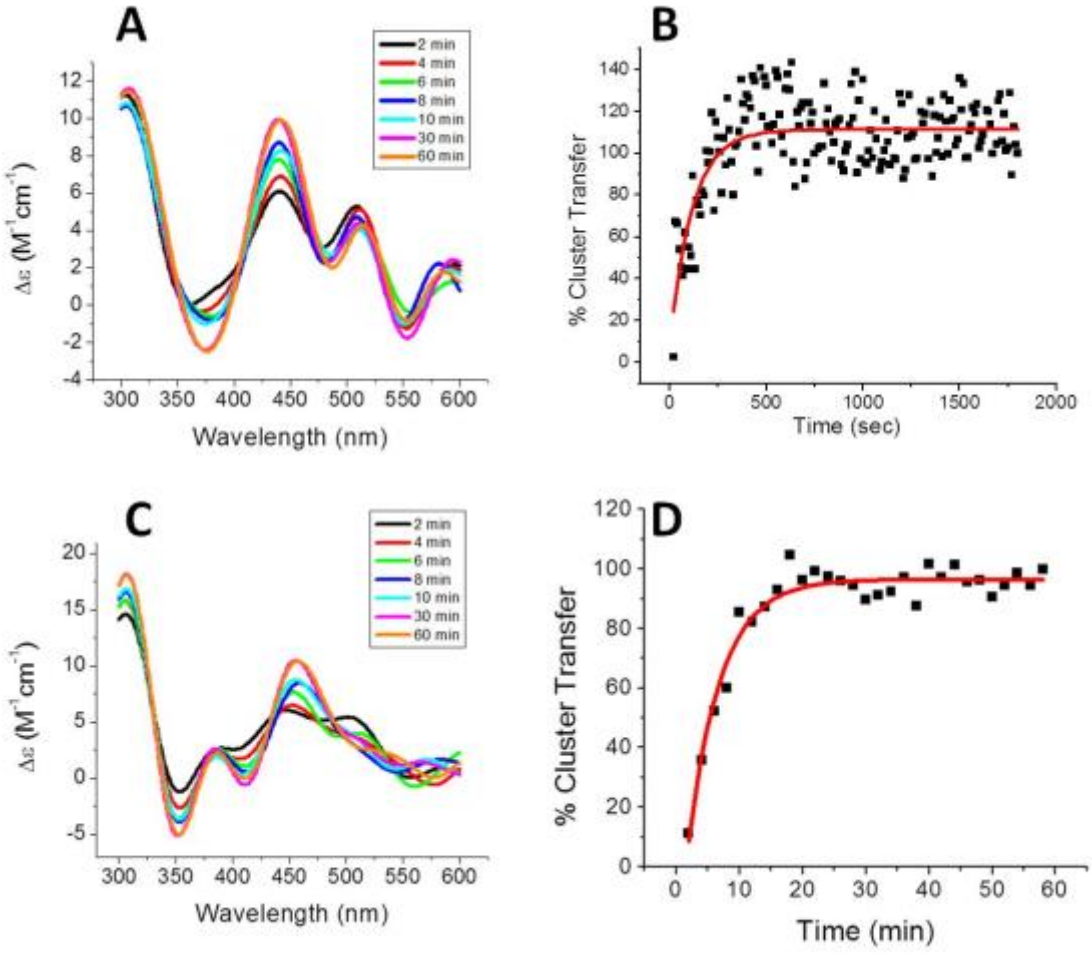

Figure 4-10 Kinetics of a representative [2Fe-2S] cluster transfer from holo reconstituted G208A NFU1 to apo targets.

(**A**) Time course for cluster transfer from G208A NFU1 to ferredoxin 1 (Fdx1) monitored by CD in 50 mM HEPES, 100 mM NaCl, pH 7.5. Spectra were recorded every 2 min after the addition of holo G208A, and converted to percent cluster transfer. Due to the rapid cluster transfer, the reaction was monitored again at intervals of 10 sec at 445 nm and percent cluster transfer data (**B**) was extracted and fit using DynaFit [89] to yield an apparent second-order rate constant 12000 ± 2800 $M^{-1}min^{-1}$ based on the concentration of the [2Fe-2S] cluster. (**C**) Time course for cluster transfer from holo G208A to apo glutaredoxin 3 (Grx3) recorded by CD under the same conditions as for Fdx1. (**D**) CD signal was converted to the percentage of cluster transferred with time to yield an apparent second-order rate constant 5600 ± 170 $M^{-1}min^{-1}$.

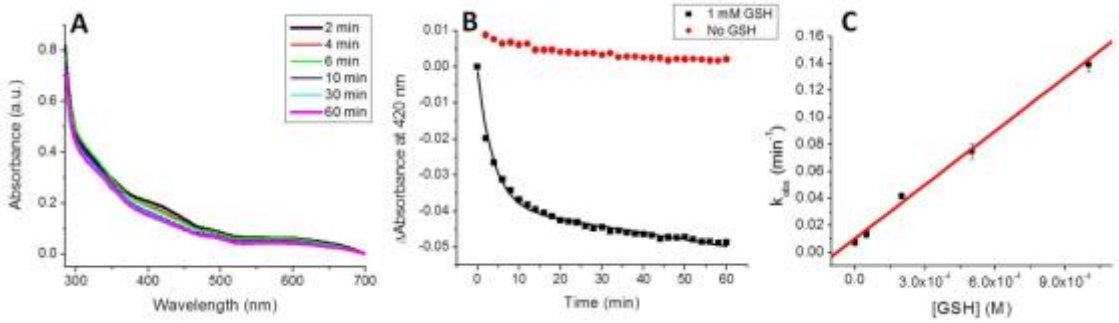

Figure 4-11 GSH extraction of the [2Fe-2S] cluster

from 10 μM reconstituted holo G208C C213A human NFU1 to form the [2Fe-2S](GS)$_4$ complex. The change in absorbance at 420 nm was monitored over the course of an hour and data were fit to an exponential decay to obtain k_{obs}. (**A**) Shows a representative UV trace for reconstituted G208C C213A NFU1 in the presence of 500 μM GSH and the corresponding decrease in absorbance at 420 nm over the course of 1 h. (**B**) The change in absorbance at 420 nm was plotted against time for each of the different concentrations of GSH and fit to an exponential to obtain k_{obs} for each concentration. Sample traces are shown for 1 mM GSH (black) and no GSH (red). (**C**) k_{obs} data was plot against the concentration of GSH and fit to a linear equation to yield an overall second-order rate constant of 133 ± 5 $M^{-1}min^{-1}$.

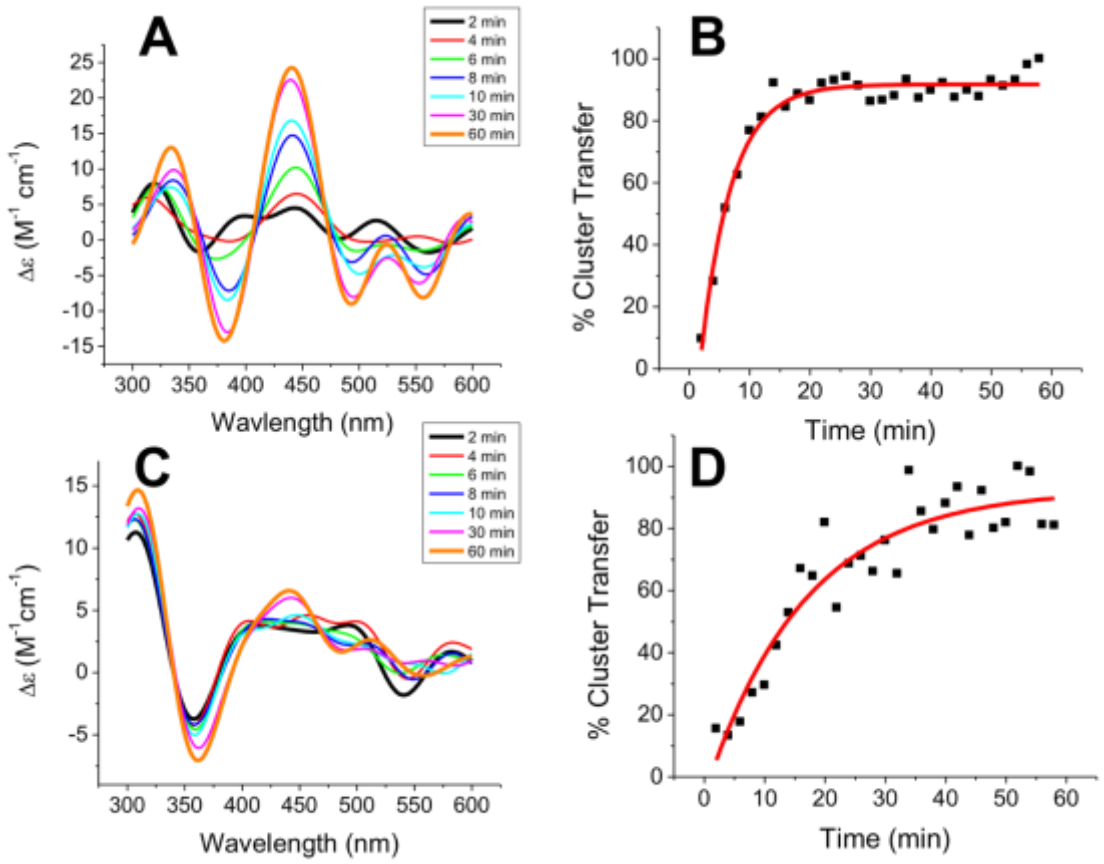

Figure 4-12 Kinetics of a representative [2Fe-2S] cluster transfer from holo reconstituted human G208C C213A NFU1 to apo human ferredoxin and glutaredoxin.

(**A**) Time course for cluster transfer to ferredoxin 1 (Fdx1) monitored by CD in 50 mM HEPES, 100 mM NaCl, pH 7.5. Spectra were recorded every 2 min following the addition of holo NFU1, and converted to percent cluster transfer (**B**) and fit using DnyaFit [89] to yield an apparent second-order rate constant 19000 ± 2900 $M^{-1}min^{-1}$ based on the concentration of the [2Fe-2S] cluster. (**C**) Time course for cluster transfer from holo human NFU1 to apo human glutaredoxin 2 (Grx2) recorded by CD under the same conditions as for Fdx1. (**D**) The CD signal was again converted to the percentage of cluster transferred with time to yield an apparent second-order rate constant of 8800 ± 3800 $M^{-1}min^{-1}$.

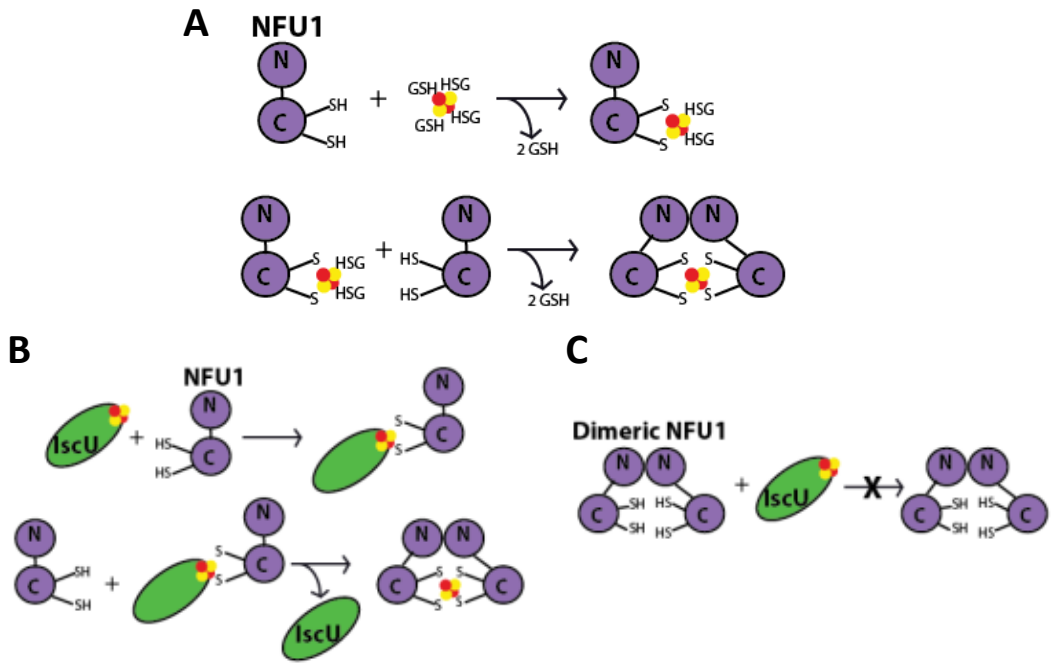

Figure 4-13 (**A**) A model for [2Fe-2S] cluster uptake by monomeric NFU1,

such as in the case of native and G208A, from the [2Fe-2S](GS)$_4$ cluster complex to form an intermediate [2Fe-2S] species with two exogenous GSH ligands. NFU1 is represented by the N and C terminal domains. A second monomeric NFU1 displaces the GSH molecules to form [2Fe-2S] dimeric NFU1. (**B**) A model for [2Fe-2S] cluster uptake by monomeric NFU1 from a [2Fe-2S] cluster scaffold, such as IscU, as in the case of native and G208S. Holo IscU interacts with monomeric NFU1 to form a transient heterodimeric complex. A second NFU1 monomeric displaces the now apo IscU to form the holo NFU1 dimer. In a case where NFU1 is a pre-formed dimer (**C**)**,** such as in the G208C mutant and the double mutants, the dimeric NFU1 is unable to form the transient complex with holo IscU and therefore unable to receive the [2Fe-2S] cluster. Adapted from [28,108].

Construct	Sequence	Construct	Sequence
Native	QGSCTSCP	G208C C210A	QCSATSCP
G208C	QCSCTSCP	G208C C210S	QCSSTSCP
G208A	QASCTSCP	G208C C213A	QCSCTSAP
G208S	QSSCTSCP	G208C C213S	QCSCTSSP

Table 4-1The series of point mutations designed in the native NFU1 construct,

relative to the native construct and the physiologically-relevant disease-causing G208C mutation. The glycine residue at position 208 was replaced with either alanine or serine, to monitor substitution effects related to size or alterations in Fe/S cluster binding. Double mutant constructs were created by maintaining the G208C mutation and replacing one of the cluster-binding cysteine residues at 210 or 213 with either alanine or serine to investigate differences in cluster-binding behavior as a result of change to the typical CXXC motif.

	T_m (°C)	ΔH_v (kcal/mol)
Native	65 ± 0.5	-26 ± 2
G208A	66 ± 2	-25 ± 6
G208C	64 ± 2	-31 ± 2
G208S	65 ± 0.5	-32 ± 2

Table 4-2 Single mutant variable temperature circular dichroism results.

Proteins at 10 μM were subjected to melting from 20 to 95 °C at 0.4 °C per min. Data were fit to a one-state melting process using equation 1 [49,108].

	α-helix	β-sheet	Random Coil
Native	47 %	21 %	33 %
G208A	21 %	22 %	58 %
G208C	37 %	17 %	46 %
G208S	25 %	20 %	55 %

Table 4-3 Percentages of single mutant secondary structural elements

measured by circular dichroism and analyzed using the analysis program CDSSTR [73] on the online Dichroweb server [75,76,108].

	T_m1 (°C)	T_m2 (°C)	T_m3 (°C)
Native	59 ± 1	--	73 ± 1
G208A	52 ± 3	--	74 ± 1
G208C	49 ± 6	64 ± 2	74 ± 4
G208S	61 ± 3	--	75 ± 1

Table 4-4 Single mutant melting temperatures determined from fits to DSC data.

The DSC profiles used for fitting are shown in Figure 2 [108].

	ΔH_{cal1}	ΔH_{v1}	ΔH_{cal2}	ΔH_{v2}	ΔH_{cal3}	ΔH_{v3}
Native	73 ± 2	39 ± 1	--	--	122 ± 2	77 ± 1
G208A	25 ± 4	34 ± 1	--	--	35 ±19	43 ± 5
G208C	5 ± 1	33 ± 4	39 ± 2	50 ± 2	23 ± 4	74 ± 16
G208S	39 ± 2	32 ± 1	--	--	34 ± 9	76 ± 7

Table 4-5 Single mutant enthalpies of melting determined by DSC

All values in kcal/mol. The DSC profiles used for data fitting are shown in Figure 2 [108].

	Monomer	With TCEP	Dimer	With TCEP	Tetramer	With TCEP
Native	45 %	44 %	52 %	44 %	0 %	0 %
G208A	70 %	76 %	22 %	14 %	2 %	1 %
G208C	29 %	30 %	58 %	60 %	6 %	1.5 %
G208S	90 %	93 %	8 %	7 %	0%	0%

Table 4-6 Analytical ultracentrifugation results of the single mutants

in the presence and absence of TCEP. The obtained molecular weights were classified according to the most likely corresponding oligomeric state [108,111].

	T_m (°C)	ΔH_v (kcal/mol)
Native	65.3 ± 0.5	-26 ± 2
G208C C210A	70 ± 3	-26 ± 1
G208C C210S	69 ± 0.5	-38 ± 10
G208C C213A	68 ± 1	-30 ± 5
G208C C213S	67 ± 0.5	-33 ± 5

Table 4-7 Double mutant variable temperature circular dichroism results.

Proteins at 10 μM were subjected to melting from 20 to 95 °C at 0.4 °C per min. Data were fit to a one-state melting process using equation 1 [108].

	α-helix	β-sheet	Random Coil
Native	0.47	0.21	0.33
G208C C210A	0.24	0.19	0.57
G208C C210S	0.19	0.21	0.61
G208C C213A	0.44	0.21	0.36
G208C C213S	0.42	0.18	0.4

Table 4-8 Percentages of double mutant secondary structural elements

measured by circular dichroism and analyzed using the analysis program CDSSTR [73] on the online Dichroweb server [75,76,108].

	T_m1 (˚C)	T_m2 (˚C)
Native	59 ± 1	73 ± 1
G208C C210A	54 ± 4	79 ± 1
G208C C210S	57 ± 4	74 ± 2
G208C C213A	48 ± 1	66 ± 2
G208C C213S	63 ± 1	72 ± 2

Table 4-9 Double mutant melting temperatures determined from fits to DSC data.

The DSC profiles used for fitting are shown in Figure 5 [49,108].

	ΔH_{cal1}	ΔH_{v1}	ΔH_{cal2}	ΔH_{v2}
Native	73 ± 2	39 ± 1	122 ± 2	77 ± 1
G208C C210A	87 ± 8	20 ± 1	119 ± 9	35 ± 5
G208C C210S	37 ± 2	30 ± 4	53 ± 3	68 ± 2
G208C C213A	115 ± 4	45 ± 6	91 ± 4	46 ± 1
G208C C213S	17 ± 7	32 ± 1	46 ± 3	50 ± 6

Table 4-10 Double mutant enthalpies of melting determined by DSC

All values in kcal/mol. The DSC profiles used for data fitting are shown in Figure 5 [49,108].

	Monomer	With TCEP	Dimer	With TCEP	Higher-Order	With TCEP
Native	45%	44%	52%	44%	--	--
C210A	40%	44%	54%	46%	1%	5.1%
C210S	33%	36%	58%	58%	1%	4%
C213A	35%	31%	46%	41%	16%	21%
C213S	21%	25%	23%	21%	47%	46%

Table 4-11 Analytical ultracentrifugation results fot the double mutant NFU1 proteins

in the presence and absence of TCEP. The obtained molecular weights were classified according to the most likely corresponding oligomeric state. The designation of higher-order includes both trimer and tetramer.

	Native	G208C	G208A	G208S
Human NFU1 to human Fdx1	4700 ± 820	2560 ± 340	12000 ± 2800	19000 ± 1700
Human NFU1 to human Fdx2	3800 ± 1250	1180 ± 220	13000 ± 1500	20000 ± 510
Human NFU1 to human Grx2	3700 ± 77	22400 ± 5000	6300 ± 380	1500 ± 97
Human NFU1 to *S. cerivisiae* Grx3	36000 ± 7700	14500 ± 3500	5600 ± 170	2900 ± 420
Human IscU to human NFU1	4750 ± 8	No transfer	No transfer	2300 ± 90
S. pombe Isa1 to human NFU1	6700 ± 1560	No transfer	No transfer	3200 ± 850
GSH-Fe-S to human NFU1	1930 ± 212	No transfer	3500 ± 500	No transfer
Human NFU1 to GSH	130 ± 22	142 ± 24	520 ± 80	210 ± 70

Table 4-12 Apparent second-order rate constants determined using CD for [2Fe-2S] cluster transfer to and from native and single mutant NFU1.

Native and G208C transfer rates were previously determined [27,28,90]. All rate constant units are $M^{-1}min^{-1}$.

	Native	G208C C213A	G208C C213S	G208C C210A	G208C C210S
Human NFU1 to human Fdx1	4700 ± 820	19000 ± 2900	5100 ± 800	23000 ± 6600	7500 ± 2000
Human NFU1 to human Fdx2	3800 ± 1250	7700 ± 1100	4100 ± 540	12000 ± 3700	3100 ± 420
Human NFU1 to human Grx2	3700 ± 80	8800 ± 3800	2500 ± 30	No transfer	No transfer
Human NFU1 to *S. cerivisiae* Grx3	36000 ± 7700	16600 ± 3000	13000 ± 4400	17100 ± 2900	7400 ± 1500
Human IscU to human NFU1	4750 ± 8	No transfer	No transfer	No transfer	No transfer
S. pombe Isa1 to human NFU1	6700 ± 1560	No transfer	No transfer	No transfer	No transfer
GSH-Fe-S to human NFU1	1930 ± 212	No transfer	No transfer	No transfer	No transfer
Human NFU1 to GSH	122 ± 22	133 ± 5	250 ± 10	60 ± 3	81 ± 8

Table 4-13 Apparent second-order rate constants determined using CD for [2Fe-2S] cluster transfer to and from native and double mutant NFU1.

Native transfer rates were previously determined [27,28,90]. All rate constant units are $M^{-1}min^{-1}$.

Appendix A : Chapter 2 Supplementary Data

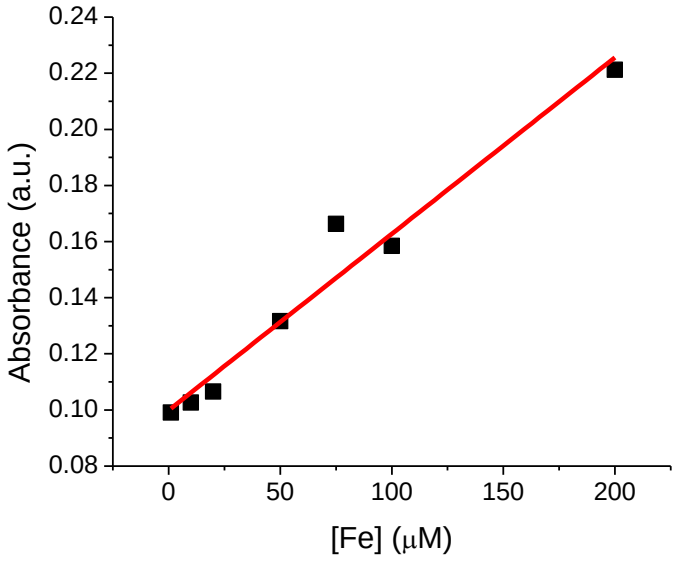

Figure A-1 Standard curve for iron quantitation.

Absorbance at 535 nm was measured by UV-Vis spectroscopy for 1 - 200 μM $FeCl_3$ standard solutions to generate the calibration curve, which was then utilized to determine the iron concentration for the holo proteins.

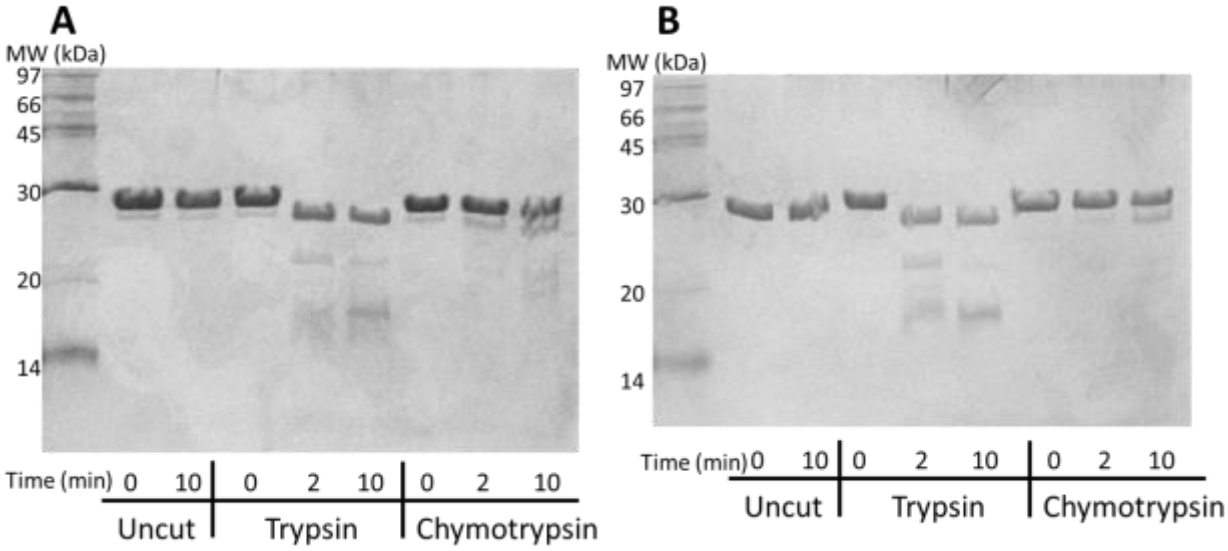

Figure A-2 Limited proteolysis of native human NFU1 (**A**) and G208C NFU1 (**B**).

Both proteins (0.5 mg/mL) were incubated with the specified protease (none, trypsin, or chymotrypsin) in a 1:100 ratio of protease:protein in 50 mM HEPES, 100 mM NaCl, 5 mM $CaCl_2$, pH 7.5. After 0, 2, 10 min at room temperature, the reaction was quenched by the addition of reducing SDS sample buffer, supplemented with 2 mM PMSF and 10 mM EDTA [125]. Samples were boiled for 5 minutes at 95 °C and separated on a 15% SDS-PAGE gel, which was visualized with Coomassie staining.

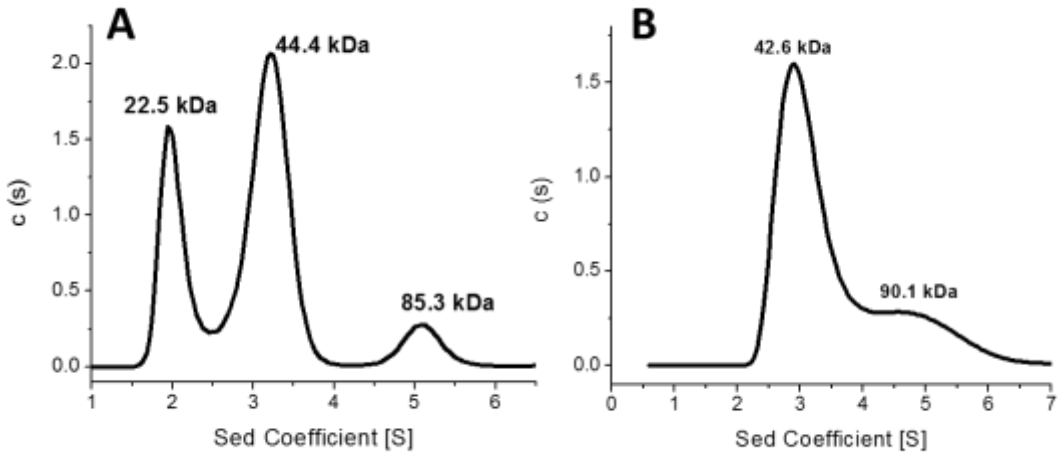

Figure A-3 Analytical ultracentrifugation profiles for holo G208C NFU1.

(**A**) Sedimentation was monitored at 280 nm, and the AUC results were fit to the Lamm equation [79,111] using a continuous distribution model to obtain the peaks and molecular weights shown above. The first peak at 22.5 kDa accounts for 25% of the sample, the second peak at 44.4 kDa accounts for 50%, and the third peak at 85.3 kDa accounts for 7%. (**B**) Sedimentation of holo G208C was monitored at 420 nm and fit the Lamm as equation as for the 280 nm trace. The first peak at 42.6 kDa accounts for 65.6% of the sample, and the second peak at 90.a kDa accounts for 16.6%.

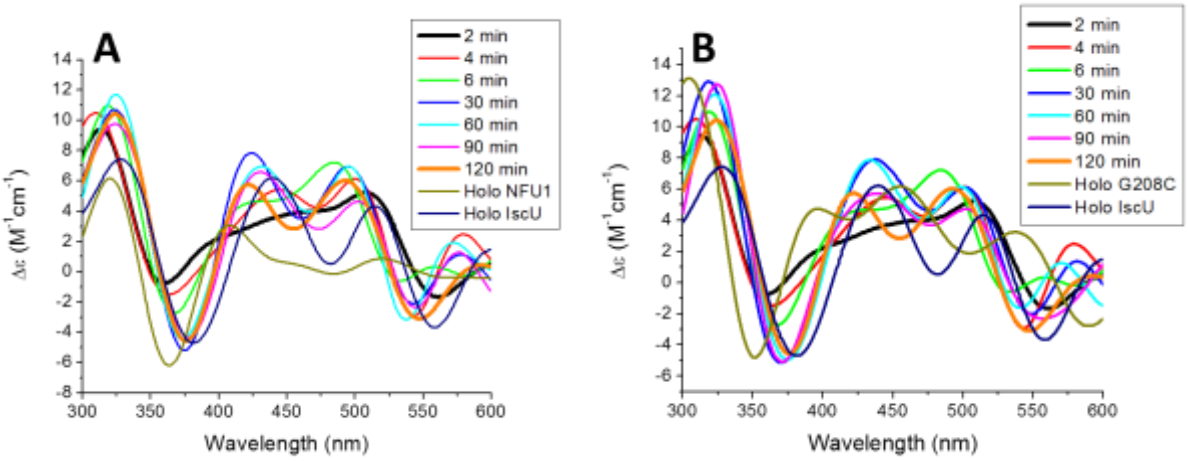

Figure A-4 Cluster transfer from IscU in the presence of chaperones.

Cluster transfer from holo human IscU (30 μM) to (**A**) apo human NFU1 (30 μM) or (**B**) apo human G208C NFU1 (30 μM). Both transfer reactions were carried out in the presence of 22 μM HspA9, 22 μM Hsc20, 40 mM MgCl2 and 2 mM ATP and monitored by UV-vis CD spectroscopy under anaerobic conditions in semi-micro 1 cm cuvette at room temperature. UV-vis CD spectra were recorded every 2 min for 60 min following addition of $MgCl_2$ and ATP, and then the cluster-bound holo human IscU.

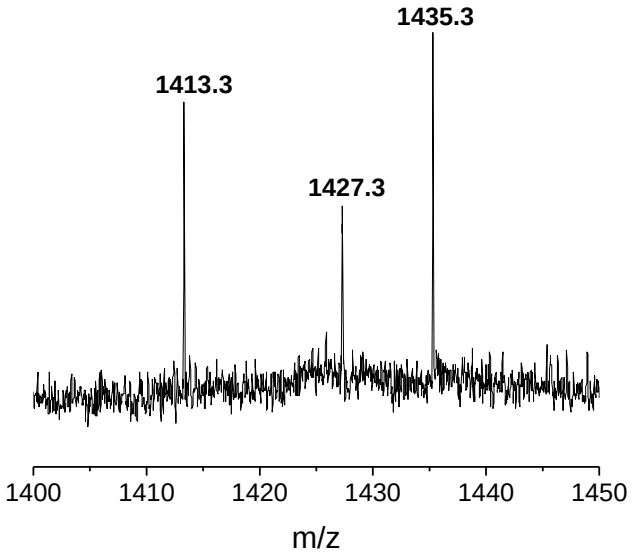

Figure A-5 ESI-MS spectrum showing the cluster complex

at 1427.3 and reaction intermediates at m/z of 1413.3 and 1435.3 representing sodium adducts of the [2Fe-2S](GS)$_4$ complex [126,127]. Holo G208C NFU1 at 100 μM was incubated anaerobically with 10 mM GSH, pH 8.6 for 2 h. The resulting reaction mixture was injected into a Bruker Micro-TOF (ESI) spectrometer in negative mode to generate the spectrum.

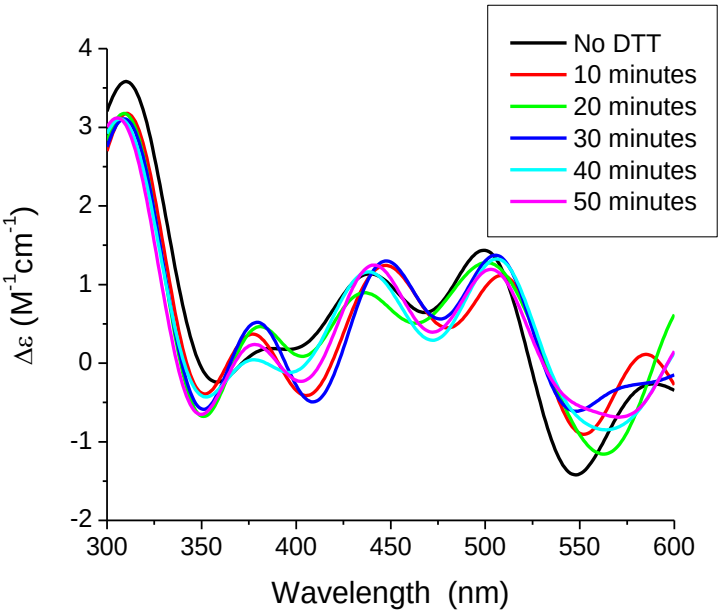

Figure A-6 DTT Incubation

Holo G208C at 20 µM was incubated with 5 mM DTT for 50 min and monitored by CD.

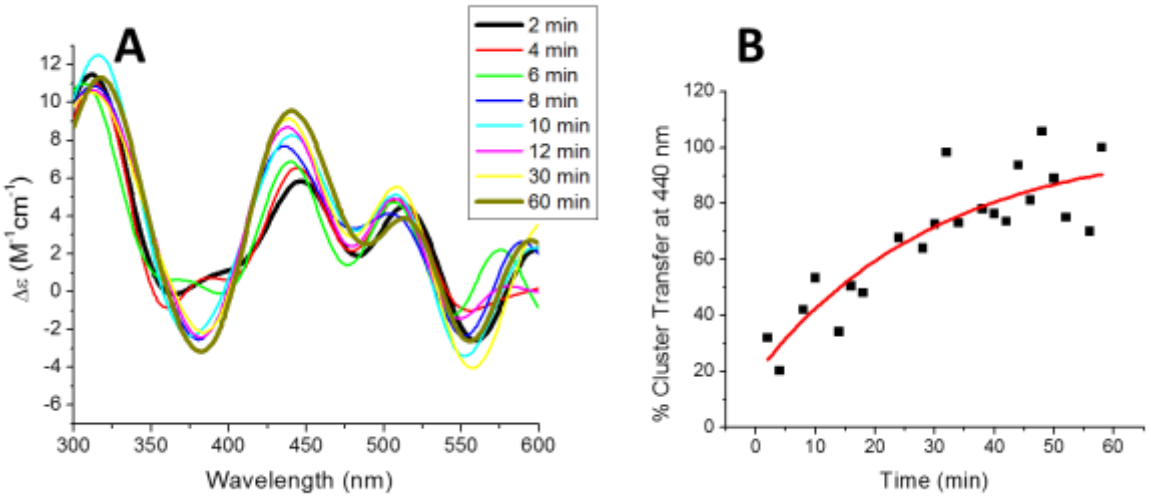

Figure A-7 Holo IscU to Fdx2 with chaperones.

Cluster transfer from holo human IscU (30 μM) to apo human Fdx2 (30 μM) in the presence of 22 μM HspA9, 22 μM Hsc20, 40 mM MgCl2 and 2 mM ATP monitored by UV-vis CD spectroscopy under anaerobic conditions in semi-micro 1 cm cuvette at room temperature. UV-vis CD spectra were recorded every 2 min for 60 min following addition $MgCl_2$ and ATP, and then the cluster bound form holo human IscU. The kinetics of appearance of the holo ferredoxin 2 CD signal **(A)** was monitored. The change in extinction values are based on the initial $[2Fe\text{-}2S]^{2+}$ cluster concentration. The apparent second order rate constants obtained for each reaction were determined as (**B**) 2400 ± 970 M^{-1} min^{-1}.

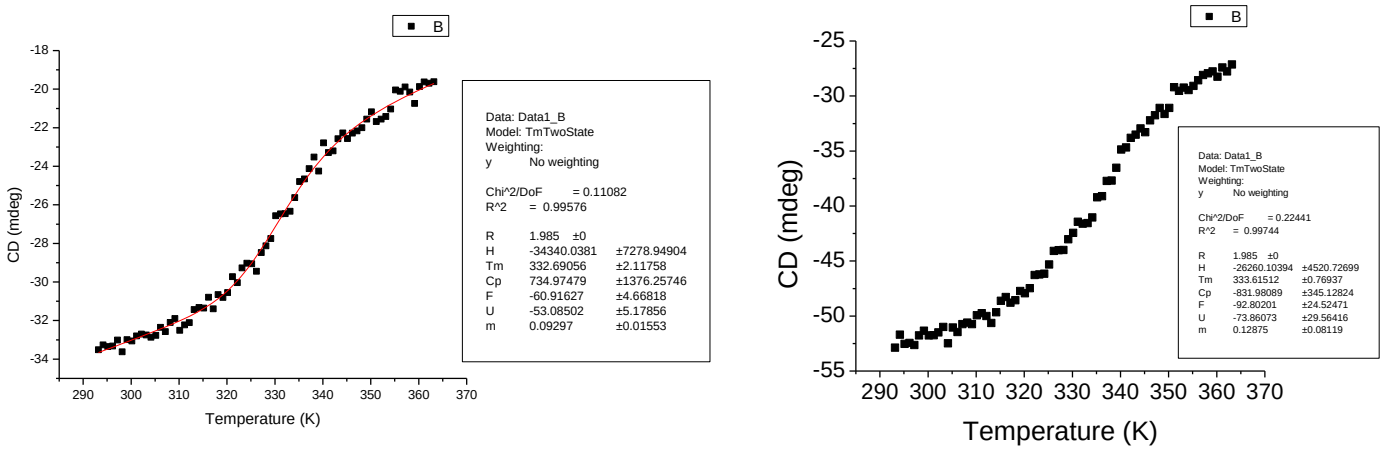

Figure A-8 Holo VTCD traces

of native NFU1 (left) and G208C NFU1 (right). Both traces were fit to a one-state model using equation 1.

	Rate Constant in the Absence of Chaperones ($M^{-1}min^{-1}$)	Rate Constant in the Presence of Chaperones ($M^{-1}min^{-1}$)
Human IscU to human Fdx2	2400 ± 1400 [27]	2400 ± 970

Table A-1 Apparent second-order rate constants

determined using CD for [2Fe-2S] cluster transfer from holo human IscU to apo human ferredoxin 2 in the absence and presence of the human co-chaperone system and MgATP. The transfer rate without the chaperone system was previously determined using the same CD method [27].

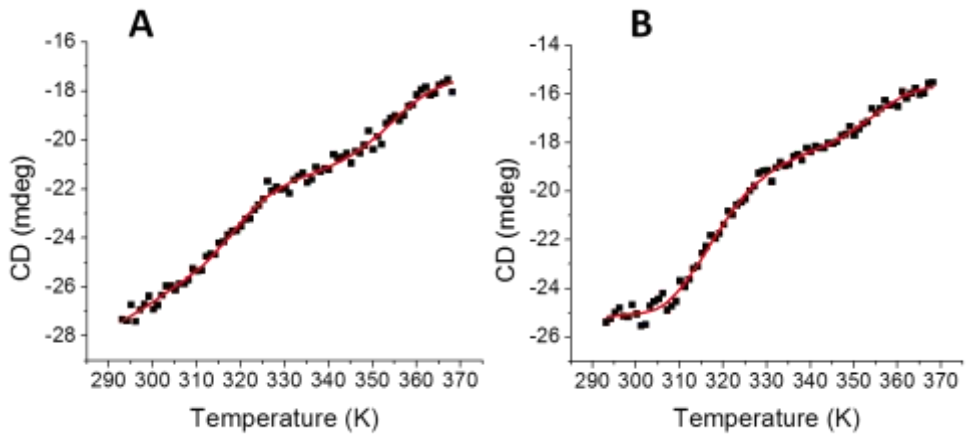

Figure B-1: VTCD trace for the melting of 10 μM (**A**) G189A and (**B**) G189K NFU1

in 40 mM phosphate, pH 7.4. Data were fit to equation 1 to obtain T_m and ΔH_V values, which are summarized in Table 1. CD units of ellipticity (mdeg) were used directly without conversion to molar ellipticity because the van't Hoff enthalpies are independent of such a factor [49].

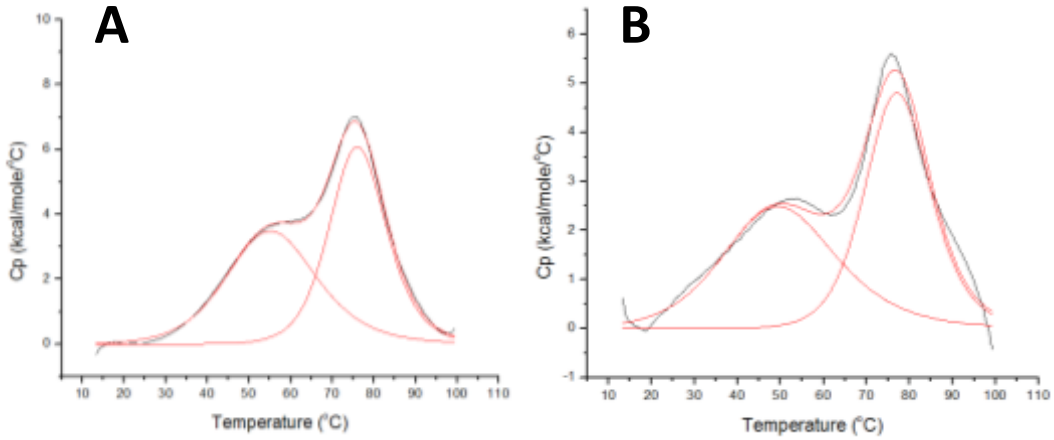

Figure B-2 Differential scanning calorimetry profiles for (**A**) 0.2 mM G189A human NFU1, (**B**) 0.15 mM G189K human NFU1

Both of the proteins were in 50 mM HEPES, 100 mM NaCl, and pH 7.4. The data were fit using Origin 7.0 to obtain T_m and ΔH_V, which are listed in Tables 3 and 4.

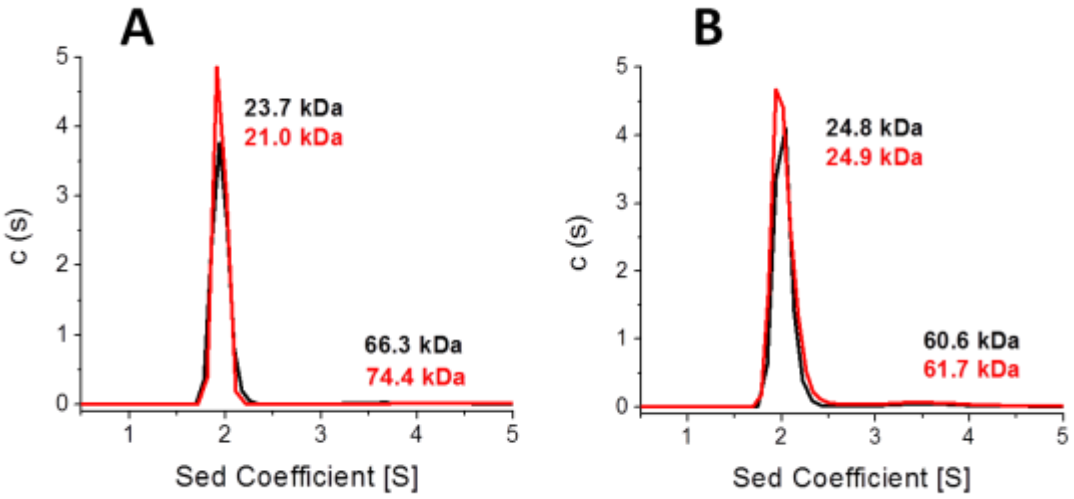

Figure B-3 AUC profile for (**A**) apo G189A NFU1 and (**B**) apo G189K NFU1

Apo protein was sedimented in the absence of TCEP (black) and in the presence of 1 mM TCEP (red). Sedimentation was monitored at 280 nm. For G189A NFU1, the first peak of the black trace at 23.7 kDa accounts for 95% of the sample, and the second peak at 66.3 kDa accounts for 3%. The first peak of the red trace at 21.0 kDa accounts for 69% of the sample, and the second peak at 74.4 kDa accounts for 2%. For G189K, the first peak of the black trace at 24.8 kDa accounts for 93% of the sample, and the second peak at 60.6 kDa accounts for 5% of the sample. The first peak of the red trace at 24.9 kDa accounts for 89% of the sample, and the second peak at 61.7 kDa accounts for 6% of the sample. The AUC results were fit to the Lamm equation [79,111] using a continuous distribution model to obtain the peaks and molecular weights shown above.

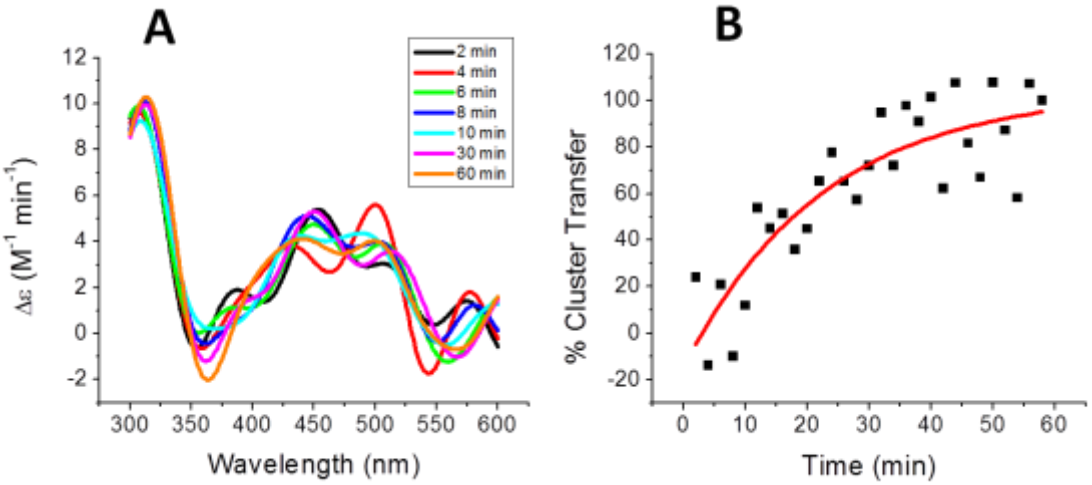

Figure B-4 A [2Fe-2S] cluster transfer from holo reconstituted *S. pombe* Isa1 to apo G189A NFU1

(**A**) Time course for cluster transfer to G189A NFU1 monitored by CD in 50 mM Hepes and 100 mM NaCl (pH 7.5). Spectra were recorded every 2 min after the addition of holo Isa1 and were converted to percent cluster transfer (**B**) to yield an apparent second-order rate constant from DynaFit of 1800 ± 100 M^{-1} min^{-1} based on the concentration of the [2Fe-2S] cluster [89].

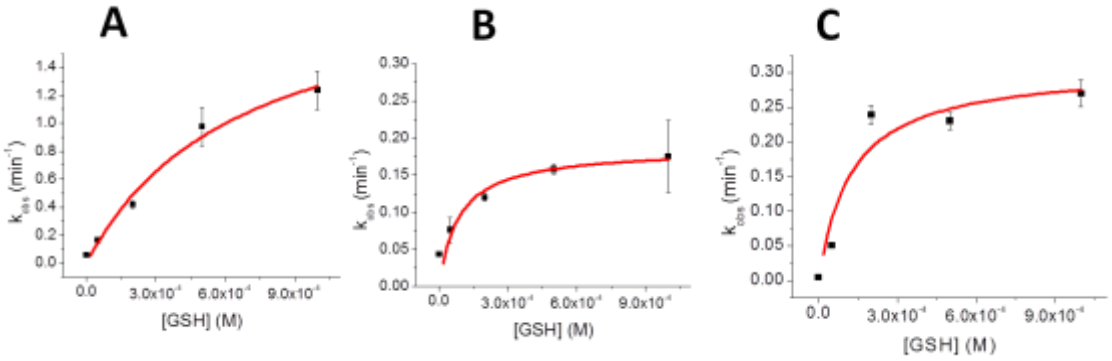

Figure B-5 GSH extraction of the [2Fe-2S] cluster from G189X NFU1
(**A**) 10 μM G189R NFU1, (**B**) 10 μM G189A NFU1, and (**C**) 10 μM G189K NFU1, to form the [2Fe-2S](GS)$_4$ complex. The change in absorbance at 420 nm was monitored over the course of one hour and the initial slopes were fit to an linear equation to obtain k_{obs} values that were subsequently plotted against GSH concentration to determine an overall second-order rate constant of 1800 ± 30 $M^{-1}min^{-1}$ for (**A**), 360 ± 70 $M^{-1}min^{-1}$ for (**B**), and 1200 ± 70 $M^{-1}min^{-1}$ for (**C**). The data were also fit to an exponential equation to determine the apparent K_d and first-order rate constants (Table S2) [26].

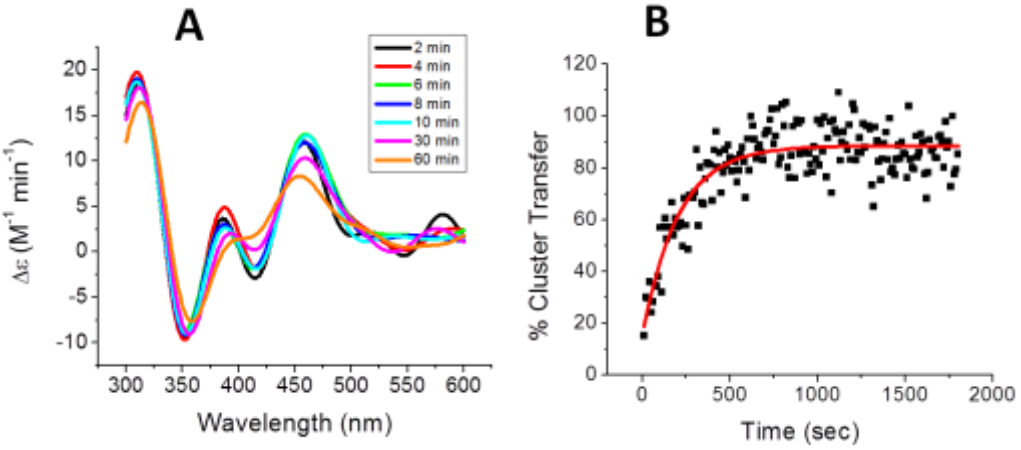

Figure B-6 A representative [2Fe-2S] cluster transfer reaction monitored using circular dichroism spectroscopy.

(**A**) Time course of [2Fe-2S] cluster transfer from holo reconstituted human G189R NFU1 to apo *S. cerevisiae* glutaredoxin 3 (Grx3) monitored by CD in 50 mM Hepes and 100 mM NaCl (pH 7.5). Spectra were recorded every 2 min after the addition of holo G189R NFU1. However transfer was too rapid to monitor, so cluster transfer was monitored from 465-455 nm every 10 sec and converted to percent cluster transfer (**B**) to determine an apparent

second-order rate constant using DynaFit of 39,500 ± 8000 M^{-1} min^{-1} based on the concentration of the [2Fe-2S] cluster [89].

Mutation	Primer
G189R – Forward	5’-CCAACTGTGCAGGAAGAT**C**GAGGGGATGTAATCT-3’
G189R – Reverse	5’-AGATTACATCCCCTC**G**ATCTTCCTGCACAGTTGG-3’
G189A – Forward	5’-AACTGTGCAGGAAGATG**C**AGGGGATGTAATCTACA-3’
G189A – Reverse	5’-TGTAGATTACATCCCCT**G**CATCTTCCTGCACAGTT-3’
G189K – Forward	5’-AATACGGCCAACTGTGCAGGAAGAT**AA**AGGGGATGTAATCT-3’
G189K – Reverse	5’-AGATTACATCCCCT**TT**ATCTTCCTGCACAGTTGGCCGTATT-3’

Table B-1 A list of primers used to conduct site-directed mutagenesis on the human NFU1 constructs.

The substituted nucleotides are in bold black and underlined.

Construct	K	k_1
G189A	0.00009 ± 0.00006	0.18 ± 0.03
G189K	0.00012 ± 0.00007	0.31 ± 0.05
G189R	0.00032 ± 0.00018	1.4 ± 0.2

Table B-2 Apparent dissociation constants K (M) for the pre-reaction complex of holo protein and GSH and first-order rate constants k_1 (min^{-1})

for formation of the [2Fe-2S](GS)$_4$ complex during cluster extraction from holo proteins by free glutathione.

Equation 4 Two-State VTCD Unfolding Model

$$\theta = \left\{ \exp\left[\left(\frac{1}{-RT}\right)\left(\Delta H_{V1}\left(1 - \frac{T}{T_{m1}}\right) - C_{p1}\left((T_{m1} - T) + T\ \ln\frac{T}{T_{m1}}\right)\right)\right] \right.$$
$$\left. \Big/ \left\{ 1 \right. \right.$$
$$\left. \left. + \exp\left[\left(\frac{1}{-RT}\right)\left(\Delta H_{V1}\left(1 - \frac{T}{T_{m1}}\right) - \ C_{p1}\left((T_{m1} - T) + T\ln\frac{T}{T_{m1}}\right)\right)\right] \right\} \right\} (F$$
$$- U_1)$$
$$+ \left\{ \exp\left[\left(\frac{1}{-RT}\right)\left(\Delta H_{V2}\left(1 - \frac{T}{T_{m2}}\right) - C_{p2}\left((T_{m2} - T) + T\ln\frac{T}{T_{m2}}\right)\right)\right] \right.$$
$$\left. \Big/ \left\{ 1 \right. \right.$$
$$\left. \left. + \exp\left[\left(\frac{1}{-RT}\right)\left(\Delta H_{V2}\left(1 - \frac{T}{T_{m2}}\right) - C_{p2}\left((T_{m2} - T) + T\ln\frac{T}{T_{m2}}\right)\right)\right] \right\} \right\} (U_1$$
$$- U_2) + U_2$$

VTCD data were fit to equation 4 for a two-state model indicative of a two-phase transition [49], where R is the ideal gas constant in calories per mole, T_m is the melting temperature in Kelvin, ΔH_V is the van't Hoff enthalpy, and C_p is the heat capacity. F and U represent the mean residue ellipticities (θ_{mr}) of the folded and unfolded protein, respectively. It has been previously determined that the first observed transition can be assigned to the secondary structure transition of the melting C-terminal domain, and the second transition is indicative of the melting of the N-terminal domain [49]. The subscripts on T_m, ΔH_V, C_p and U denote the transition parameters on the separate protein domains, with 1 for the C-terminal domain and 2 for the N-terminal domain.

Appendix C : Chapter 4 Supplementary Data

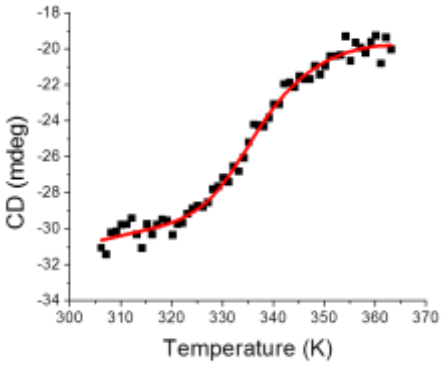

Figure C-1 VTCD trace for the melting of 10 μM G208S

in 40 mM phosphate, pH 7.4. Data were fit to equation 1 to obtain T_m and ΔH_V, which are summarized in Table 2. CD units of ellipticity (mdeg) were used directly without conversion to molar ellipticity because the van't Hoff enthalpies are independent of such a factor [49].

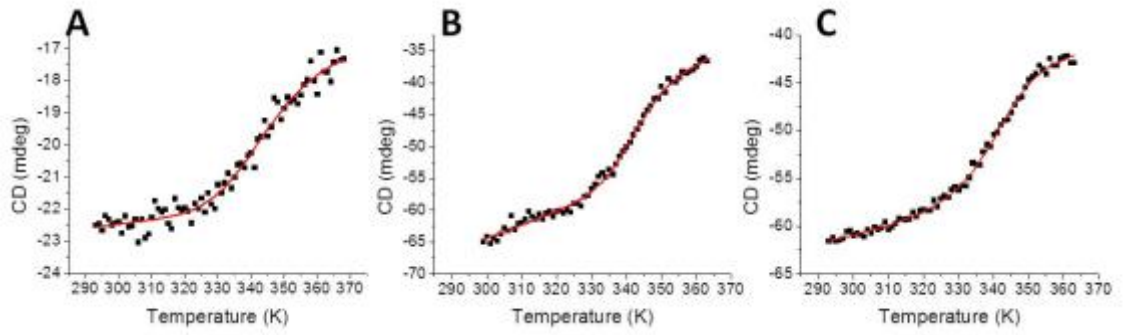

Figure C-2 VTCD traces

for the melting of (**A**) 10 μM G208C C210A, (**B**) 10 μM G208C C210S, and (**C**) 10 μM G208C C213S in 40 mM phosphate, pH 7.4. Data were fit to equation 1 to obtain T_m and ΔH_V, which are summarized in Table 2. CD units of ellipticity (mdeg) were used directly without conversion to molar ellipticity because the van't Hoff enthalpies are independent of such a factor [49].

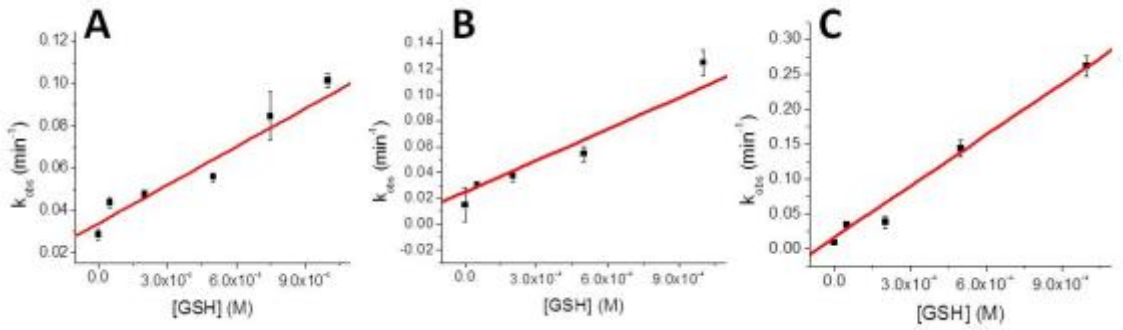

Figure C-3 GSH extraction of the [2Fe-2S] cluster

from (**A**) 10 μM G208C C210A, (**B**) 10 μM G208C C210S, and (**C**) 10 μM G208C C213S, to form the [2Fe-2S](GS)$_4$ complex. The change in absorbance at 420 nm was monitored over the course of one hour and data were fit to an exponential to obtain k_{obs} values that were subsequently plotted against GSH concentration to determine an overall second-order rate constant of 250 ± 10 $M^{-1}min^{-1}$ for (**A**), 60 ± 3 $M^{-1}min^{-1}$ for (**B**), and 81 ± 8 $M^{-1}min^{-1}$ for (**C**).

Mutation	Primer
G208A - Forward	5’-CAGCTGAAACTCCAGG**C**TTCTTGTACCAGCTGC-3’
G208A - Reverse	5’-GCAGCTGGTACAAGAA**G**CCTGGAGTTTCAGCTG-3’
G208S - Forward	5’-GTACAGCTGAAACTCCAG**TC**TTCTTGTACCAGCTGCCC-3’
G208S - Reverse	5’-GGGCAGCTGGTACAAGAA**GA**CTGGAGTTTCAGCTGTAC-3’
G208C C210A - Forward	5’-CTGAAACTCCAG**T**GTTCT**GC**TACCAGCTGCCCTAGTTC-3’
G208C C210A - Reverse	5’-GAACTAGGGCAGCTGGTA**GC**AGAAC**A**CTGGAGTTTCAG-3’
G208C C210S - Forward	5’-GCTGAAACTCCAG**T**GTTCTT**C**TACCAGCTGCC-3’
G208C C210S - Reverse	5’-GGCAGCTGGTA**G**AAGAAC**A**CTGGAGTTTCAGC-3’
G208C C213A - Forward	5’-CCAG**T**GTTCTTGTACCAGC**GC**CCCTAGTTCAATCATTACT-3’
G208C C213A - Reverse	5’-AGTAATGATTGAACTAGGG**GC**GCTGGTACAAGAAC**A**CTGG-3’
G208C C213S - Forward	5’-CAG**T**GTTCTTGTACCAGCT**C**CCCTAGTTCAATCAT-3’
G208C C213S - Reverse	5’-ATGATTGAACTAGGG**G**AGCTGGTACAAGAAC**A**CTG-3’

Table C-1 A list of primers used to conduct site-directed mutagenesis on the human NFU1 constructs.

The substituted nucleotides are in bold black and underlined, and the Gly208Cys mutation is in bold red.

References

[1] Maret, W. (2016). The Metals in the Biological Periodic System of the Elements: Concepts and Conjectures. International Journal of Molecular Sciences 17, 66.

[2] Andreini, C., Bertini, I. and Rosato, A. (2009). Metalloproteomes: A bioinformatic approach. Acc Chem Res 42, 1471-1479.

[3] Cowan, J.A. (1997) Inorganic Biochemistry: An Introduction, Wiley-VCH, Inc.

[4] Hayden, J.A., Brophy, M.B., Cunden, L.S. and Nolan, E.M. (2013). High-Affinity Manganese Coordination by Human Calprotectin Is Calcium-Dependent and Requires the Histidine-Rich Site Formed at the Dimer Interface. Journal of the American Chemical Society 135, 775-787.

[5] (2013) Interrelations between Essential Metal Ions and Human Diseases, Springer

[6] Gaeta, A. and Hider, R.C. (2009). The crucial role of metal ions in neurodegeneration: the basis for a promising therapeutic strategy. British Journal of Pharmacology 146, 1041-1059.

[7] Chen, P., Miah, M.R. and Aschner, M. (2016). Metals and neurodegeneration. F1000Research 5, 366.

[8] Muckenthaler, M.U., Galy, B. and Hentze, M.W. (2008). Systemic Iron Homeostasis and the Iron-Responsive Element/Iron-Regulatory Protein (IRE/IRP) Regulatory Network. Annual Review of Nutrition 28, 197-213.

[9] Zhang, A.S. and Enns, C.A. (2008). Iron Homeostasis: Recently Identified Proteins Provide Insight into Novel Control Mechanisms. Journal of Biological Chemistry 284, 711-715.

[10] Kakhlon, O. and Cabantchik, Z.I. (2002). The labile iron pool: Characterization, measurement, and participation in cellular processes Free Radic Biol Med 33, 1037-1046.

[11] Anderson, G.J. and Vulpe, C.D. (2009). Mammalian iron transport. Cellular and Molecular Life Sciences 66, 3241-3261.

[12] Johnson, D.C., Dean, D.R., Smith, A.D. and Johnson, M.K. (2005). Structure, function, and formation of biological iron-sulfur clusters. Annu Rev Biochem 74, 247-281.

[13] Lill, R. and Muehlenhoff, U. (2008). Maturation of iron-sulfur proteins in eukaryotes: mechanisms, connected processes, and diseases. Annu. Rev. Biochem. 77

[14] Maio, N. and Rouault, T.A. (2015). Iron–sulfur cluster biogenesis in mammalian cells: New insights into the molecular mechanisms of cluster delivery. Biochim. Biophys. Acta 1853, 1493-1512.

[15] Stehling, O., Wilbrecht, C. and Lill, R. (2014). Mitochondrial iron–sulfur protein biogenesis and human disease. Biochimie 100, 61-77.

[16] Fontecave, M. (2006). Iron-sulfur clusters: ever-expanding roles. Nat Chem Biol 2, 171-174.

[17] Baltscheffsky, H. (1996) Origin and Evolution of Biological Enegy Conversion, Wiley-VCH

[18] Tan, G., Liu, D., Pan, F., Zhao, J., Li, T., Ma, Y., Shen, B. and Lyu, J. (2016). His-87 ligand in mitoNEET is crucial for the transfer of iron sulfur clusters from mitochondria to cytosolic aconitase. Biochem Biophys Res Commun 470, 226-232.
[19] Bak, D.W. and Elliott, S.J. (2014). Alternative FeS cluster ligands: tuning redox potentials and chemistry. Curr Opin Chem Biol 19, 50-58.
[20] Harmer, Jenny E. et al. (2014). Structures of lipoyl synthase reveal a compact active site for controlling sequential sulfur insertion reactions. Biochem J 464, 123-133.
[21] Huang, J. and Cowan, J.A. (2009). Iron–sulfur cluster biosynthesis: role of a semi-conserved histidine. Chem Commun, 3071-3073.
[22] Maio, N. and Rouault, T.A. (2016). Mammalian Fe–S proteins: definition of a consensus motif recognized by the co-chaperone HSC20. Metallomics 8, 1032-1046.
[23] Markley, J.L., Kim, J.H., Dai, Z., Bothe, J.R., Cai, K., Frederick, R.O. and Tonelli, M. (2013). Metamorphic protein IscU alternates conformations in the course of its role as the scaffold protein for iron–sulfur cluster biosynthesis and delivery. FEBS Lett. 587, 1172-1179.
[24] Lill, R. and Mühlenhoff, U. (2008). Maturation of iron-sulfur proteins in eukaryotes: mechanisms, connected processes, and diseases. Annu. Rev. Biochem. 77, 669-700.
[25] Kim, J.H., Bothe, J.R., Alderson, T.R. and Markley, J.L. (2015). Tangled web of interactions among proteins involved in iron–sulfur cluster assembly as unraveled by NMR, SAXS, chemical crosslinking, and functional studies. Biochim Biophys Acta 1853, 1416-1428.
[26] Fidai, I., Wachnowsky, C. and Cowan, J.A. (2016). Glutathione-complexed [2Fe-2S] clusters function in Fe-S cluster storage and trafficking. J Biol Inorg Chem 21, 887-901.
[27] Fidai, I., Wachnowsky, C. and Cowan, J.A. (2016). Mapping cellular Fe–S cluster uptake and exchange reactions – divergent pathways for iron–sulfur cluster delivery to human ferredoxins. Metallomics 8, 1283-1293.
[28] Wachnowsky, C., Fidai, I. and Cowan, J.A. (2016). Iron-sulfur cluster exchange reactions mediated by the human Nfu protein. J Biol Inorg Chem 21, 825-836.
[29] Li, J. and Cowan, J.A. (2015). Glutathione-coordinated [2Fe–2S] cluster: a viable physiological substrate for mitochondrial ABCB7 transport. Chem Commun 51, 2253-2255.
[30] Qi, W., Li, J., Chain, C.Y., Pasquevich, G.A., Pasquevich, A.F. and Cowan, J.A. (2012). Glutathione complexed Fe-S centers. J Am Chem Soc 134, 10745-8.
[31] Qi, W., Li, J. and Cowan, J.A. (2014). A structural model for glutathione-complexed iron–sulfur cluster as a substrate for ABCB7-type transporters. Chem. Commun. 50, 3795.
[32] Cameron, J.M. et al. (2011). Mutations in iron-sulfur cluster scaffold genes NFU1 and BOLA3 cause a fatal deficiency of multiple respiratory chain and 2-oxoacid dehydrogenase enzymes. Am J Hum Genet 89, 486-95.

[33] Ajit Bolar, N. et al. (2013). Mutation of the iron-sulfur cluster assembly gene IBA57 causes severe myopathy and encephalopathy. Hum. Mol. Genet. 22, 2590-2602.
[34] Debray, F.-G. et al. (2015). Mutation of the iron-sulfur cluster assembly gene IBA57 causes fatal infantile leukodystrophy. J Inherit Metab Dis 38, 1147-1153.
[35] Al-Hassnan, Z.N. et al. (2015). ISCA2 mutation causes infantile neurodegenerative mitochondrial disorder. J Med Genet 52, 186-194.
[36] Baker, P.R. et al. (2013). Variant non ketotic hyperglycinemia is caused by mutations in LIAS, BOLA3 and the novel gene GLRX5. Brain 137, 366-379.
[37] Lossos, A. et al. (2015). Fe/S protein assembly gene IBA57 mutation causes hereditary spastic paraplegia. Neurology 84
[38] Navarro-Sastre, A. et al. (2011). A fatal mitochondrial disease is associated with defective NFU1 function in the maturation of a subset of mitochondrial Fe-S proteins. Am J Hum Genet 89, 656-667.
[39] Ye, H. and Rouault, T.A. (2010). Human Iron−Sulfur Cluster Assembly, Cellular Iron Homeostasis, and Disease. Biochemistry 49, 4945-4956.
[40] Lasserre, J.P. et al. (2015). Yeast as a system for modeling mitochondrial disease mechanisms and discovering therapies. Dis. Model Mech. 8, 509-526.
[41] Galluzzi, L., Kepp, O., Trojel-Hansen, C. and Kroemer, G. (2012). Mitochondrial Control of Cellular Life, Stress, and Death. Circulation Research 111, 1198-1207.
[42] Lill, R. et al. (2012). The role of mitochondria in cellular iron-sulfur protein biogenesis and iron metabolism. Biochim. Biophys. Acta 1823, 1491-508.
[43] Tort, F., Ferrer-Cortes, X. and Ribes, A. (2016). Differential diagnosis of lipoic acid synthesis defects. J Inherit Metab Dis 39, 781-793.
[44] Stehling, O., Wilbrecht, C. and Lill, R. (2014). Mitochondrial iron-sulfur protein biogenesis and human disease. Biochimie 100, 61-77.
[45] Invernizzi, F., Ardissone, A., Lamantea, E., Garavaglia, B., Zeviani, M., Farina, L., Ghezzi, D. and Moroni, I. (2014). Cavitating leukoencephalopathy with multiple mitochondrial dysfunction syndrome and NFU1 mutations. Front. Genet. 5
[46] Nizon, M. et al. (2014). Leukoencephalopathy with cysts and hyperglycinemia may result from NFU1 deficiency. Mitochondrion 15, 59-64.
[47] Ahting, U. et al. (2015). Clinical, biochemical, and genetic spectrum of seven patients with NFU1 deficiency. Front Genet 06
[48] Lill, R. and Muehlenhoff, U. (2008). Maturation of iron-sulfur proteins in eukaryotes: mechanisms, connected processes, and diseases. Annu. Rev. Biochem. 77, 669-700.
[49] Li, J., Ding, S. and Cowan, J.A. (2013). Thermodynamic and structural analysis of human NFU conformational chemistry. Biochemistry 52, 4904-4913.
[50] Liu, Y. and Cowan, J.A. (2007). Iron sulfur cluster biosynthesis. Human NFU mediates sulfide delivery to ISU in the final step of [2Fe-2S] cluster assembly. Chem Commun, 3192-4.
[51] Liu, Y. and Cowan, J.A. (2009). Iron−sulfur cluster biosynthesis: characterization of a molten globule domain in human NFU. Biochemistry 48, 7512-7518.

[52] Tong, W.H., Jameson, G.N.L., Huynh, B.H. and Rouault, T.A. (2003). Subcellular compartmentalization of human Nfu, an iron-sulfur cluster scaffold protein, and its ability to assemble a [4Fe-4S] cluster. Proc. Natl. Acad. Sci. U.S.A. 100, 9762-9767.

[53] Angelini, S., Gerez, C., Choudens, S.O.d., Sanakis, Y., Fontecave, M., Barras, F. and Py, B. (2008). NfuA, a new factor required for maturing Fe/S proteins in *Escherichia coli* under oxidative stress and iron starvation conditions. J. Biol. Chem. 283, 14084-14091.

[54] Gao, H. et al. (2013). *Arabidopsis thaliana* Nfu2 accommodates [2Fe-2S] or [4Fe-4S] clusters and is competent for *in vitro* maturation of chloroplast [2Fe-2S] and [4Fe-4S] cluster-containing proteins. Biochemistry 52, 6633-6645.

[55] Nishio, K. and Nakai, M. (2000). Transfer of iron-sulfur cluster from NifU to apoferredoxin. J. Biol. Chem. 275, 22615-22618.

[56] Py, B. et al. (2012). Molecular organization, biochemical function, cellular role and evolution of NfuA, an atypical Fe-S carrier. Mol. Microbiol. 86, 155-171.

[57] Yabe, T. (2004). The *Arabidopsis* chloroplastic NifU-like protein CNFU, which can act as an iron-sulfur cluster scaffold protein, is required for biogenesis of ferredoxin and photosystem I. Plant Cell 16, 993-1007.

[58] Cai, K., Liu, G., Frederick, Ronnie O., Xiao, R., Montelione, Gaetano T. and Markley, John L. (2016). Structural/functional properties of human NFU1, an intermediate [4Fe-4S] carrier in human mitochondrial iron-sulfur cluster biogenesis. Structure

[59] Ganesh, S. (2003). The Lafora disease gene product laforin interacts with HIRIP5, a phylogenetically conserved protein containing a NifU-like domain. Hum. Mol. Gen. 12, 2359-2368.

[60] Melber, A., Na, U., Vashisht, A., Weiler, B.D., Lill, R., Wohlschlegel, J.A. and Winge, D.R. (2016). Role of Nfu1 and Bol3 in Iiron-sulfur cluster transfer to mitochondrial clients. eLife 5, e15991.

[61] Touraine, B., Boutin, J.-P., Marion-Poll, A., Briat, J.-F., Peltier, G. and Lobréaux, S. (2004). Nfu2: a scaffold protein required for [4Fe-4S] and ferredoxin iron-sulphur cluster assembly in *Arabidopsis* chloroplasts. Plant J. 40, 101-111.

[62] Bandyopadhyay, S., Naik, S.G., O'Carroll, I.P., Huynh, B.H., Dean, D.R., Johnson, M.K. and Dos Santos, P.C. (2008). A proposed role for the *Azotobacter vinelandii* NfuA protein as an intermediate iron-sulfur cluster carrier. J. Biol. Chem. 283, 14092-14099.

[63] Ferrer-Cortès, X. et al. (2012). Protein expression profiles in patients carrying NFU1 mutations. Contribution to the pathophysiology of the disease. J Inherit Metab Dis 36, 841-847.

[64] Foster, M.W., Mansy, S.S., Hwang, J., Penner-Hahn, J.E., Surerus, K.K. and Cowan, J.A. (2000). A mutant human IscU protein contains a stable $[2Fe\text{-}2S]^{2+}$ center of possible functional significance. J Am Chem Soc 122, 6805-6806.

[65] Mansy, S.S., Xiong, Y., Hemann, C., Hille, R., Sundaralingam, M. and Cowan, J.A. (2002). Crystal structure and stability studies of C77S HiPIP: a serine ligated [4Fe-4S] cluster. Biochemistry 41, 1195-1201.

[66] Nuth, M., Yoon, T. and Cowan, J.A. (2002). Iron-sulfur cluster biosynthesis: characterization of iron nucleation sites for assembly of the $[2Fe\text{-}2S]^{2+}$ cluster core in IscU proteins. J Am Chem Soc 124, 8774-8775.

[67] Xia, B., Cheng, H., Bandarian, V., Reed, G.H. and Markley, J.L. (1996). Human ferredoxin: overproduction in *Escherichia coli*, reconstitution *in vitro*, and spectroscopic studies of iron-sulfur cluster ligand cysteine-to-serine mutants. Biochemistry 35, 9488-9495.

[68] Qi, W., Li, J. and Cowan, J.A. (2013). Human ferredoxin-2 displays a unique conformational change. Dalton Trans. 42, 3088-3091.

[69] Qi, W. and Cowan, J.A. (2011). Mechanism of glutaredoxin-ISU [2Fe-2S] cluster exchange. Chem Commun 47, 4989-91.

[70] Wu, G., Mansy, S.S., Hemann, C., Hille, R., Surerus, K.K. and Cowan, J.A. (2002). Iron-sulfur cluster biosynthesis: characterization of *Schizosaccharomyces pombe* Isa1. J Biol Inorg Chem 7, 526-32.

[71] Luo, W.-I., Dizin, E., Yoon, T. and Cowan, J.A. (2010). Kinetic and structural characterization of human mortalin. Protein Expr Purif 72, 75-81.

[72] Yoon, T. (2005) Functional and structural studies of human frataxin: An iron chaperone protein for mitochondrial iron-sulfur cluster and heme biosynthesis. In Chemistry ed.^eds), pp. 168. The Ohio State University, Columbus.

[73] Sreerama, N. and Woody, R.W. (2000). Estimation of protein secondary structure from CD spectra: Comparison of CONTIN, SELCON and CDSSTR methods with an expanded reference set. Anal Chem 287, 252-260.

[74] Janes, R.W. (2008) Reference Datasets Circular Dichroism and Synchrotron Radiation Circular Dichroism Spectroscopy of Proteins. . In Modern Techniques in Circular Dichroism and Synchrotron Radiation Circular Dichroism Spectroscopy (Wallace, B.A. and Janes, R.W., ed.^eds). IOS Press, Amsterdam.

[75] Whitmore, L. and Wallace, B.A. (2004). DICHROWEB, an online server for protein secondary structure analyses from circular dichroism spectroscopic data. Nucleic Acids Res 32, W668-W673.

[76] Whitmore, L. and Wallace, B.A. (2008). Protein secondary structure analyses from circular dichroism spectroscopy: Methods and reference databases. Biopolymers 89, 392-400.

[77] Krebs, C., Agar, J.N., Smith, A.D., Frazzon, J., Dean, D.R., Huynh, B.H. and Johnson, M.K. (2001). IscA, an alternate scaffold for Fe-S cluster biosynthesis. Biochemistry 40, 14069-14080.

[78] Wu, S.-p., Wu, G., Surerus, K.K. and Cowan, J.A. (2002). Iron-sulfur cluster biosynthesis. Kinetic analysis of [2Fe-2S] cluster transfer from holo ISU to apo Fd: role of redox chemistry and a conserved aspartate. Biochemistry 41, 8876-8885.

[79] Lamm, O. (1929). Die Differentialgleichung der Ultrazentrifugierung. Ark Mat Astr Fys, 1-4.

[80] Schuck, P. (2000). Size-distribution analysis of macromolecules by sedimentation velocity ultracentrifugation and Lamm equation modeling. Biophys. J. 78, 1606-1619.

[81] Moulis, J.-M. and Meyer, J. (1982). Characterization of the selenium-substituted 2[4Fe-4Se] ferredoxin from *Clostridium pasteurianum*. Biochemistry 21, 4762-4771.
[82] Qi, W., Li, J., Chain, C.Y., Pasquevich, G.A., Pasquevich, A.F. and Cowan, J.A. (2013). Glutathione-complexed iron–sulfur clusters. Reaction intermediates and evidence for a template effect promoting assembly and stability. Chem Commun 49, 6313.
[83] Mapolelo, D.T. et al. (2013). Monothiol glutaredoxins and A-type proteins: partners in Fe–S cluster trafficking. Dalton Trans 42, 3107.
[84] Shakamuri, P., Zhang, B. and Johnson, M.K. (2012). Monothiol glutaredoxins function in storing and transporting [2Fe-2S] clusters assembled on IscU scaffold proteins. J Am Chem Soc 134, 15213-15216.
[85] Bonomi, F., Iametti, S., Morleo, A., Ta, D. and Vickery, L.E. (2008). Studies on the mechanism of catalysis of iron-sulfur cluster transfer from IscU[2Fe2S] by HscA/HscB chaperones. Biochemistry 47, 12795–12801.
[86] Bonomi, F., Iametti, S., Morleo, A., Ta, D. and Vickery, L.E. (2011). Facilitated transfer of IscU–[2Fe2S] clusters by chaperone-mediated ligand exchange. Biochemistry 50, 9641-9650.
[87] Wu, S.-P., Mansy, S.S. and Cowan, J.A. (2005). Iron-sulfur cluster biosynthesis. Molecular chaperone DnaK promotes IscU-bound [2Fe-2S] cluster stability and inhibits cluster transfer activity. Biochemistry 44, 4284-4293.
[88] Chandramouli, K. and Johnson, M.K. (2006). HscA and HscB stimulate [2Fe-2S] cluster transfer from IscU to apoferredoxin in an ATP-dependent reaction. Biochemistry 45, 11087-11095.
[89] Kuzmic, P. (1996). Program DYNAFIT for the analysis of enzyme kinetic data: Application to HIV proteinase. Anal Biochem 237, 260-273.
[90] Wachnowsky, C., Fidai, I. and Cowan, J.A. (2016). Cytosolic iron-sulfur cluster transfer: a proposed kinetic pathway for the reconstitution of glutaredoxin 3. FEBS Lett 590, 4531-4540.
[91] Stephens, P.J., Thomson, A.J., Dunn, J.B.R., Keiderling, T.A., Rawlings, J., Rao, K.K. and Hall, D.O. (1978). Circular Dichroism and Magnetic Circular Dichroism of Iron-Sulfur Proteins. Biochemistry 22, 4770-4778.
[92] Broom, H.R., Vassall, K.A., Rumfeldt, J.A.O., Doyle, C.M., Tong, M.S., Bonner, J.M. and Meiering, E.M. (2016). Combined isothermal titration and differential scanning calorimetry define three-state thermodynamics of fALS-associated mutant apo SOD1 dimers and an increased population of folded monomer. Biochemistry 55, 519-533.
[93] Doyle, C.M., Rumfeldt, J.A., Broom, H.R., Broom, A., Stathopulos, P.B., Vassall, K.A., Almey, J.J. and Meiering, E.M. (2013). Energetics of oligomeric protein folding and association. Arch Biochem Biophys 531, 44-64.
[94] Kelley, L.A., Mezulis, S., Yates, C.M., Wass, M.N. and Sternberg, M.J.E. (2015). The Phyre2 web portal for protein modeling, prediction and analysis. Nat. Protoc. 10, 845-858.

[95] Pace, C.N. and Scholtz, J.M. (1998). A helix propensity scale based on experimental studies of peptides and protein. Biophys J 75, 422-427.
[96] Maio, N. and Rouault, T.A. (2015). Iron–sulfur cluster biogenesis in mammalian cells: New insights into the molecular mechanisms of cluster delivery. Biochim Biophys Acta 1853, 1493-1512.
[97] Shan, Y. and Cortopassi, G. (2016). Mitochondrial Hspa9/Mortalin regulates erythroid differentiation via iron-sulfur cluster assembly. Mitochondrion 26, 94-103.
[98] Maio, N., Singh, A., Uhrigshardt, H., Saxena, N., Tong, W.-H. and Rouault, Tracey A. (2014). Cochaperone binding to LYR motifs confers specificity of iron sulfur cluster delivery. Cell Metab 19, 445-457.
[99] Uzarska, M.A. et al. (2016). Mitochondrial Bol1 and Bol3 function as assembly factors for specific iron-sulfur proteins. eLife 5, e15991.
[100] Muhlenhoff, U., Richhardt, N., Gerber, J. and Lill, R. (2002). Characterization of iron-sulfur protein assembly in isolated mitochondria. A requirement for ATP, NADH, and reduced iron. J. Biol. Chem. 277, 29810-29816.
[101] Lundberg, M., Johansson, C., Chandra, J., Enoksson, M., Jacobsson, G., Ljung, J., Johansson, M. and Holmgren, A. (2001). Cloning and expression of a novel human glutaredoxin (Grx2) with mitochondrial and nuclear isoforms. J. Biol. Chem. 276, 26269-26275.
[102] Chung, W.H., Kim, K.D. and Roe, J.H. (2005). Localization and function of three monothiol glutaredoxins in *Schizosaccharomyces pombe*. Biochem. Biophys. Res. Commun. 330, 604-10.
[103] Seyda, A. et al. (2001). A Novel Syndrome Affecting Multiple Mitochondrial Functions, Located by Microcell-Mediated Transfer to Chromosome 2p14-2p13. Am. J. Hum. Genet. 68, 386-396.
[104] Fajac, I. and De Boeck, K. (2017). New horizons for cystic fibrosis treatment. Pharmacology & Therapeutics 170, 205-211.
[105] Colca, J.R., McDonald, W.G., Waldon, D.J., Leone, J.W., Lull, J.M., Bannow, C.A., Lund, E.T. and Mathews, W.R. (2004). Identification of a novel mitochondrial protein ("mitoNEET") cross-linked specifically by a thiazolidinedione photoprobe. Am J Physiol Endocrinol Metab 286, E252-E260.
[106] Wiley, S.E., Murphy, A.N., Ross, S.A., van der Geer, P. and Dixon, J.E. (2007). MitoNEET is an iron-containing outer mitochondrial membrane protein that regulates oxidative capacity. Proceedings of the National Academy of Sciences 104, 5318-5323.
[107] Ferrer-Cortès, X. et al. (2016). A leaky splicing mutation in NFU1 is associated with a particular biochemical phenotype. Consequences for the diagnosis. Mitochondrion 26, 72-80.
[108] Wachnowsky, C., Wesley, N.A., Fidai, I. and Cowan, J.A. (2017). Understanding the molecular basis for Multiple Mitochondrial Dysfunctions Syndrome 1 (MMDS1) - Impact of a disease-causing Gly208Cys substitution on structure and activity of NFU1 in the Fe/S cluster biosynthetic pathway. J Mol Biol doi: 10.1016/j.jmb.2017.01.021

[109] Tonduti, D. et al. (2015). New spastic paraplegia phenotype associated to mutation of NFU1. Orphanet J Rare Dis 10, 13.
[110] Wu, S.-p., Wu, G., Surerus, K.K. and Cowan, J.A. (2002). Iron-sulfur cluster biosynthesis. Kinetic analysis of [2Fe-2S] cluster transfer from holo ISU to apo Fd: role of redox chemistry and a conserved aspartate. Biochemistry 41, 8876-8885.
[111] Schuck, P. (2000). Size-distribution analysis of macromolecules by sedimentation velocity ultracentrifugation and Lamm equation modeling. Biophys J 78, 1606-1619.
[112] Qi, W., Li, J., Chain, C.Y., Pasquevich, G.A., Pasquevich, A.F. and Cowan, J.A. (2012). Glutathione Complexed Fe–S Centers. Journal of the American Chemical Society 134, 10745-10748.
[113] Mapolelo, D.T. et al. (2013). Monothiol glutaredoxins and A-type proteins: partners in Fe-S cluster trafficking. Dalton Trans 42, 3107-15.
[114] Liu, Y., Qi, W. and Cowan, J.A. (2009). Iron-sulfur cluster biosynthesis: functional characterization of the N- and C-terminal domains of human NFU. Biochemistry 48, 973-980.
[115] Harris, T.V. and Szilagyi, R.K. (2016). Protein environmental effects on iron-sulfur clusters: A set of rules for constructing computational models for inner and outer coordination spheres. J Comput Chem 37, 1681-1696.
[116] Tsang, S.H., Wang, R., Nakamaru-Ogiso, E., Knight, S.A.B., Buck, C.B., You, J. and Banks, L. (2016). The oncogenic small tumor antigen of merkel cell polyomavirus is an iron-sulfur cluster protein that enhances viral DNA replication. J Virol 90, 1544-1556.
[117] Netz, D.J.A., Genau, H.M., Weiler, B.D., Bill, E., Pierik, A.J. and Lill, R. (2016). The conserved protein Dre2 uses essential [2Fe-2S] and [4Fe-4S] clusters for its function in cytosolic iron-sulfur protein assembly. Biochem J 473, 2073-2085.
[118] Hurley, J.K. et al. (1997). Iron-sulfur cluster cysteine-to-serine mutants of *Anabaena* [2Fe-2S] ferredoxin exhibit unexpected redox properties and are competent in electron transfer to ferredoxin:NADP+ reductase. Biochemistry 36, 15109-15117.
[119] Greenfield, N.J. (2007). Using circular dichroism collected as a function of temperature to determine the thermodynamics of protein unfolding and binding interactions. Nat Protoc 1, 2527-2535.
[120] Spiller, Michael P., Ang, Swee K., Ceh-Pavia, E., Fisher, K., Wang, Q., Rigby, Stephen E.J. and Lu, H. (2013). Identification and characterization of mitochondrial Mia40 as an iron–sulfur protein. Biochem J 455, 27-35.
[121] Ohnishi, T. (1998). Iron–sulfur clustersrsemiquinones in complex I. Biochem Biophys Acta 1364, 186-206.
[122] Levitan, A., Danon, A. and Lisowsky, T. (2004). Unique features of plant mitochondrial sulfhydryl oxidase. J Biol Chem 279, 20002-8.
[123] Abdel-Ghany, S.E., Ye, H., Garifullina, G.F., Zhang, L., Pilon-Smits, E.A.H. and Pilon, M. (2005). Iron-sulfur cluster biogenesis in chloroplasts. Involvement of the scaffold protein CpIscA. Plant Physiol 138, 161-172.

[124] Xiao, Z. et al. (1998). The rubredoxin from *Clostridium pasteurianum*: Mutation of the iron cysteinyl ligands to serine. Crystal and molecular structures of oxidized and dithionite-treated forms of the Cys42Ser mutant. J Am Chem Soc 120, 4135-4150.

[125] Kudryashova, E., Quintyn, R., Seveau, S., Lu, W., Wysocki, Vicki H. and Kudryashov, Dmitri S. (2014). Human defensins facilitate local unfolding of thermodynamically unstable regions of bacterial protein toxins. Immunity 41, 709-721.

[126] Marinoni, E.N., de Oliveira, J.S., Nicolet, Y., Raulfs, E.C., Amara, P., Dean, D.R. and Fontecilla-Camps, J.C. (2012). (IscS-IscU)2 complex structures provide insights into Fe2S2 biogenesis and transfer. Angew Chem Int Ed Engl 51, 5439-42.

[127] Qi, W., Li, J., Chain, C.Y., Pasquevich, G.A., Pasquevich, A.F. and Cowan, J.A. (2013). Glutathione-complexed iron-sulfur clusters. Reaction intermediates and evidence for a template effect promoting assembly and stability. Chemical Commun 49, 6313-5.